Analysis and Compensation of Nonlinear Impairments in Fiber-Optic Communication Systems

ANALYSIS AND COMPENSATION OF NONLINEAR IMPAIRMENTS IN FIBER-OPTIC COMMUNICATION SYSTEMS

BY

XIAOJUN LIANG, M.A.Sc.

A THESIS

SUBMITTED TO THE DEPARTMENT OF ELECTRICAL AND COMPUTER ENGINEERING

AND THE SCHOOL OF GRADUATE STUDIES

OF MCMASTER UNIVERSITY

IN PARTIAL FULFILMENT OF THE REQUIREMENTS

FOR THE DEGREE OF

DOCTOR OF PHILOSOPHY

Doctor of Philosophy (2015) McMaster University

(Electrical and Computer Engineering) Hamilton, Ontario, Canada

TITLE:	Analysis and Compensation of Nonlinear Impairments in Fiber-Optic Communication Systems
AUTHOR:	Xiaojun Liang M.A.Sc., (Optical Engineering) Huazhong University of Science and Technology,Wuhan, China
SUPERVISOR:	Prof. Shiva Kumar
NUMBER OF PAGES:	xxi, 179

To my beloved parents

Abstract

Fiber optic communications make the backbone of telecommunications. Optical fiber is an excellent transmission medium due to its low loss, high bandwidth and robustness. However, the dispersive and nonlinear effects of an optical fiber lead to signal distortions. Propagation impairments accumulate over fiber distance and seriously distort the signal in long-haul communication systems. Transmission performance can be significantly improved by compensating for fiber dispersion and nonlinear effects. In this thesis, we carry out theoretical analysis of fiber nonlinear effects and develop analytical models to characterize different kinds of nonlinearities. Moreover, we investigate various digital and optical methods to compensate for dispersive and nonlinear distortions, which significantly enhance transmission performance, spectral efficiency and system capacity.

Fiber dispersion is a linear effect and can be well-characterized by the dispersion coefficient and the transfer function. On the other hand, fiber nonlinearity is a much more complicated effect. In most fiber optic communication systems, the major fiber nonlinear effect is the Kerr nonlinearity that arises from the dependence of refractive index on the signal intensity. We focus on the theoretical analysis of Kerr nonlinear effects in optical fibers. Practically, most fiber optic links are dispersion dominant, meaning that dispersive effect is much stronger than the nonlinear effect. Therefore,

a perturbation theory is applicable which assumes the nonlinear distortion to be a small perturbation to the linear field solution due to dispersion only. Based on a first order perturbation theory, we derive analytical models for various fiber nonlinear effects, including self-phase modulation (SPM), cross-phase modulation (XPM) and intra-channel four wave mixing (IFWM).

Based on the nonlinear distortion field calculated using a first order perturbation theory, we carry out statistical analysis to obtain the variance of XPM effects in coherent wavelength division multiplexing (WDM) fiber-optic systems. For systems using non-Gaussian pulses, the analytical XPM model is not available due to the difficulty in evaluating integrals. We use a summation of time-shifted Gaussian pulses to fit non-Gaussian pulse shapes so that the analytical model can deal with arbitrary pulse shapes. The analytically estimated XPM variance is found to be in good agreement with numerical simulations.

Moreover, we develop a novel recursive perturbation theory to model signal propagation in fiber optic links. We express signal fields using orthogonal sampling functions which allows recursive operation of perturbation calculation. The recursive perturbation theory improves both the modeling accuracy and computational cost as compared to the conventional first order perturbation theory.

Also, we derive an exact solution of nonlinear Schrödinger equation (NLSE) for impulse input in the presence of pre-dispersion. It is found that if the complex weights of a sequence of impulses at the input have a secant-hyperbolic envelope and a proper chirp factor, they will propagate over long distances without exchanging energy. To describe their interaction, a discrete version of NLSE is derived. The discrete NLSE is found to admit fundamental and higher order soliton solutions in the presence

of high pre-dispersion. We have obtained the nonlinear eigenmodes of the highly pre-dispersed fiber-optic system which may be useful for the description of signal propagation, and signal and noise interaction.

For the purpose of compensation, we develop various digital and optical methods. We investigate a digital back propagation (DBP) scheme with optimal step sizes to compensate for fiber dispersion and nonlinearities. By optimizing the step size of each section through minimizing the area mismatch between the exponential profile of the effective nonlinear coefficient and its stepwise approximation, system reach is significantly enhanced without additional computational cost and system complexity.

We study a digital compensation scheme based on the perturbation theory to mitigate XPM distortions in dispersion-managed fiber-optic communication systems. A hard-decision unit at the receiver is used to estimate data for the calculation of XPM fields using the perturbation technique. The perturbation technique is shown to be effective in mitigating XPM distortions. However, wrong estimations in the hard-decision unit result in performance degradation. A hard-decision correction method is proposed to correct the wrong estimations, which brings significant performance improvements. The perturbation-based XPM compensation scheme requires much less computational cost as compared with conventional DBP, since it only requires one-stage (or two-stage when hard-decision correction is applied) compensation and symbol-rate signal processing.

Also, we develop a multi-stage scheme based on a recursive perturbation theory to compensate for intra-channel nonlinear impairments is investigated. In each stage the first order theory is used to calculate the nonlinear distortions occurring in a distance much shorter than the entire fiber-optic link, which improves the accuracy

and the summation of the signal field and the first order field of the previous stage is used as the unperturbed solution for the next stage, which further improves the accuracy. Moreover, the accumulated dispersion in one compensation stage is much smaller than that of the entire link which significantly reduces the computational cost of perturbation calculation since the cost is proportional to the amount of accumulated dispersion. Numerical simulations of a single-channel fiber-optic system shows that the multi-stage perturbation technique brings significant performance improvements and computational complexity reduction as compared with the single-stage compensation scheme.

Other than digital methods, we propose an ideal optical back propagation (OBP) scheme to compensate for dispersion and nonlinear effects of the transmission fibers is investigated. The scheme consists of an optical phase conjugator (OPC), N spans of dispersion-decreasing fibers (DDFs) and amplifiers, placed at the end of the fiber optic link. It is shown that a combination of DDFs and amplifiers can compensate for the nonlinear effects exactly. An analytical expression for the dispersion profile of the DDF is derived. Numerical simulations of WDM fiber-optic systems show that the proposed OBP scheme can enhance the system reach significantly as compared to DBP. Moreover, it is hard to use digital techniques to compensate for nonlinear impairments in fiber optic networks with complex mesh configurations, due to the lack of path information of signal propagation. In contrast, OBP is applicable to network systems by placing an OBP module after each transmission fiber and the propagation impairments of each transmission fiber are compensated by the OBP module following it.

Acknowledgements

I would like to express the deepest gratitude to my research supervisor Prof. Shiva Kumar for providing me the opportunity of Ph.D. study and for his constant encouragement, inspiring guidance and insightful discussions throughout the period of this work. Also, I would like to thank Prof. Shiva Kumar for always being supportive, tolerant and caring like a friend.

I would like to express my sincere thanks to the committee members, Prof. Xun Li, Prof. Wei-Ping Huang, Prof. Mohamed Bakr and Prof. Steve Hranilovic, for their valuable comments and suggestions during my research. I would like to thank Dr. Sina N. Shahi for the helpful discussions about optical fiber nonlinear effects. I would like to thank all my friends and colleagues in the Photonics group, Jianwei Mu, Lin Han, Yu Li, Kan He, Lanxin Deng, Qingyi Guo, Xiao Deng, Zhengkai Chen, Ting Luo, Yefeng Wen, Haibo Liang, Tingxia Li, Rui Tang, Yunfei Cai, Zeyu Hu, Qiudi Ding, Shovasis K. Biswas, Sangzhi Zhao and Chenyu Yang, for their friendship and help. I would like to thank all the ECE department staff for providing me all the conveniences and assistance in my study.

Finally, I am deeply grateful to my dear wife, Jing, for her love and support, and for the constant companionship throughout the memorable time.

Abbreviations

ADC	analog-to-digital converter
ASE	amplified spontaneous emission
A-M	additive-multiplicative
BER	bit error rate
BPF	band pass filter
CPR	carrier phase recovery
CW	continuous wave
DBP	digital back propagation
DC	dispersion compensator
DCF	dispersion compensating fiber
DDF	dispersion-decreasing fiber
DFT	discrete Fourier transform
DM	dispersion-managed
DMUX	demultiplxer
DSP	digital signal processing
DST	discrete self-trapping
DU	dispersion-uncompensated
EDC	electronic dispersion compensation

EDFA	Erbium doped fiber amplifier
ERP	enhanced regular perturbation
FBG	fiber Bragg grating
FEC	forward error correction
FFT	fast Fourier transforms
FIR	finite impulse response
FWM	four-wave mixing
GN	Gaussian noise
GTO	Gaussian type orbital
GVD	group-velocity dispersion
HDF	high-dispersion fiber
HNLF	highly nonlinear fiber
IDFT	inverse discrete Fourier transform
IFWM	intra-channel four wave mixing
IIR	infinite impulse response
ISI	inter-symbol interference
IST	inverse scattering transform
IXPM	intra-channel cross-phase modulation
LMS	least mean squares
LO	local oscillator
LPF	low pass filter
LSM	least squares method
MAM	minimum area mismatch
MMSE	minimum mean-square error

MUX	multiplexer
NDF	negative dispersion fiber
NLIN	nonlinear interference noise
NLSE	nonlinear Schrödinger equation
NZDSF	non-zero dispersion-shifted fiber
OBP	optical back propagation
OBPF	optical back propagation fiber
OFDM	orthogonal frequency-division multiplexing
OPC	optical phase conjugation
OPLL	optical phase locked loop
OSNR	optical signal-to-noise ratio
PCTW	phase-conjugated twin wave
PDM	polarization division multiplexing
PMD	polarization mode dispersion
PSD	power spectral density
QAM	quadrature amplitude modulation
QPSK	quadrature phase shift keying
SPM	self-phase modulation
SSFS	split-step Fourier scheme
SSMF	standard single mode fiber
TF	transmission fiber
WDM	wavelength division multiplexing
XPM	cross-phase modulation

Contents

List of Figures

Chapter 1

Introduction

1.1 Fiber-optic communication systems

Fiber-optic communication systems are lightwave systems that transmit information from one place to another by sending electromagnetic signals through an optical fiber [1, 2]. A fundamental fiber-optic communication system consists of an optical transmitter, a fiber-optic link and an optical receiver. The optical transmitter converts an electrical signal to an optical signal using an optical modulator. After signal propagation in the fiber-optic link, the optical receiver converts the optical signal back into an electrical signal. One significant advantage of fiber-optic communication systems is the high bandwidth (and hence high transmission data rate) due to the use of a high-frequency laser carrier ($\sim$ 200 THz), which is five orders of magnitude higher than that of the microwave systems ($\sim$ 1 GHz). Fiber-optic communication systems have been deployed worldwide since 1980s and have revolutionized the telecommunication industry.

1.2 Impairments in fiber-optic links

Optical signals will be distorted while propagating through an optical fiber, due to fiber loss, dispersion and nonlinearity. The loss of silica fibers can be made as small as 0.2 dB/km. However, in long haul transmission systems, signal attenuation becomes significant and has to be compensated in order to recover high quality signal. Fiber loss can be compensated using Erbium doped fiber amplifiers (EDFAs) which add amplified spontaneous emission (ASE) noise. Optical fiber is a dispersive medium whose refractive index is dependent on frequency. As a result, different frequency components of an optical pulse propagate at different speeds leading to pulse broadening and intersymbol interference (ISI). Another origin of signal impairments is fiber nonlinear effects [3]. The dominant fiber nonlinear effect in fiber-optic communication systems is the Kerr effect, namely the dependence of the refractive index on the intensity of the optical pulse. In a single channel fiber-optic link, the Kerr effect results

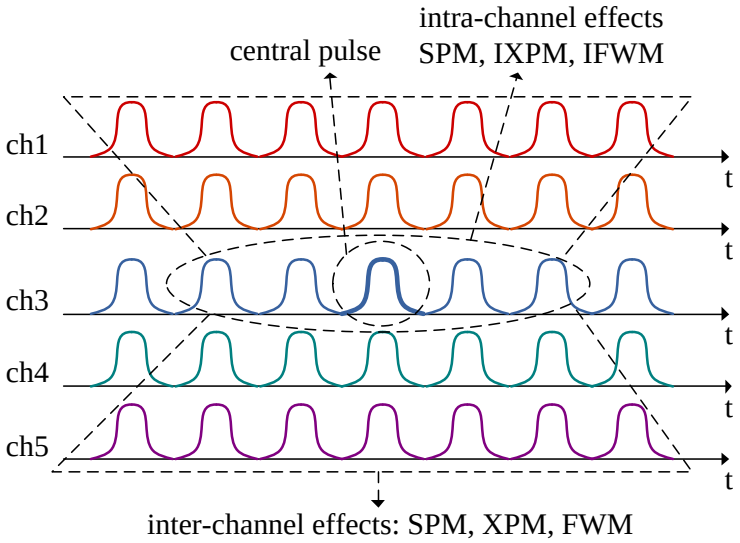

Figure 1.1: Nonlinear interactions in a WDM fiber optic communication system

in self-phase modulation (SPM), intra-channel cross-phase modulation (IXPM), and intra-channel four wave mixing (IFWM) [3]. SPM and IXPM mean the intensity-dependent nonlinear phase shifts added to an optical pulse due to the presence of the same pulse and a neighboring pulse, respectively. Nonlinear interaction among signal pulses centered at lT_s, mT_s and nT_s leads to a ghost pulse centered at $(l+m-n)T_s$, which is known as IFWM. As shown in Fig. 1.1, the intra-channel effects are due to the nonlinear interactions of optical pulses of a same channel (e.g. ch3). In a wavelength division multiplexing (WDM) system, the Kerr effect results in self-phase modulation (SPM), cross-phase modulation (XPM), and four wave mixing (FWM) [3]. As shown in Fig. 1.1, SPM, XPM and FWM correspond to the nonlinear interactions of one, two and three WDM channels, respectively. Due to the power variance of an optical pulse, SPM effect brings a phase shift to the pulse itself. This phase change also leads to a change in the pulse's frequency spectrum. In the case when multiple signal channels co-propagate in a single fiber, the power fluctuations of one signal channel produce a phase shift to another channel, which is due to the XPM effect [4, 5]. Also, nonlinear interaction among signal channels centered at frequencies f_1, f_2 and f_3 gives rise to a fourth frequency $(f_1+f_2-f_3)$ due to the scattering of the incident photons, which is known as the FWM effect [6, 7]. In polarization division multiplexing (PDM) systems, the two principal polarizations have slightly different group velocities and also the birefringence varies randomly with distance along the fiber. These polarization fluctuations produce linear (intensity independent) and nonlinear (intensity dependent) signal pulse broadening and distortions, known as linear and nonlinear polarization mode dispersion (PMD), respectively [8, 9]. Moreover, nonlinear interactions between signal and ASE noise will result in additional signal

impairments, known as the Gordon-Mollenauer effects [10]. The amplitude fluctuations resulted from ASE noise will be converted to a phase noise since the refractive index is dependent on the signal intensity.

1.3 Compensation techniques for fiber dispersive and nonlinear effects

Fiber-optic communication technology has been advancing rapidly for several decades. The transmission capacity of a fiber-optic link is enhanced by a factor of 10 every four years [11]. The technology breakthroughs starting from 1980s that promotes fiber-optic communications include the development of low-loss single mode fibers, the use of EDFA, the WDM technique, and the use of advanced modulation formats in coherent transmission systems enabled by high-speed digital signal processing (DSP). Currently, the transmission capacity of fiber-optic communication systems is mainly limited by the Kerr nonlinear effect in optical fibers. At low signal power, transmission performance is limited by ASE noise, so the capacity can be enhanced by increasing signal power. At high signal power, however, fiber nonlinear effects dominate and make it impossible to enhance transmission performance by simply increasing signal power. Various optical and digital compensation techniques have been investigated to partially or fully compensate for fiber nonlinear effects, or the combined effect of fiber dispersion and nonlinearities.

1.3.1 Optical dispersion compensation

The concept of compensation for signal distortions using optical techniques dates

back to decades ago. In 1994, Antos and Smith [12] designed and fabricated a dispersion compensating fiber (DCF) with large negative waveguide dispersion for the LP_{01} mode to compensate for the dispersion of transmission fiber. The length of the DCF is chosen to obtain a negative dispersion that is equal in magnitude to the positive dispersion accumulated in the transmission fiber so that the net pulse broadening is zero. Hill *et al.* [13] employed a fiber Bragg grating (FBG) to compensate for dispersion in fiber-optic networks. FBGs exhibit large dispersion when used in reflection mode and the sign of dispersion is easily controlled. A relatively short Bragg grating is shown to compensate for dispersion of an optical fiber that is tens of kilometers long.

1.3.2 Mid-point optical phase conjugation

Signal distortions due to propagation in an optical fiber result from the interplay of dispersion and nonlinearity. Pepper and Yariv [14] showed theoretically that the signal propagation distortions can be compensated by the use of a phase conjugation mirror. Fisher *et al.* [15] demonstrated numerically that the temporal distortion and spectral broadening of a pulse generated by the combined effect of group-velocity dispersion (GVD) and SPM is removed by conjugating the signal near the mid-point of the fiber-optic link. In WDM systems, Watanabe and Chikama [16] demonstrated the compensation of FWM using mid-point OPC. In 2009, Martelli *et al.* [17] demonstrated OPC for polarization multiplexed signals. In fiber-optic communication systems, mid-point optical phase conjugation (OPC) can undo the distortions due to fiber dispersion and nonlinearity, if the nonlinearity, dispersion, and power profiles are symmetric with respect to OPC location. However, for systems using lumped amplification such as

EDFA, the power profile with respect to OPC is not symmetric, which limits the compensation performance of OPC. A much better symmetry of power profile is available in fiber-optic systems with Ramam amplification. Solis-Trapala *et al.* [18] showed by experiments that mid-point OPC brings a significant performance improvement in a WDM system with dispersion-flattened non-zero dispersion-shifted fibers (NZDSFs) and bidirectional Ramam pumping amplification.

1.3.3 Optical back propagation

Optical back propagation (OBP) has been proposed for the compensation of fiber dispersive and nonlinear effects by Kumar *et al.* [19–21]. In Ref. [19], an OBP module is designed and placed at the end of a fiber-optic link to compensate fiber dispersive and nonlinear effects. The OBP module consists of DCFs and nonlinearity compensators, which undo distortions by reversing signal propagation. The nonlinearity compensator imparts a phase shift that is equal in magnitude to the nonlinear phase shift due to fiber propagation, but opposite in sign. The effective negative nonlinear coefficient of the nonlinearity compensator is realized using a pair of highly nonlinear fibers (HNLFs). This OBP scheme provides good transmission performance, but it requires pumps and polarization alignment of the pumps with signal, which increases the complexity of the receiver. In Ref. [20], an improved OBP scheme that does not need pump is presented, wherein the OBP module consists of an OPC followed by short lengths of high-dispersion fibers (HDFs) and HNLFs, concatenated in a way analogous to the split-step Fourier scheme (SSFS) used for solving the nonlinear Schrödinger equation (NLSE). The HDF provides the accumulated dispersion that is the same as the corresponding transmission fiber section and the set of HDF

and HNLF provides a nonlinear phase shift that is the same as the corresponding transmission fiber section. It is shown that the OBP scheme provides better transmission performance as compared with mid-point OPC when the lumped amplifiers are used [20]. In Ref. [21], the OBP scheme is further improved by optimizing the accumulated dispersion of each section of FBGs and the nonlinear phase shift of each section of HNLFs in the OBP module. The optimization is achieved by minimizing the mismatch between the area under the exponentially increasing nonlinearity profile and its stepwise approximation provided by the OBP module and is shown that the minimal area mismatch (MAM) technique leads to significant reach enhancement as compared to uniform spacing for the given step size [21].

1.3.4 Phase-conjugated twin wave

Recently, Liu *et al.* [22] proposed to compensate for Kerr nonlinearity using phase-conjugated twin waves (PCTWs). They showed that the nonlinear distortions of a pair of phase-conjugated twin waves are anticorrelated and as a result, nonlinear distortions due to signal-signal nonlinear interactions are canceled by coherent superimposition of the twin waves. In experiments, the two orthogonal polarizations are used at twin waves and the data modulated on one polarization is the conjugation copy of that of the other polarization. The PCTW approach reduces the nonlinear distortions significantly, but halves the spectral efficiency since the data on one polarization is only a conjugated copy of the data on the other polarization. The PCTW approach provides a method of trading spectral efficiency for transmission performance. Yoshida *et al.* [23] proposed a method based on joint processing of two

pairs of PCTWs to improve transmission performance without loss of spectral efficiency. The single set PCTW is modified by combining two sets of PCTWs in a single carrier so as to increase the spectral efficiency. A quadrature pulse shaping technique is introduced to reduce the crosstalk between the two sets of PCTW signals. In Ref. [24], Liu *et al.* generalized the PCTW concept to twining two signals in orthogonal dimensions, such as two waves that propagate along an orthogonal spatial path or occupy two different carrier frequencies. Yi *et al.* [25] employed optical orthogonal frequency-division multiplexing (OFDM) sub-carriers as twin waves. They showed by experiments that signal tolerance to both laser phase noise and XPM phase noise is improved in an optical OFDM system by the PCTW technique.

1.3.5 Digital dispersion compensation

Recent advances in DSP have enabled the digital compensation of signal impairments in coherent fiber-optic communication systems [26]. Coherent detection provides the amplitude as well as phase information of the received signal, allowing compensation of linear and nonlinear impairments using DSP in the digital domain. Taylor [27] demonstrated the compensation of chromatic dispersion using coherent detection and DSP, without using the optical phase locked loops (OPLLs). Dispersion is compensated by an off-line equalizer which divides the spectrum of the received signal with the dispersion transfer function of the transmission fiber. Savory [28] showed that dispersion compensation can be realized in the time domain using a finite impulse response (FIR) filter, which has a non-recursive structure and can be implemented using a tapped delay line. The number of FIR taps required grows linearly with accumulated dispersion, which results in high power consumption in long-haul systems.

Alternatively, Goldfarb and Li [29] demonstrated the compensation of chromatic dispersion using an infinite impulse response (IIR) filter. IIR filters are shown to be more computational efficient as compared to FIR filters but requires buffering. For systems with large accumulated dispersion, it would be more efficient to compensate for chromatic dispersion in the frequency domain using fast Fourier transforms (FFTs) rather than using time domain filters. Ip and Kahn [30] investigated a digital equalizer for compensation of chromatic dispersion and PMD in polarization multiplexed coherent fiber-optic systems. They found that the digital equalizer can fully compensate chromatic dispersion and first order PMD distortion, provided that the oversampling rate is at least 3/2 and sufficient number of equalizer taps are employed. The optimal tap settings are derived based on the minimum mean-square error (MMSE) criterion, which is shown to be a valid performance criterion despite the potential non-Gaussianity of crosstalk and ISI. Tsukamoto *et al.* [31] experimentally demonstrated the compensation of dispersion using DSP in a coherent fiber-optic system with homodyne detection.

1.3.6 Digital back propagation

Signal propagation in an optical fiber is well described by the NLSE, which is an invertible equation. In the absence of ASE noise, distortions due to signal-signal nonlinear interactions can be calculated by solving NLSE and as a result, the transmitted signal can be exactly recovered by propagating the signal in the backward direction in a virtual fiber in the digital domain, which will undo all deterministic distortions. In digital back propagation (DBP), the optical signal is converted into a digital signal and then passes through an virtual fiber that has loss, dispersion and

nonlinear coefficient the same in magnitude but the opposite in sign as those of the transmission fiber. Roberts *et al.* [32] proposed a nonlinear pre-compensation method based on DBP in a single-channel fiber-optic system. The desired signal waveform at the receiver is used as the input to DBP. Pre-distortions are added to the signal during back propagation in the virtual fiber. The back propagated signal is then used to determine the nonlinear filter coefficients in the transmitter. The pre-distortions in the transmitted signal cancel with the distortions accumulated in the real fiber propagation. DBP can be also implemented as post-compensation by putting the virtual fiber after coherent detection and using the distorted signal as the input to DBP. Post-compensation has better flexibility than pre-compensation since it allows various adapative compensation techniques. Li *et al.* [33] and Ip and Kahn [34] applied DBP using post-compensation in WDM systems. In Ref. [33], Li *et al.* used FIR filters for the dispersion step and a parallel architecture was designed to facilitate real-time implementation. They showed by numerical simulations that two samples per symbol hardware sampling with up-sampling in the digital domain are sufficient to achieve significant nonlinearity compensation. In Ref. [34], Ip and Kahn investigated a non-iterative asymmetric SSFS for solving the inverse NLSE in DBP. Simulations showed that three samples per symbol are required for DBP to achieve good numerical accuracy. Mateo *et al.* [35] investigated the impact of XPM and FWM on electronic impairment compensation using DBP in coherent WDM systems. Coupled NLSE and total-field NLSE are used to study the impacts of XPM and FWM, respectively. The inverse NLSEs are solved using symmetric iterative SSFS. Simulation results show that XPM is the most important source of nonlinear distortion and is much stronger

than FWM. As compared with coupled NLSE, DBP based on total-field NLSE provides more precise compensation since it compensates for FWM distortions. However, FWM effect is phase sensitive, so that its compensation requires the phases of received signals in different WDM channels to be preserved. This is difficult to achieve since different WDM channels have different LO lasers. To maintain the phase relation in different WDM channels, the LO lasers must be phase-locked. On the other hand, DBP based on coupled NLSE can maintain high accuracy with better computational efficiency and low system latency. Also, it is shown in [35] that for DBP based on coupled NLSE, the step size is determined by the walk-off effect between two separated WDM channels. The compensation of FWM requires implementing DBP based on the total-field NLSE, which needs enormous computational resources. Although FWM effect is negligible as compared with XPM effect in long-haul systems with large accumulated dispersion, FWM distortion becomes substantial in the low-dispersion region or in dispersion-managed systems due to the increased degree of phase matching. Mateo and Li [36] proposed a DBP scheme based on an enhanced coupled NLSE for full compensation of XPM and partial compensation of FWM, where only significant FWM interactions between neighboring channels are included. A significant reduction in computational complexity is achieved as compared with the total-field NLSE based DBP, while good compensation performance is maintained. Mateo *et al.* [37] investigated an advanced split-step DBP based on the coupled NLSE to reduce the computational cost by factoring out the dispersive walk-off effect between WDM channels, which sets the limit to DBP step size. This advanced SSFS method relaxes the computational load by a factor of 4. The computational cost of DBP is an important issue for real-time implementation in practical systems. For single-channel and

WDM systems, the required number of steps per fiber span varies from a few steps to tens of steps in DBP. Du and Lowery [38] proposed a filtered DBP scheme to reduce the computational cost. In filtered DBP, a low pass filter (LPF) is used to filter the signal before nonlinearity compensation in each DBP step and the position of nonlinear compensation in each step is optimized. They found that the required number of DBP steps per fiber span can be less than one in a single-channel fiber-optic system.

In fiber-optic communication systems, signal distortion is usually dominated by fiber dispersion and nonlinear distortion can be considered as a small perturbation. For the case of dispersion managed (DM) systems, signal distortion due to fiber dispersion repeats itself with every dispersion period. This periodic behavior of signal distortion may be employed to simplify the implementation of DBP. Zhu and Li [39] proposed a folded DBP scheme for DM communication systems. In folded DBP, nonlinear distortions accumulated in multiple (K) fiber spans are approximated by the nonlinear distortion accumulated in a single span with the same dispersion map and K times the nonlinearity. Simulation results show that for DM transoceanic transmission systems, folded DBP reduces the computational complexity by up to two orders of magnitude as compared to conventional DBP, with negligible penalty. However, the advantage in computational cost and compensation performance of folded DBP degrade when the residual dispersion per span (RDSP) increases, due to the break of periodicity of signal waveform evolution. Later, Zhu and Li [40] investigated an improved folded DBP that works even when RDSP is large, called dispersion-folded (D-folded) DBP. In D-folded DBP, the dispersion map is divided into multiple divisions according to the value of accumulated dispersion. Multiple (M) fiber segments of different fiber spans may have a same dispersion map division, that is, they have

the same accumulated dispersion. Therefore, the nonlinear distortions of these fiber segments can be compensated using a single fiber segment with M times the nonlinearity. However, in the split steps, the power levels and effective fiber lengths are different due to the loss of periodicity. To solve this problem, weighting factors are introduced to modify the nonlinear phase shift at every DBP step. The weighting factors are calculated off-line and stored in look-up tables. Liu *et al.* [41] experimentally demonstrated efficient mitigation of intra-channel and inter-channel nonlinear impairments in dispersion managed WDM fiber-optic systems using dispersion folded DBP.

In polarization multiplexed WDM systems, signals on different polarizations rotate differently due to PMD. Nonlinear interactions among different channels are dependent on their polarization status, indicating that PMD may affect the compensation performance of DBP. Yaman and Li [42] investigated the implementation of DBP in PDM transmission systems. They showed by simulations that PMD substantially impairs the DBP technique. In order to effectively compensate inter-channel nonlinear distortions, rotations of the polarization status have to be followed at every fiber span in DBP implementation. Mateo *et al.* [43] reported an improved split step DBP for PDM transmission systems. DBP is implemented on a channel-by-channel basis based on a system of coupled equations derived from the Manakov equations which describe the average polarization evolution of the vector NLSE. The inter-polarization mixing effects are included by introducing new terms in the split step formulation. Moreover, the effect of dispersive walk-off between WDM channels is factorized by including the relative delay between different channels, which substantially increases the DBP step size.

1.3.7 Perturbation-based digital compensation

DBP provides a universal compensation technique for signal impairments in fiber-optic links, which is able to remove all deterministic impairments provided that the DBP step size is sufficiently small. The implementation of DBP is based on solving the inverse NLSE numerically in the digital domain using SSFS, which demands enormous computational resources and limits the most implementation of DBP to off-line signal processing. Alternatively, analytical or semi-analytical solutions of the NLSE may be employed in digital compensation schemes in order to substantially reduce computational complexity. In fiber-optic communication systems, dispersion is the dominant effect and nonlinearity can be considered as a small perturbation. Therefore, perturbation theory can be applied to find analytical or semi-analytical solutions to the NLSE. Mecozzi *et al.* [44] presented a first order perturbation analysis in time domain for intra-channel nonlinear effects for highly dispersed systems with Gaussian pulses. The signal field propagatin in an optical fiber is divided into two parts: the unperturbed solution which is the solution due to fiber dispersion and loss, but in the absence of nonlinearity, and the perturbation correction which is the first order field due to nonlinearity. Nonlinear interaction among optical pulses results in time jitter and echo pulses. Kumar and Yang [45] developed a second order perturbation theory to study the SPM and XPM effects in fiber-optic links. They found that if the dispersion distance is comparable to or larger than the nonlinear length, the accuracy of first order perturbation theory is not adequate to describe nonlinear effects, while the second order theory still provides good accuracy in this case. Analytical expressions are derived for SPM and XPM distortions for both first order and second order perturbation theories. Poggiolini *et al.* [46] provided a Gaussian noise (GN) model

based on a perturbation theory to describe the nonlinear distortions in dispersion uncompensated (DU) transmission systems. In the GN model, the nonlinear interaction distortions in DU links are assumed to be additive Gaussian noise. Based on this assumption, a semi-analytical expression is obtained for the power spectral density (PSD) of nonlinear distortions. The GN model is shown to provide good agreement with both simulation and experimental results. In Ref. [47], Dar *et al.* compared the time domain perturbation theory with the GN model. The nonlinear distortion is shown to be not additive Gaussian, but rather it depends on the data modulated on the channel of interest and on the modulation format of the interfering channel. Mecozzi *et al.* [48] developed a general first order perturbation theory for signal propagation in fiber-optic links. The perturbation theory applies to optical pulses propagating in a fiber-optic link in the presence of ASE noise and Kerr nonlinearity. An analytical expression is obtained to calculate the deviation in complex amplitude of the distorted signal at the center symbol slot of a given channel.

Perturbation theory has been applied in digital compensation schemes in fiber-optic communication systems. Tao *et al.* [49] investigated a perturbation based digital pre-compensation scheme to mitigate intra-channel nonlinear distortions. At the transmitter, the nonlinear distortions are calculated based on the first order perturbation theory using the input data and the perturbation coefficient matrix. The perturbation coefficient matrix is calculated off-line and stored in a look up table. The transmitted signal is obtained by subtracting the nonlinear distortions from the input signal. Fiber dispersive and nonlinear effects introduce distortions to the transmitted signal, and these distortions cancel with the pre-distortions added in the transmitter.

Therefore, the output signal of the fiber-optic link become the same as the input signal at the transmitter. This perturbation based pre-compensation scheme provides a transmission performance similar to that of a DBP with step size equal to the fiber span length. Perturbation based compensation scheme can also be implemented at the receiver side. Oyama *et al.* [50] proposed a decision-aided compensation scheme based on perturbation theory for compensating intra-channel nonlinear effects. The information data required for perturbation calculation is lost at the receiver side, but the estimated data obtained by hard-decision is used instead of the input data for perturbation calculation. This scheme uses one-stage compensation and symbol rate operation. They found that the receiver-side perturbation based scheme has similar compensation performance as the transmitter-side perturbation based scheme. In the perturbation theory, the first order correction or the nonlinear distortion of a given symbol is calculated by considering its nonlinear interaction with neighboring symbols, where single and double summations involving the perturbation coefficient matrix X_{mn} needs to be calculated. The coefficient X_{mn} corresponds to the nonlinear interaction of the mth, nth, and $(m+n)$th symbols which produces a nonlinear distortion to the symbol at the 0th symbol. The computational effort for the double summation is substantial in long haul transmission systems where the accumulated dispersion is high resulting in a large number of interacting neighboring symbols. Therefore, the reduction of implementation complexity of perturbation based compensation schemes is of great research interest. Gao *et al.* [51, 52] reduced the complexity of perturbation based pre-compensation using symmetric electronic dispersion compensation (EDC) and pulse shaping. Using symmetric EDC, the perturbation coefficients X_{mn} are calculated based on half of the entire fiber link length indicating a

reduced accumulated dispersion as well as the number of interacting neighboring symbols. Also, with symmetric EDC, complex multiplications in perturbation calculation become real multiplications. Therefore, the computational complexity is significantly reduced. In Ref. [53], Gao *et al.* showed that the computational complexity of the perturbation based compensation can be reduced using joint pre-compensation and selective decision-aided post-compensation. In practice, perturbation compensation only needs to be applied to the symbols that are close to the decision boundaries as these are most likely related with error symbols. Such a selective compensation is hard to be implemented at the transmitter due to the difficulty of identify distortions before pre-compensation. In Ref. [53], part of the perturbation compensation is performed at the transmitter and the other part is applied at the receiver with selective compensation, which results in a reduction of the effective number of multiplications by a factor of 4. Zhuge *et al.* [54] investigated a coefficient quantization method to reduce the complexity of perturbation based compensation schemes. In perturbation calculation, the nonlinear distortion is calculated by the multiplication of three data symbols and one perturbation coefficient. For quadrature phase shift keying (QPSK) systems, the multiplication of three data symbols still produces a QPSK symbol, and hence the multiplications can be replaced using a digital logical operation. Also, the number of distinct values in the perturbation coefficient matrix can be substantially reduced using quantization. Therefore, the majority operations in perturbation calculation become a large number of summations and a small number (equal to the number of distinct values in the perturbation coefficient matrix) of multiplications. Experimental results show that three distinct perturbation coefficients are sufficient in a per-distortion scheme for a fiber-optic system with symmetric EDC, which still

brings substantial transmission performance improvement.

1.4 Contributions of the thesis

This thesis focuses on the theoretical analysis and compensation techniques of signal impairments due to fiber dispersive and nonlinear effects in fiber-optic communication systems. In Chapter 2, analytical modeling of XPM effect in coherent WDM fiber-optic communication systems is investigated. XPM distortion is calculated using a first order perturbation theory and then statistical analysis is carried out to calculate XPM variance based on quadrature amplitude modulation (QAM). For systems with non-Gaussian pulses, the XPM variance cannot be calculated analytically, due to the difficulty in evaluating integrals explicitly. We introduced a method of using a summation of time-shifted Gaussian pulses to fit non-Gaussian pulse shapes so that the analytical model can deal with arbitrary pulse shapes. The analytically estimated XPM variance is found to be in good agreement with numerical simulations.

In Chapter 3, we studied a digital back propagation (DBP) scheme with optimal step sizes for the compensation of fiber dispersive and nonlinear effects. The optimal step sizes are obtained by minimizing the area mismatch between the exponential profile of the effective nonlinear coefficient and its stepwise approximation. Numerical simulations show that system reach is significantly enhanced without additional computational cost and system complexity. To simulate randomly changing birefringence in PDM systems, the vector NLSE is used for signal propagation and an adaptive least mean squares (LMS) equalizer is employed at the receiver to compensate for PMD.

In Chapter 4, we investigated a perturbation-based digital compensation scheme

to mitigate XPM distortions in dispersion-managed fiber-optic communication systems. The data information required for the perturbation calculation of XPM fields is obtained using a hard-decision unit at the receiver. The intra-channel nonlinear distortions are removed by intra-channel DBP based on split-step Fourier scheme before the hard-decision unit. The perturbation technique is shown to be effective in mitigating XPM distortions. However, wrong estimations in the hard-decision unit result in performance degradation. A hard-decision correction method is proposed to correct the wrong estimations. Numerical simulations show that the perturbation-based XPM compensation scheme brings significant performance improvements. The perturbation-based XPM compensation scheme requires much less computational cost as compared with conventional DBP based on the coupled NLSE, since it only requires one-stage (or two-stage when hard-decision correction is applied) compensation and symbol-rate signal processing.

In Chapter 5, a recursive perturbation theory to model the fiber-optic system is developed. Using this perturbation theory, a multi-stage compensation technique is investigated for the mitigation of intra-channel nonlinear impairments. The input signals of different compensation stages are expressed using the same basis functions so that the coefficient matrix X_{mn} for perturbation calculation is the same for all stages. The multi-stage compensation is implemented recursively, the output signal of one compensation stage is used as the input of the next compensation stage. In each stage the first order theory is used to calculate the nonlinear distortions occurring in a distance much shorter than the entire fiber-optic link, which improves the accuracy and the summation of the signal field and the first order field of the previous stage is used as the unperturbed solution for the next stage, which further improves the

accuracy. Moreover, the accumulated dispersion in one compensation stage is much smaller than that of the entire link which significantly reduces the size of the coefficient matrix X_{mn}, leading to reductions both in computational complexity and the required memory for storing X_{mn}. Simulation results show that the multi-stage perturbation technique brings significant performance improvements and computational complexity reduction as compared with the single-stage compensation scheme.

In Chapter 6, we studied an OBP scheme that employs dispersion-decreasing fibers (DDFs) to fully compensate for dispersion and nonlinearity in fiber-optic links. The scheme consists of an OPC, N spans of DDFs and amplifiers, placed at the end of the fiber optic link. In order to compensate for the nonlinear effects of the transmission fibers exactly, the nonlinear coefficient of the back propagation fiber has to increase exponentially with distance or equivalently the power in the back propagation fiber should increase exponentially with distance if the nonlinear coefficient is constant. We find that a combination of DDFs and amplifiers can compensate for the nonlinear effects exactly. An analytical expression for the dispersion profile of the DDF is derived. Numerical simulations show that the proposed OBP scheme can enhance the system reach significantly as compared to DBP.

In Chapter 7, we derived an exact solution of NLSE for impulse input in the presence of pre-dispersion. The phase factor of the exact solution is obtained in a closed form using the exponential integral. It is found that if the complex weights of a sequence of impulses at the input have a secant-hyperbolic envelope and a proper chirp factor, they will propagate over long distances without exchanging energy. To describe their interaction, a discrete version of NLSE is derived. In the context of discrete NLSE, if the effective dispersion length is much longer than the effective nonlinear

length, we have obtained the nonlinear eigenmodes of the highly pre-dispersed fiber-optic system which may be useful for the description of signal propagation, and signal and noise interaction.

The research work has resulted in the following publications:

Journal papers:

1. X. Liang, S. Kumar, and J. Shao, "Ideal optical backpropagation of scalar NLSE using dispersion-decreasing fibers for WDM transmission," Optics Express, vol. 21, no. 23, pp. 28668-28675, (2013).
2. J. Shao, S. Kumar, and X. Liang, "Digital back propagation with optimal step size for polarization multiplexed transmission," *IEEE* Photonics Technology Letters, vol. 25, no. 23, pp. 2327-2330, (2013).
3. S. N. Shahi, S. Kumar, and X. Liang, "Analytical modeling of cross-phase modulation in coherent fiber-optic system," Optics Express, vol. 22, no. 2, pp. 1426-1439, (2014).
4. X. Liang and S. Kumar, "Analytical modeling of XPM in dispersion-managed coherent fiber-optic systems," Optics Express, vol. 22, no. 9, pp. 10579-10592, (2014).
5. J. Shao, X. Liang, and S. Kumar, "Comparison of split-step Fourier schemes for simulating fiber optic communication systems," *IEEE* Photonics Journal, vol. 6, no. 4, pp. 7200515, (2014).
6. X. Liang, S. Kumar, J. Shao, M. Malekiha, and D. V. Plant, "Digital compensation of cross-phase modulation distortions using perturbation technique for dispersion-managed fiber-optic systems," Optics Express, vol. 22, no. 17, pp. 20634-20645,

(2014).

7. X. Liang and S. Kumar, "Multi-stage perturbation theory for compensating intra-channel nonlinear impairments in fiber-optic links," Optics Express, vol. 22, no. 24, pp. 29733-29745, (2014).
8. S. Kumar, J. Shao, and X. Liang, "Impulse response of nonlinear Schrödinger equation and its implications for pre-dispersed fiber-optic communication systems," Optics Express, vol. 22, no. 26, pp. 32282-32292, (2014).

Conference papers:

1. X. Liang and S. Kumar, "An analytical XPM model for dispersion-managed fiber optic systems," in Proc. of SPIE, Photonics North (Montreal Canada, 2014), paper 928805.
2. J. Shao, X. Liang, and S. Kumar, "An efficient scheme of split-step Fourier method for fiber optic communication systems," in Proc. of SPIE, Photonics North (Montreal Canada, 2014), paper 928806.
3. Q. Ding, X. Liang, and S. Kumar, "Comparisons of LMS equalizers for PMD mitigation in polarization-multiplexed coherent fiber optic systems," in Proc. of SPIE, Photonics North (Montreal Canada, 2014), paper 928808.
4. X. Liang and S. Kumar, A multi-stage perturbation technique for intra-channel nonlinearity compensation, in Optical Fiber Communication Conference, OSA Technical Digest (Optical Society of America, 2015), paper Th3D.1.

Book chapter:

X. Liang, J. Shao, and S. Kumar, "Optical back propagation for compensation of

dispersion and nonlinearity in fiber-optic transmission systems", in the book *Odyssey of Light in Nonlinear Optical Fibers: Theory and Applications*, K. Porsezian and R. Ganapathy, ed., CRC Press, 2015. (in press)

Chapter 2

Analytical modeling of XPM effect in dispersion-managed systems

2.1 Introduction

The modeling of cross-phase modulation (XPM) distortion in fiber-optic systems with direct detection [45, 55–61] and with coherent detection [46–48, 62–68] has drawn significant interest. Poggiolini *et al.* [46] and Carena *et al.* [62] have modeled the nonlinear interference noise (NLIN) in dispersion-uncompensated (DU) transmission systems as excess additive Gaussian noise and its variance is calculated using a perturbation technique. Dar *et al.* [47] have analyzed the properties of NLIN in a DU fiber-optic system with large dispersion and found that the NLIN is not additive Gaussian, but rather it depends strongly on the data transmitted in the channel. In this chapter, we develop an analytical expression for the XPM variance of a probe Gaussian pulse due to its interaction with other channels of a wavelength division multiplexing (WDM) system [69]. Then, we extend the analysis to arbitrary pulse

shapes and study the scaling laws of the XPM variance with residual dispersion per span, the number of WDM channels and transmission distance [70].

For a non-Gaussian pulse, the XPM variance cannot be calculated analytically without additional approximations. In DU systems, the stationary phase approximation can be used to circumvent the difficulty in explicitly evaluating integrals and analytical expressions are still available for the variance of nonlinear distortions [47, 69, 71]. However, the stationary phase approximation technique requires a large accumulated dispersion, which becomes inaccurate for dispersion-managed (DM) systems. The modeling of XPM variance in DM systems has become a challenging problem and in this chapter, we develop a simple analytical expression for the XPM variance in DM systems with arbitrary pulse shapes. We use the summation of time-shifted Gaussian pulses to fit a non-Gaussian pulse, which not only provides a good approximation of the non-Gaussian pulse but also allows analytical derivation of the XPM variance. We note that a similar method has been successfully applied in quantum chemistry, where a summation of Gaussian functions ($\sum_k \exp(-a_k x^2)$) is used to approximate an exponential function ($\exp(-bx)$) [72]. The summation of Gaussian functions is used in modeling electronic orbitals, named as Gaussian type orbitals (GTOs) [73]. Despite the fact that Gaussian functions are not mutually orthogonal, GTOs form a complete basis set and have gained dominance in calculating electronic wave functions due to its simplicity in explicitly evaluating integrals. In this chapter, we use a similar technique and approximate a non-Gaussian pulse by a summation of time-shifted Gaussian pulses. The fitting parameters are calculated using the least squares method (LSM).

The analytical expressions developed in this chapter are used to study the XPM

impairments in DM systems based on quadrature phase shift keying (QPSK) and 16-quadrature amplitude modulation (16-QAM). Scaling laws of the XPM variance with launch power, residual dispersion per span, number of channels and number of spans are studied. We found that the XPM variance depends on the power levels of the probe channel for 16-QAM, i.e., the variance is higher for constellation points close to the edge than those close to the center. This is the consequence of strong phase noise due to the XPM [48] and the manifestation of the non-additive nature of XPM noise [47]. The frequency-domain approach of [46, 62, 63] treats the XPM variance as white noise whose variance is independent of the signal power levels. Although such an approach is acceptable for systems in which amplified spontaneous emission (ASE) noise is the dominant penalty, it could lead to inaccurate results when XPM variance is comparable to ASE variance. The XPM variance is highest for the resonant dispersion map with zero accumulated dispersion per span ($\Psi_{res} = 0$ ps/nm) and it decreases monotonically with $|\Psi_{res}|$. The XPM variance increases almost quadratically with the number of spans when $\Psi_{res} = 0$ ps/nm due to the coherent addition of XPM distortions. However, when $|\Psi_{res}|$ is large, the XPM variance scales almost linearly with the number of spans since the correlation between XPM distortions occurring in different spans becomes close to zero. Typically, the XPM variance scales as N_s^r where N_s is the number of fiber spans, and $r \in [1, 2]$ for different values of residual dispersion, similar to the intra-channel four wave mixing (IFWM) variance [71].

2.2 Analytical XPM model for Gaussian pulses

The evolution of the optical field envelope in a fiber-optic link is described by the nonlinear Schrödinger equation (NLSE). Ignoring the higher-order dispersion and

higher-order/delayed nonlinear effects, the NLSE can be written as

$$i\frac{\partial q}{\partial z} - \frac{\beta_2(z)}{2}\frac{\partial^2 q}{\partial t^2} + \gamma_0|q|^2 q = -i\frac{\alpha(z)}{2}q, \tag{2.1}$$

where q is the optical field envelope; $\beta_2(z)$, γ_0 and $\alpha(z)$ are the dispersion, nonlinear and loss/gain profiles, respectively. Using the transformation

$$q(z,t) = \exp[-w(z)/2]u(z,t), \tag{2.2}$$

where $w(z) = \int_0^z \alpha(s)ds$, we obtain

$$i\frac{\partial u}{\partial z} - \frac{\beta_2(z)}{2}\frac{\partial^2 u}{\partial t^2} + \gamma(z)|u|^2 u = 0, \tag{2.3}$$

where $\gamma(z) = \gamma_0 \exp[-w(z)]$. Let us first consider the nonlinear interaction between two channels of a WDM system. The total field envelope can be written as

$$u = u_1 + u_2, \tag{2.4}$$

where u_k is the field envelope of the kth channel, $k = 1, 2$. Substituting Eq. (2.4) into Eq. (2.3) and ignoring the four wave mixing (FWM) terms, we get

$$i\frac{\partial u_k}{\partial z} - \frac{\beta_2(z)}{2}\frac{\partial^2 u_k}{\partial t^2} = -\gamma(z)\left[|u_k|^2 + 2|u_l|^2\right]u_k, \quad k = 1, 2 \quad \text{and} \quad l = 3 - k. \tag{2.5}$$

Without loss of generality, we consider the interaction between a pulse of channel 1 (probe) in symbol slot 0 and multiple pulses in channel 2 (pump) modulated with random data. We assume that the leading order solution of Eq. (2.5) is linear and

treat the nonlinear terms on the right-hand side as perturbations. The input fields to the optical fiber can be written as

$$u_1(0,t) = \sqrt{P}a_0 g(0,t), \tag{2.6}$$

$$u_2(0,t) = \sqrt{P}\sum_{n=-N}^{N} b_n g(0,t-nT_s)\exp(-i\Omega t), \tag{2.7}$$

$$g(0,t) = \exp\left(-\frac{t^2}{2T_0^2}\right), \tag{2.8}$$

where P is the power, $(2N+1)$ is the total number of symbols, T_s is the symbol interval, Ω is the channel separation in radians, T_0 is the half-width at 1/e-intensity point of the Gaussian pulse. For QAM format, the data a_0 and b_n are given by

$$a_0 \quad \text{or} \quad b_n = \frac{x_n + iy_n}{\sqrt{2}}, \tag{2.9}$$

where $x_n = 1, 3, 5, \cdots, (X-1)$; $y_n = 1, 3, 5, \cdots, (Y-1)$. X and Y are the number of amplitude levels of the in-phase and quadrature components, respectively. When $X = 2$ and $Y = 2$, we obtain QPSK format. Using the perturbation technique, we take γ_0 as a small parameter and expand the field in channel k into a series

$$u_k = u_k^{(0)} + \gamma_0 u_k^{(1)} + \gamma_0^2 u_k^{(2)} + ..., \quad k = 1, 2, \tag{2.10}$$

where $u_k^{(m)}$ denotes the mth-order solution. The linear solution satisfies Eq. (2.5) with $\gamma_0 = 0$,

$$i\frac{\partial u_k^{(0)}}{\partial z} - \frac{\beta_2(z)}{2}\frac{\partial^2 u_k^{(0)}}{\partial t^2} = 0. \tag{2.11}$$

Solving Eq. (2.11), we find the linear solution as [69]

$$u_1^{(0)}(z,t) = \frac{\sqrt{P}T_0}{T_1} a_0 \exp\left(-\frac{t^2}{2T_1^2}\right), \tag{2.12}$$

$$u_2^{(0)}(z,t) = \frac{\sqrt{P}T_0}{T_1} \sum_n b_n \exp\left[-\frac{(t-\tau_n)^2}{2T_1^2} - i\Omega t + i\theta(z)\right], \tag{2.13}$$

where

$$T_1 = \sqrt{T_0^2 - iS(z)}, \tag{2.14}$$

$$\tau_n = nT_s + S(z)\Omega, \tag{2.15}$$

$$\theta(z) = S(z)\Omega^2/2, \tag{2.16}$$

$$S(z) = \int_0^z \beta_2(s)ds. \tag{2.17}$$

To find the first-order solution, we substitute Eq. (2.10) into Eq. (2.5) and collect all the terms that are proportional to γ_0. We find the governing equation for the first-order solution as

$$i\frac{\partial u_k^{(1)}}{\partial z} - \frac{\beta_2(z)}{2}\frac{\partial^2 u_k^{(1)}}{\partial t^2} = -e^{-w(z)}\left[|u_k^{(0)}|^2 + 2|u_l^{(0)}|^2\right]u_k^{(0)}, \quad k = 1,2 \quad \text{and} \quad l = 3-k. \tag{2.18}$$

Before solving Eq. (2.18), consider the following differential equation

$$i\frac{\partial f}{\partial z} - \frac{\beta_2(z)}{2}\frac{\partial^2 f}{\partial t^2} = F(z,t), \tag{2.19}$$

where the forcing function $F(z,t)$ is in the form

$$F(z,t) = \eta(z)\exp\left\{-\sum_{k=1}^{3}[t - C_k(z)]^2 R_k(z)\right\}, \tag{2.20}$$

The solution of Eq. (2.19) is given by [45, 69]

$$f(z,t) = -i\int_0^z \frac{\eta(s)}{\sqrt{\delta(z,s)R(s)}}\exp\left[-\sum_{k=1}^{3} C_k^2 R_k + \frac{C^2}{R}\right]\exp\left[\frac{(D+it)^2}{\delta(z,s)}\right]ds, \tag{2.21}$$

where

$$R = R_1 + R_2 + R_3, \tag{2.22}$$

$$C = C_1R_1 + C_2R_2 + C_3R_3, \tag{2.23}$$

$$D = iC/R, \tag{2.24}$$

$$\delta(z,s) = \left[1 - iRA(z,s)\right]/R, \tag{2.25}$$

$$A(z,s) = 2[S(z) - S(s)]. \tag{2.26}$$

For the first order correction for u_1 due to the XPM term $2|u_2^{(0)}|^2u_1^{(0)}$ in Eq. (2.18), the corresponding forcing function $F(z,t)$ is

$$\begin{aligned} F(z,t) &= -2e^{-w(z)}|u_2^{(0)}|^2u_1^{(0)} \\ &= 2P^{3/2}a_0\eta(z)\sum_m\sum_n b_m b_n^* \exp\left\{-\sum_{k=1}^{3}[t - C_k(z)]^2 R_k(z)\right\}, \end{aligned} \tag{2.27}$$

where

$$\eta(z) = \frac{-T_0^3\exp[-w(z)]}{T_1(z)|T_1(z)|^2}, \tag{2.28}$$

$$C_1(z) = \tau_m(z), \quad C_2(z) = \tau_n(z), \quad C_3(z) = 0, \tag{2.29}$$

$$R_1 = R_3 = \frac{1}{2T_1^2}, \quad R_2 = \frac{1}{2(T_1^*)^2}, \tag{2.30}$$

Using Eq. (2.21), the first order correction for u_1 due to XPM is obtained as

$$u_1^{(1),XPM}(L_{tot}, t) = i2P^{3/2}a_0 \sum_m \sum_n b_m b_n^* X_{mn}(L_{tot}, t), \tag{2.31}$$

where

$$X_{mn}(L_{tot}, t) = \int_{-\infty}^{\infty} U_{mn}(L_{tot}, t')h_{RX}(t - t')dt', \tag{2.32}$$

$$U_{mn}(L_{tot}, t) = \int_0^{L_{tot}} \frac{-\eta'(s)}{\sqrt{\delta(L_{tot}, s)R(s)}} \exp\left[\frac{(D + it)^2}{\delta(L_{tot}, s)}\right] ds, \tag{2.33}$$

$$\eta'(s) = \eta(s)\exp\left(-\sum_{k=1}^{3} C_k^2 R_k + \frac{C^2}{R}\right), \tag{2.34}$$

Here, L_{tot} is the total transmission distance and $h_{RX}(t)$ is the impulse response of the receiver filter. The integrations in Eqs. (2.32) and (2.33) are evaluated numerically using Simpsons 1/3 rule with step sizes $dt = T_s/8$ and $ds = 0.1$ km.

From Eq. (2.10), we see that the first order XPM distortion is

$$\delta u_1 = \gamma_0 u_1^{(1),XPM}. \tag{2.35}$$

The XPM variance can be calculated by

$$Var\{\delta u_1\} = E\{|\delta u_1|^2\} - |E\{\delta u_1\}|^2. \tag{2.36}$$

For QAM signals, we define

$$K_1 = E\{|b_n|^2\}, \quad K_2 = E\{|b_n|^4\}. \tag{2.37}$$

For QPSK, $K_1 = K_2 = 1$, while for 16-QAM, $K_1 = 5$, $K_2 = 33$. Using Eqs. (2.31), (2.35) and (2.36) and applying statistical analysis to the data a_0 and b_n, the XPM variance is found as [69]

$$\sigma_{XPM}^2 = 4\gamma_0^2 P^3 |a_0|^2 \left[(K_2 - K_1^2) \sum_m |X_{mm}|^2 + K_1^2 \sum_{\substack{m \\ m \neq n}} \sum_n |X_{mn}|^2 \right]. \tag{2.38}$$

2.3 Analytical XPM model for non-Gaussian pulses

A non-Gaussian pulse $h(t)$ is approximated by a summation of time-shifted Gaussian pulses as [70]

$$h'(t) = \sum_{k=1}^{K} \xi_k \exp\left[-\frac{(t - \mu_k T_s)^2}{2(\theta_k T_s)^2} \right], \tag{2.39}$$

where ξ_k, μ_k and θ_k are fitting parameters; K is the number of time-shifted Gaussian functions. We use the least squares method (LSM) to optimize the fitting parameters. The detailed derivation of the LSM is given in the Appendix A. As an example, Fig. 2.1 shows the Gaussian fitting of the two most commonly used pulse shapes in optical communications: a Nyquist pulse $x_1(t)$ and a raised cosine pulse $x_2(t)$, which are respectively defined as:

$$x_1(t) = \text{sinc}\left(\frac{t}{T_s}\right) \frac{\cos(a\pi t/T_s)}{1 - (2at/T_s)^2}, \tag{2.40}$$

$$x_2(t) = \begin{cases} 1, & |t| < \frac{1-a}{2T_s} \\ \frac{1}{2}\left[1 - \sin\left(\frac{\pi T_s}{a}(|t| - \frac{1}{2T_s})\right)\right], & \frac{1-a}{2T_s} \leq |t| \leq \frac{1+a}{2T_s} \\ 0, & |t| > \frac{1+a}{2T_s} \end{cases} \tag{2.41}$$

where a is the roll-off factor, $0 < a < 1$. The fitting parameters optimized by LSM are given in Tables. 2.1 and 2.2. This example shows that only a few ($K = 6$) time-shifted Gaussian pulses are enough to achieve good fitting of the Nyquist pulse and the raised cosine pulse. We found that the required number of Gaussian pulses increases when the roll-off factor decreases. For example, the required numbers are 10 and 16 when the roll-off factor is 0.2 and 0.1, respectively. When the roll-off factor is greater than 0.6, six Gaussian pulses are sufficient.

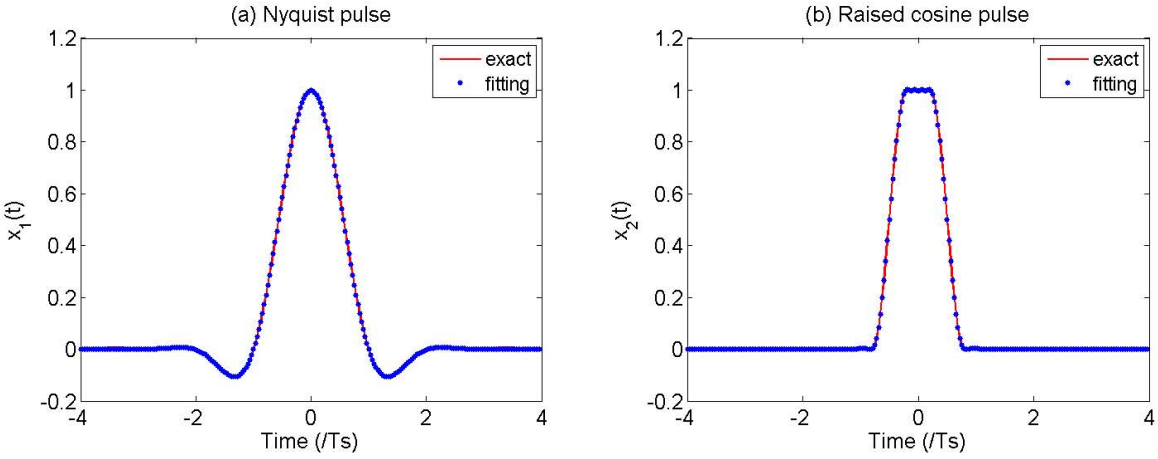

Figure 2.1: Fitting a Nyquist pulse $x_1(t)$ and a raised cosine pulse $x_2(t)$ using a summation of time-shifted Gaussian functions. (roll-off factor = 0.6, number of Gaussian functions = 6)

Using Eq. (2.39), the XPM variance for systems with non-Gaussian pulses can be derived following the similar procedure as the Gaussian pulse case. The XPM

Table 2.1: Fitting parameters optimized by LSM (Nyquist pulse, $x_1(t)$)

k	1	2	3	4	5	6
ξ_k	0.5342	0.5342	-0.2588	-0.2588	0.0289	0.0289
μ_k	0.0042	-0.0042	0.9884	-0.9884	1.8314	-1.8314
θ_k	0.5909	0.5909	0.4932	0.4932	0.3781	0.3781

Table 2.2: Fitting parameters optimized by LSM (Raised cosine pulse, $x_2(t)$)

k	1	2	3	4	5	6
ξ_k	0.0350	0.0350	-0.0632	-0.0632	0.9106	0.9106
μ_k	0.0482	-0.0482	0.7283	-0.7283	0.2542	-0.2542
θ_k	0.0470	0.0470	0.0931	0.0931	0.2239	0.2239

distortion for the case of non-Gaussian pulse is given by (see the Appendix B)

$$u_1^{(1),XPM,NG}(L_{tot},t) = i2P^{3/2}a_0 \sum_m \sum_n b_m b_n^* Y_{mn}(L_{tot},t), \tag{2.42}$$

where

$$Y_{mn}(L_{tot},t) = \int_{-\infty}^{\infty} V_{mn}(L_{tot},t')h_{RX}(t-t')dt', \tag{2.43}$$

$$V_{mn}(L_{tot},t) = \int_0^{L_{tot}} \sum_{k_1=1}^{K}\sum_{k_2=1}^{K}\sum_{k_3=1}^{K} \frac{-\eta'(s)}{\sqrt{\delta(L_{tot},s)R(s)}} \exp\left[\frac{(D+it)^2}{\delta(L_{tot},s)}\right] ds, \tag{2.44}$$

where the parameters are the same as those defined for the Gaussian pulse case, except for the following ones:

$$T_{1,k} = \sqrt{(\theta_k T_s)^2 - iS(z)}, \tag{2.45}$$

$$\eta(z) = -e^{-w(z)}\xi_{k_1}\xi_{k_2}\xi_{k_3}\frac{\theta_{k_1}\theta_{k_2}\theta_{k_3}T_s^2}{T_{1,k_1}T_{1,k_2}^* T_{1,k_3}}, \tag{2.46}$$

$$C_1(z) = \tau_{m,k_1}, \quad C_2(z) = \tau_{n,k_2}, \quad C_3(z) = \mu_{k_3}T_s, \tag{2.47}$$

$$R_1(z) = \frac{1}{2T_{1,k_1}^2}, \quad R_2(z) = \frac{1}{2(T_{1,k_2}^*)^2}, \quad R_3(z) = \frac{1}{2T_{1,k_3}^2}, \tag{2.48}$$

$$\tau_{n,k} = (n + \mu_k)T_s + S(z)\Omega. \tag{2.49}$$

The XPM variance for systems with non-Gaussian pulses is

$$\sigma_{XPM}^2(t) = |a_0|^2 G(t), \tag{2.50}$$

where

$$G(t) = 4\gamma_0^2 P^3 \left[(K_2 - K_1^2) \sum_m |Y_{mm}|^2 + K_1^2 \sum_m \sum_{\substack{n \\ m \neq n}} |Y_{mn}|^2 \right]. \tag{2.51}$$

So far we assumed that there is only one symbol (at the symbol slot 0) in the probe channel and Eq. (2.50) provides the variance as a function of time t for this case. Here, we consider the modification of Eq. (2.50) for the case of a known symbol a_0 in the symbol slot 0 of the probe channel and random symbols in the neighboring slots of the probe channel. Since the Nyquist pulse $x_1(t)$ has a pulse width larger than the symbol period, the XPM variance given by Eq. (2.50) has non-zero values even when t is larger than the duration of the symbol slot 0, which means that the interaction of a pulse in symbol slot 0 of the probe channel with the symbol sequence of the pump channel introduces distortion on the pulse in the neighboring symbol slot $k, k \in [-M, M], k \neq 0$, and M is the number of neighboring symbol slots up to which the XPM distortion is significant. In the case that multiple random symbols present in the probe channel, the calculation of the overall XPM variance at the center of any given symbol slot (eg. symbol slot 0) needs to take into account both contributions from the interaction of the current symbol with the pump as well as

those from the interaction of the neighboring symbols with the pump. As the data on the neighboring symbol slots of the probe channel is random, the variance contribution of the neighboring symbols needs to be averaged over the random data $|a_n|^2$. The overall XPM variance at the center of the symbol slot 0 can be calculated as

$$\sigma^2_{XPM,overall} = |a_0|^2 G(0) + E\{|a_n|^2\} \sum_{\substack{k=-M \\ k\neq 0}}^{M} G(kT_s). \tag{2.52}$$

The first term in Eq. (2.52) represents the XPM variance of the pulse in the symbol slot 0 of the probe channel with the pump and the second term represents that of the pulses in the neighboring symbol slots of the probe channel with the pump. For QPSK, $E\{|a_n|^2\} = 1$, while for 16-QAM, $E\{|a_n|^2\} = 5$. The first term in Eq. (2.52) is proportional to $|a_0|^2$, which implies that the XPM variance could have multiple levels as an M-QAM constellation has multiple power levels. For example, the 16-QAM system has three XPM variance levels, i.e., $|a_0|^2$ can take any one of the values [1, 5, 9]. The capability of estimating multiple XPM variance levels rather than only one averaged level will permit more accurate bit error rate (BER) estimation in practical fiber-optic communication systems.

In summary, the analytical XPM model can be applied in both DU and DM systems, and can deal with arbitrary pulse shapes. Also, the model is valid for M-QAM modulation formats and can be used to estimate the multiple levels of the XPM variance.

2.4 Simulation results and discussions

To validate the analytical model, we carried out Monte-Carlo simulations of DM coherent fiber-optic systems. The numerical simulations are done by self-developed Matlab codes. We build subroutines for different components of fiber optic communication systems, including optical transmitter, fiber link, optical amplifiers, filters and coherent receivers. We also implemented Matlab codes for various digital signal processing (DSP) algorithms such as carry phase recovery (CPR). To simulate signal propagation in optical fibers, we use the standard split-step Fourier scheme (SSFS) to numerically solve the NLSE. The step size is chosen to ensure that the maximum nonlinear phase change within each step is smaller than 0.0005 radian.

The XPM variances obtained by numerical simulations are compared with the analytical results calculated using Eq. (2.52). The WDM fiber-optic system considered in this chapter is shown in Fig. 2.2. Unless otherwise specified, the system configuration is as follows: symbol rate per channel = 28 Gbaud, modulation = QPSK or 16-QAM, pulse shape = Nyquist pulse ($x_1(t)$) with a roll-off factor of 0.6, number of WDM channels = 5, channel spacing = 50 GHz, amplifier spacing = 80 km, number of fiber spans = 10, number of symbols simulated = 32768 per channel. The dispersion, loss, and nonlinear coefficients of the transmission fiber are D_{TF} = 16.5 ps/nm/km, α_{TF} = 0.2 dB/km, and γ_{TF} = 1.1 $\mathrm{W^{-1}km^{-1}}$, respectively. For the dispersion compensating fiber (DCF), D_{DCF} = -117.7 ps/nm/km, α_{DCF} = 0.5 dB/km, and γ_{DCF} = 4.4 $\mathrm{W^{-1}km^{-1}}$. Gain of the first and second stages of the amplifiers are G_1 = 16 dB and G_2 = 5.2 dB, respectively. The residual dispersion per span (defined as: $\Psi_{res} = D_{TF}L_{TF} + D_{DCF}L_{DCF}$) is 100 ps/nm. Half of the accumulated residual dispersion is compensated in the digital-domain at the transmitter, and the other half

at the receiver. We ignore the ASE noise, laser phase noise and polarization effects, since the primary focus is to validate the analytical model for XPM variance. The central channel is demultiplexed using a 50 GHz optical filter. The received signal passes through the coherent receiver front end and then through the digital signal processing (DSP) unit with four samples per symbol. The intradyne receiver selects the channel of interest (middle channel in our case). In the DSP unit, digital back propagation (DBP) is followed by a post- dispersion compensation filter and then by a noise limiting filter. The intra-channel distortion is removed by DBP at the receiver [33]. The step size of DBP is 0.1 km. DBP compensates only for dispersion and intra-channel nonlinear effects of the fiber-optic channel. To compensate for pre-dispersion, post-dispersion compensation filter is used. A second order Gaussian filter with a 3-dB bandwidth of 28 GHz is used as a noise limiting filter. Without loss of generality, we consider only the XPM variance of the central channel. The numerical variances are calculated for various power levels of QAM.

Fig. 2.3 shows the overall XPM variance as a function of average launch power per channel, P_{ave}. P_{ave} is related to P (the power defined in Eq. (2.6)) by the pulse shape and the modulation format. For the Nyquist pulse ($x_1(t)$) with a roll-off factor of 0.6, P_{ave}(dB) = P(dB) - 0.71 dB for QPSK, and P_{ave}(dB) = P(dB) + 6.27 dB for 16-QAM. The XPM variance is proportional to P^3, as shown in Eq. (2.51). For 16-QAM, the overall XPM scales linearly with $|a_0|^2$, as shown in Eq. (2.52). Fig. 2.3(c) shows the mean XPM variance for 16-QAM, by taking an average over $|a_0|^2$. The analytical results agree quite well with the numerical results for both QPSK and 16-QAM systems. In the analytical calculation, the XPM variance contributions of six neighboring symbols are included, namely $M = 3$ in Eq. (2.52). In the systems

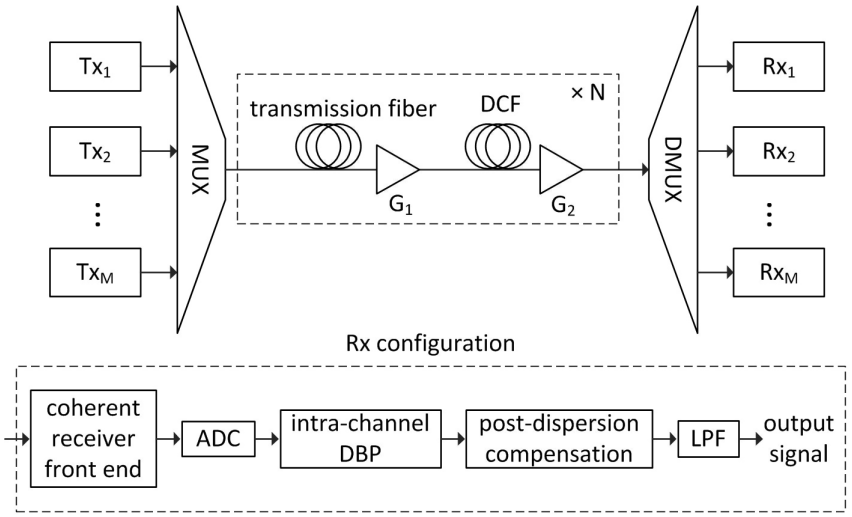

Figure 2.2: Schematic of a dispersion-managed WDM fiber-optic transmission system. Tx: transmitter, Rx: receiver, MUX: multiplexer, DMUX: demultiplexer, DCF: dispersion compensating fiber, ADC: analog-to-digital convertor, LPF: low pass filter.

considered here, symbols further than $M = 3$ have negligible impact on the overall XPM variance. The discrepancies are within 7% and 8% for QPSK and 16-QAM systems, respectively. The discrepancy is defined as

$$\text{discrepancy} = \frac{|\sigma^2_{XPM}(\text{numerical}) - \sigma^2_{XPM}(\text{analytical})|}{\sigma^2_{XPM}(\text{numerical})} \times 100\%. \tag{2.53}$$

Fig. 2.4 shows the constellation of the received signal, after compensating for the average nonlinear phase rotation. As can be seen, the XPM noise on the edge constellation points of 16-QAM is higher than those close to the center since larger power leads to larger XPM variance (see the first term of Eq. (2.52)). The phase noise component in the case of 16-QAM is significantly higher than for QPSK, in accordance with the findings of [47, 48]. From Fig. 2.3(b), we see that the XPM variance depends on the power levels of the probe pulse.

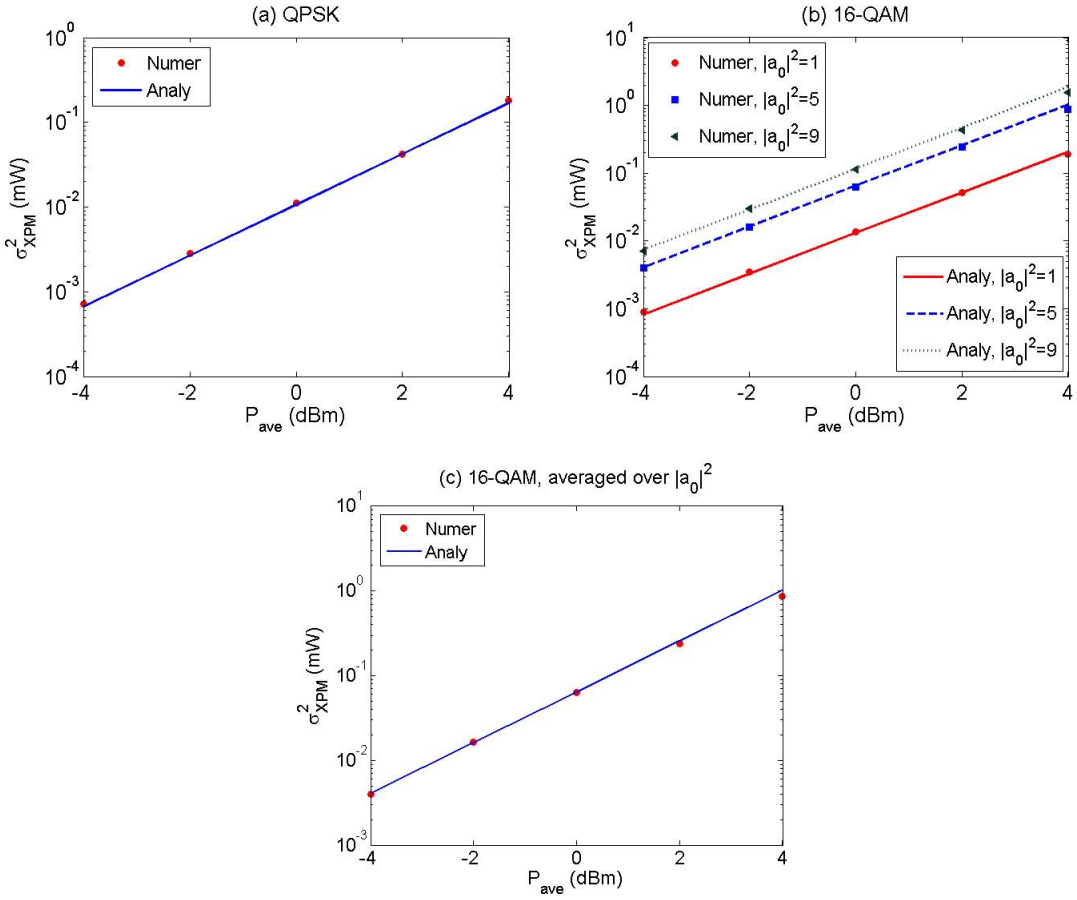

Figure 2.3: XPM variance vs. average launch power per channel (P_{ave}). (Number of WDM channels = 5, transmission distance = 800 km, residual dispersion per span = 100 ps/nm, amplifier ASE noise is ignored.)

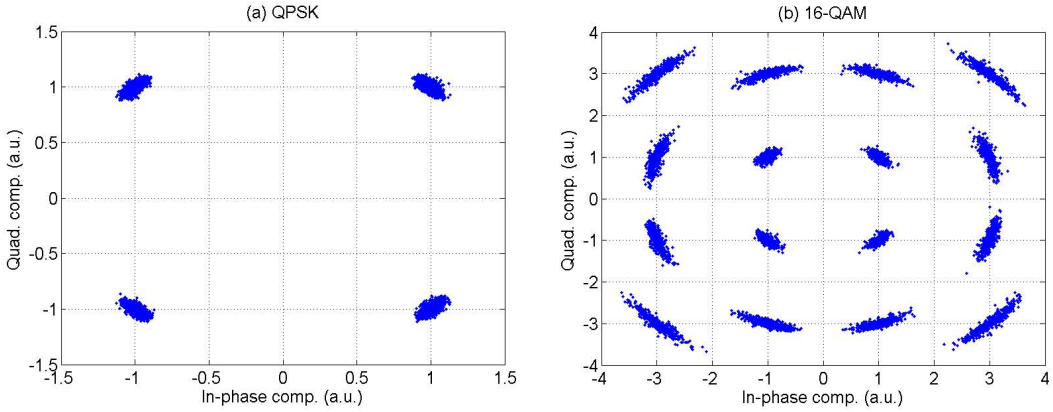

Figure 2.4: Constellation of received signal (P_{ave} = 4 dBm, number of fiber span = 1, Ψ_{res} = 0 ps/nm).

Fig. 2.5 shows the overall XPM variance as a function of residual dispersion per span. The XPM variance reaches a peak value in the case of resonant dispersion map (i.e., $\Psi_{res} = 0$ ps/nm), since the XPM fields of different fiber spans add up constructively in this case. The XPM variance decreases monotonically with $|\Psi_{res}|$. The discrepancies are within 7% and 8% for QPSK and 16-QAM systems, respectively.

Fig. 2.6 shows the overall XPM variance as a function of the number of WDM channels. As the number of channels increases beyond 5, the variance increase sub-linearly, similar to the results obtained for the direct detection systems [55]. The discrepancies are within 5% and 8% for QPSK and 16-QAM systems, respectively.

Fig. 2.7 shows the overall XPM variance as a function of the number of fiber spans N_s. For 16-QAM, the results for the case of $|a_0|^2 = 5$ are plotted. The discrepancies are within 8% and 10% for QPSK and 16-QAM systems, respectively. Using a curve fitting to the simulation results, we find that the XPM variance for the QPSK system scales as $N_s^{1.99}$, $N_s^{1.71}$ and $N_s^{1.56}$ when the residual dispersion per span is 0, 50 and 100 ps/nm, respectively. For the 16-QAM system, the XPM variance scales as $N_s^{1.96}$, $N_s^{1.82}$

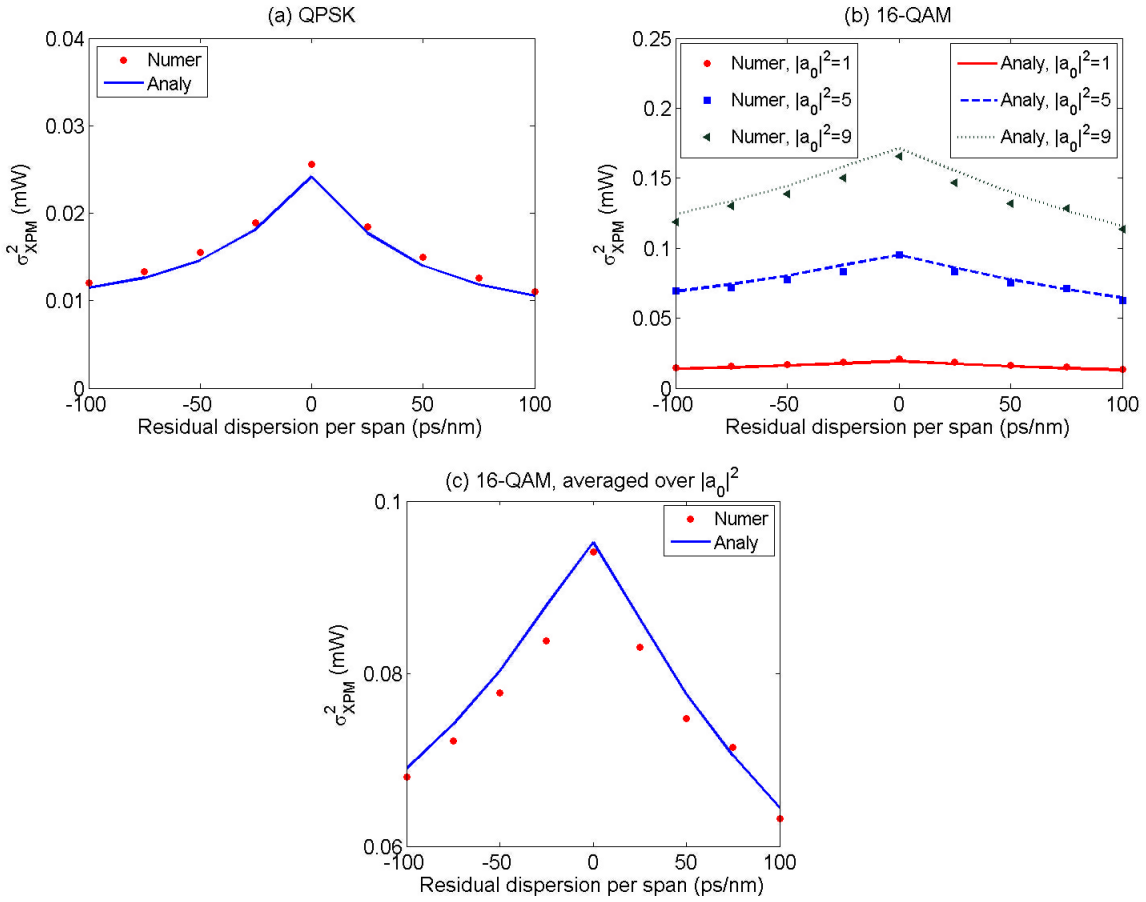

Figure 2.5: XPM variance versus residual dispersion per span. (P_{ave} = 0 dBm, number of WDM channels = 5, transmission distance = 800 km, amplifier ASE noise is ignored.)

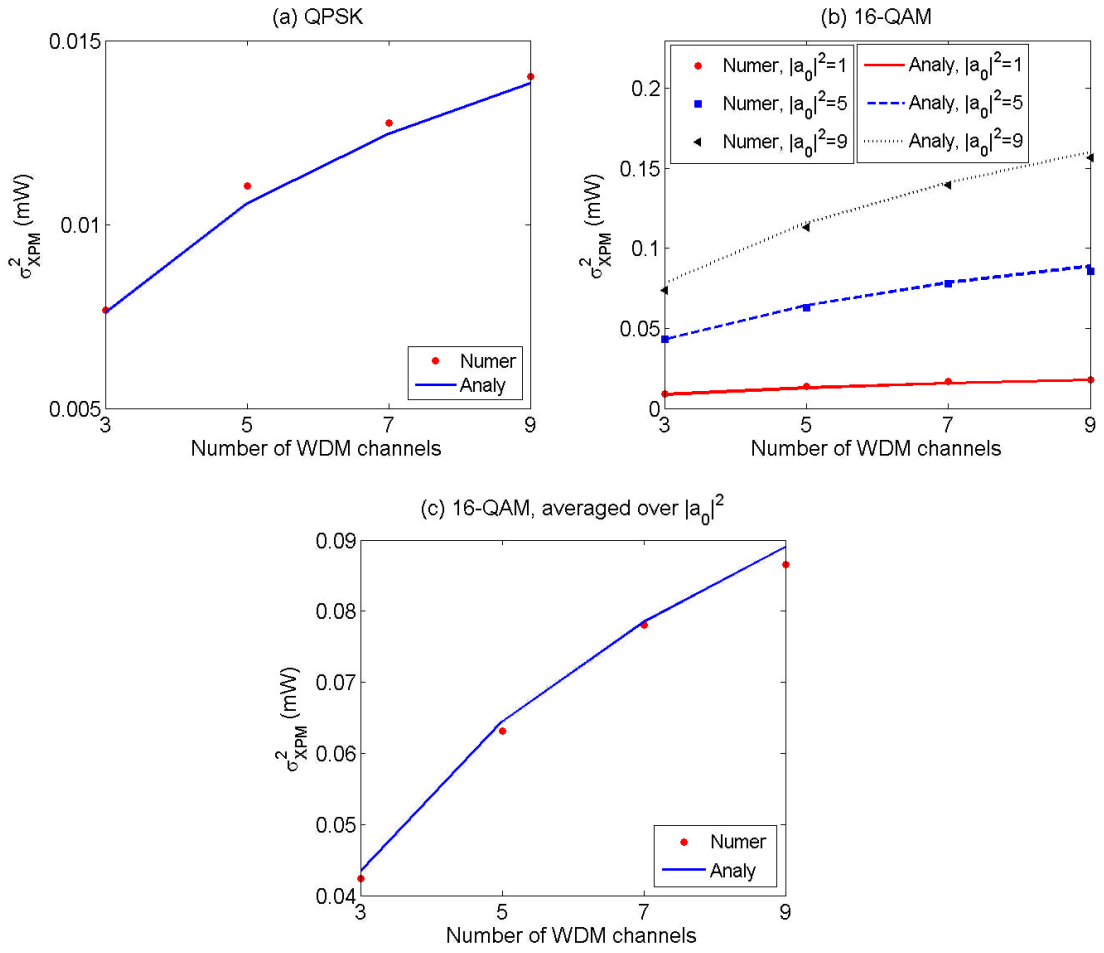

Figure 2.6: XPM variance versus number of WDM channels. (P_{ave} = 0 dBm, transmission distance = 800 km, residual dispersion per span = 100 ps/nm, amplifier ASE noise is ignored.)

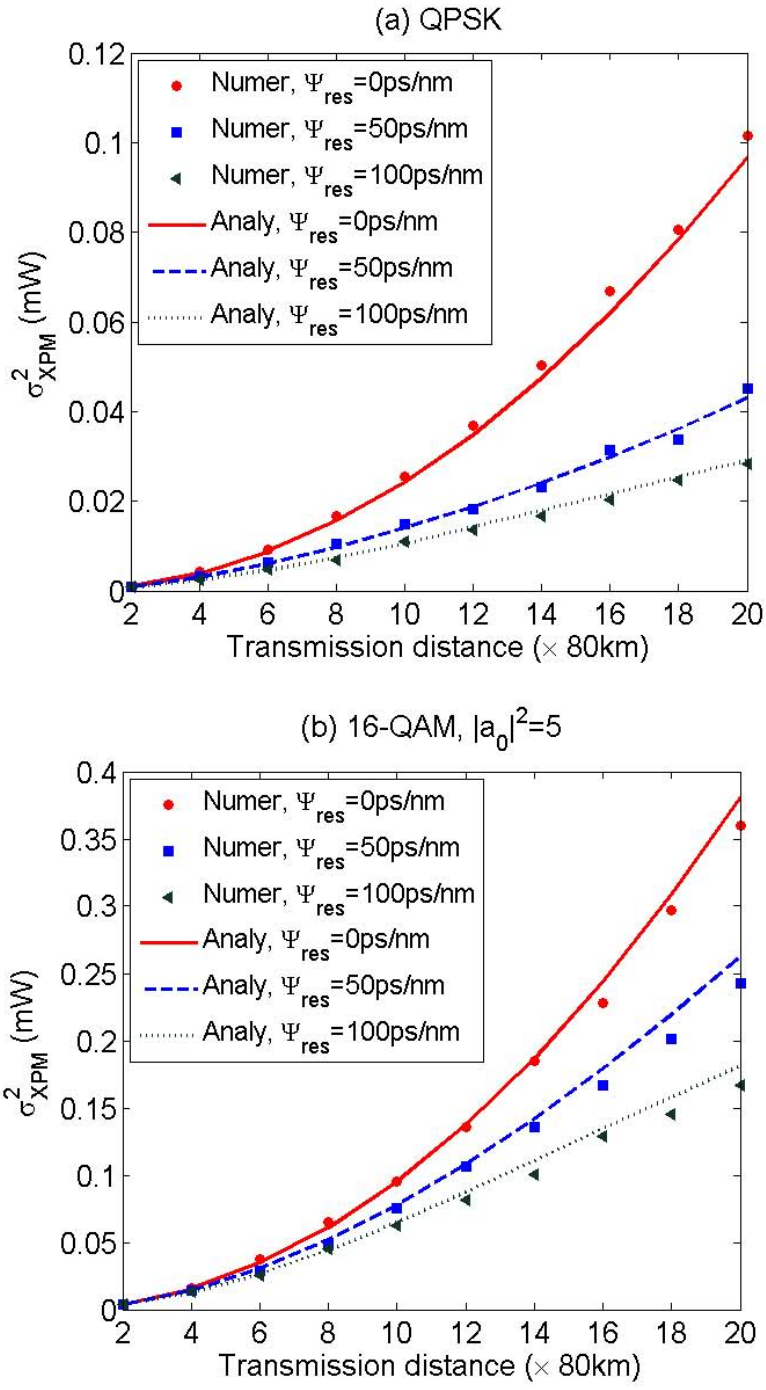

Figure 2.7: XPM variance versus transmission distance. (P_{ave} = 0 dBm, number of WDM channels = 5, residual dispersion per span = 100 ps/nm, amplifier ASE noise is ignored.)

and $N_s^{1.72}$ when the residual dispersion per span is 0, 50 and 100 ps/nm, respectively. For a resonant dispersion map (i.e., $\Psi_{res} = 0$ ps/nm), the XPM field of every fiber span is identical and will coherently add up so that the XPM noise scales linearly with distance and hence, the variance increases quadratically with distance. As the residual dispersion increases, the degree of correlation between XPM noise occurring in different spans decreases and hence the total XPM variance scales linearly with distance for large $|\Psi_{res}|$. Typically, the XPM variance scales as N_s^r where $r \in [1, 2]$ for different values of residual dispersion, similar to the IFWM variance [71].

2.5 Conclusions

We have developed an analytical model for the XPM variance in coherent fiber-optic systems. A first order perturbation technique is used to calculate the XPM distortion and then statistical analysis is carried out to calculate XPM variance for systems based on QAM. For arbitrary pulse shapes, the XPM variance cannot be calculated analytically, due to the difficulty in evaluating integrals explicitly. We have introduced a method of using the summation of time-shifted Gaussian pulses to fit arbitrary pulse shapes. Using the LSM to optimize the fitting parameters, a good approximation of the Nyquist pulse and the raised cosine pulse is achieved by using only a few time-shifted Gaussian pulses. As a result, analytical derivation of the XPM variance becomes possible for arbitrary pulse shapes. Moreover, the analytical model can be used to estimate the multiple levels of XPM variance in an M-QAM system rather than only one averaged variance level, which will permit more accurate BER estimation. The analytical XPM model has been validated by extensive numerical simulations of dispersion-managed coherent WDM fiber-optic

systems. The discrepancies between the analytical XPM variances and the numerical results are within 10% in all the simulations.

Chapter 3

Digital back propagation with optimal step size for polarization multiplexed transmission systems

3.1 Introduction

Linear and nonlinear fiber impairments due to dispersion and nonlinearity can be compensated using digital back propagation (DBP) [35, 38, 42, 74–77]. In DBP, typically split-step Fourier scheme (SSFS) is used to solve the NLSE in digital domain and it provides significant performance improvement if the step size is sufficiently small. In practice, the choice of step size is usually determined by the trade-off between performance and implementation complexity. In [74], the step size used to solve the NLSE is chosen equal to the amplifier spacing and in [35, 42], sub-amplifier spacing step size is chosen, but the step size is uniform. In this chapter, a DBP scheme with non-uniform step size based on minimum area mismatch (MAM) is investigated

[78]. For the ideal compensation of dispersion and nonlinearity, the power in the virtual fiber should increase exponentially with distance if the nonlinear coefficient is constant or equivalently the nonlinear coefficient should increase exponentially with distance if the power is fixed. This ideal exponential profile can be approximated by a stepwise increasing profile. The nonlinear coefficients of these virtual fiber sections (or steps) are obtained by minimizing the area mismatch between the ideal exponential profile and its stepwise approximation. The dispersion and nonlinear coefficients of each virtual fiber section are optimized using the Lagrange function. For the given number of virtual fiber sections, the MAM scheme outperforms the uniform spacing scheme without additional computational cost. In [38], the step size is chosen larger than the amplifier spacing so as to lower the computational complexity and power consumption. However, the method proposed in this chapter is not valid for such cases.

3.2 DBP and SSFS

Let us first consider a single-span system with constant fiber dispersion, nonlinear and loss coefficients. The evolution of the field envelope in a fiber is described by the NLSE (see Eq. 2.1 in Chapter 2),

$$\frac{\partial q}{\partial z} = (N + D)q, \tag{3.1}$$

where D denotes the fiber dispersion effect,

$$D = -i\frac{\beta_2}{2}\frac{\partial^2}{\partial t^2}, \tag{3.2}$$

and N denotes the nonlinear and loss effects,

$$N(t,z) = i\gamma|q(t,z)|^2 - \frac{\alpha}{2}. \tag{3.3}$$

The formal solution of Eq. (3.1) can be obtained as follows:

$$q(t,L) = Mq(t,0), \tag{3.4}$$

where

$$M = \exp\left\{\int_0^L [N(t,z) + D(t)]dz\right\}, \tag{3.5}$$

and L is the fiber length. Multiplying Eq. (3.4) by M^{-1} on both sides, we find

$$q(t,0) = M^{-1}q(t,L), \tag{3.6}$$

where

$$M^{-1} = \exp\left\{-\int_0^L [N(t,z) + D(t)]dz\right\} \tag{3.7}$$

In Eq. (3.6), $q(t,L)$ represents the received field envelope which is distorted due to fiber dispersion and nonlinear effects. If we multiply the received field by the inverse fiber operator, M^{-1}, distortions due to fiber dispersion and nonlinear effects can be completely undone. Eq. (3.6) with M^{-1} given by Eq. (3.7) is equivalent to solving the following partial differential equation,

$$\frac{\partial q_b}{\partial z} = -[N + D]q_b, \tag{3.8}$$

or

$$\frac{\partial q_b}{\partial(-z)} = [N + D]q_b, \tag{3.9}$$

with the initial condition $q_b(t, 0) = q(t, L)$. Since Eq. (3.9) is nothing but Eq. (3.1) with $z \to -z$, this technique is referred to as *back propagation*. Eq. (3.8) may be rewritten as

$$\frac{\partial q_b}{\partial z} = [N_b + D_b]q_b, \tag{3.10}$$

with $q_b(t, 0) \equiv q(t, L)$ and

$$D_b = -D = i\beta_2 \frac{\partial^2}{\partial t^2}, \tag{3.11}$$

$$N_b = -N = -i\gamma|q_b|^2 + \frac{\alpha}{2}. \tag{3.12}$$

The NLSE with reversed signs of dispersion, loss and nonlinear coefficients is solved in digital domain to undo the distortion caused by the transmission fiber. Figs. 3.1 and 3.2 illustrates the forward and backward propagation.

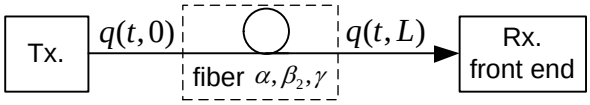

Figure 3.1: Propagation in a single-span fiber (Forward propagation). Tx: transmitter, Rx: receiver.

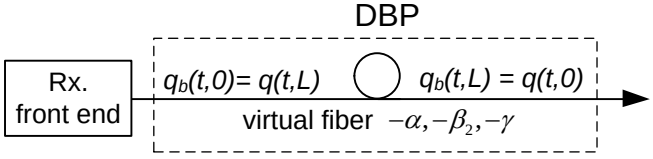

Figure 3.2: Backward propagation in the virtual fiber. Rx: receiver.

Eq. (3.10) can be solved numerically using the split-step Fourier scheme (SSFS) [3]. In Eq. (3.10), the operators N_b and D_b act simultaneously and N_b changes with

z, which makes it harder to realize the operator M^{-1} numerically. However, over a small propagation step, Δz, D_b and N_b may be approximated to act one after the other. Hence, this technique is known as split-step technique. Let us first consider the unsymmetric split-step scheme. The received field $q(t, L) = q_b(t, 0)$. We wish to find $q_b(t, \Delta z)$ which corresponds to $q(t, L - \Delta z)$. The operator M^{-1} in this propagation step can be approximated as

$$\begin{aligned} M^{-1} &= \exp\left\{\int_0^{\Delta z} [N_b(t,z) + D_b(t)]dz\right\} \\ &\cong \exp\left\{\int_0^{\Delta z} [N_b(t,z)]dz\right\} \exp\left[D_b(t)\Delta z\right]. \end{aligned} \tag{3.13}$$

And

$$q_b(t, \Delta z) = M^{-1} q_b(t, 0) \cong \exp\left[\int_0^{\Delta z} N_b(t,z)dz\right] q_b^l(t, \Delta z), \tag{3.14}$$

where

$$q_b^l(t, \Delta z) = \exp[D_b(t)\Delta z] q_b(t, 0). \tag{3.15}$$

The linear solution $q_b^l(t, \Delta z)$ is obtained using fiber linear transfer function [3]

$$q_b^l(t, \Delta z) = F^{-1}\left[\tilde{q}_b^l(\omega, \Delta z)\right], \tag{3.16}$$

where

$$\tilde{q}_b^l(\omega, \Delta z) = \tilde{q}_b^l(\omega, 0) \exp\left[-i\beta_2 \Delta z \omega^2/2\right], \tag{3.17}$$

$$\tilde{q}_b^l(\omega, 0) = F\left[q_b^l(t, 0)\right], \tag{3.18}$$

F and F^{-1} indicate Fourier transformation and inverse Fourier transformation, respectively. For the nonlinear operator, Eq. (3.14) is formally equivalent to the following equation

$$\frac{\partial q_b}{\partial z} = N_b q_b = \left(-i\gamma|q_b|^2 + \frac{\alpha}{2}\right) q_b, \tag{3.19}$$

with $q_b(t,0) = q_b^l(t,\Delta z)$. Let

$$q_b = A\exp(i\theta). \tag{3.20}$$

Substituting Eq. (3.20) into Eq. (3.19) and separating the real and imaginary parts, we find

$$\frac{dA}{dz} = \frac{\alpha}{2}A, \tag{3.21}$$

$$\frac{d\theta}{dz} = -\gamma|A|^2. \tag{3.22}$$

Solving Eqs. (3.21) and (3.22), we find

$$q_b(t,\Delta z) = q_b(t,0)\exp(-i\gamma\Delta z_{eff}|q_b(t,0)|^2 + \alpha\Delta z), \tag{3.23}$$

where

$$\Delta z_{eff} = \frac{\exp(\alpha\Delta z) - 1}{\alpha}, \tag{3.24}$$

$$q_b(t,0) = A(t,0)\exp[i\theta(t,0)]. \tag{3.25}$$

With $q_b(t,0) = q_b^l(t,\Delta z)$, Eq. (3.23) becomes

$$q_b(t,\Delta z) = q_b^l(t,\Delta z)\exp(-i\gamma\Delta z_{eff}|q_b^l(t,\Delta z)|^2 + \alpha\Delta z). \tag{3.26}$$

Fig. 3.3 illustrates the unsymmetric SSFS. This technique can be summarized as

follows:

(i) Initial field $q_b(t,0)$ is known. First, the nonlinear and loss effects (N_b) are ignored and the output of a lossless, linear fiber $q_b^l(t,\Delta z)$ is calculated using the Fourier transformation technique.

(ii) Next, fiber dispersion (D_b) is ignored. The NLSE is analytically solved with the initial condition $q_b(t,0) = q_b^l(t,\Delta z)$ and the field envelope at Δz, $q_b(t,\Delta z)$ is calculated using Eq. (3.26).

(iii) $q_b(t,2\Delta z)$ is calculated by repeating steps (i) and (ii) with $q_b(t,\Delta z)$ as the initial condition.

This process is repeated until $z = L$. The step size Δz should be chosen sufficiently small so that the absolute value of the nonlinear phase shift accumulated over a distance Δz should be much smaller than π.

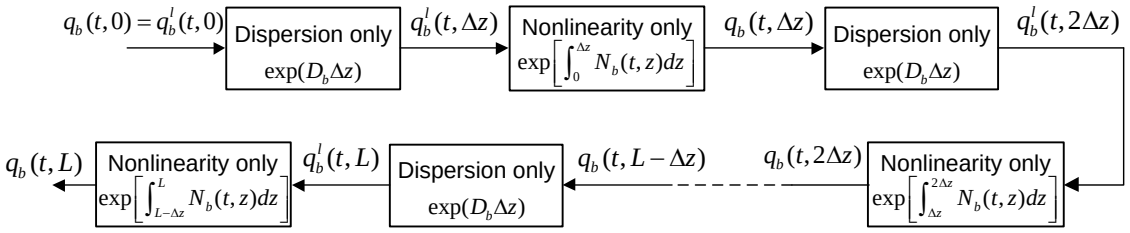

Figure 3.3: Unsymmetric split-step Fourier scheme for backward propagation.

A disadvantage of the unsymmetric SSFS is that the step size has to be really small as the error scales as Δz^2 [3]. The step size can be made significantly larger using the symmetric SSFS which is described as follows. From Eq. (3.10), we have

$$q_b(t,\Delta z) = \exp\left\{\int_0^{\Delta z} [N_b(t,z) + D_b(t)]dz\right\} q_b(t,0). \tag{3.27}$$

$q_b(t, \Delta z)$ can be approximated as

$$q_b(t, \Delta z) = \left\{ \exp\left[\frac{D_b \Delta z}{2}\right] \exp\left[\int_0^{\Delta z} N_b(t, z) dz\right] \exp\left[\frac{D_b \Delta z}{2}\right] \right\} q_b(t, 0). \qquad (3.28)$$

The above scheme is known as symmetric SSFS. Fig. 3.4 illustrates the symmetric SSFS. First, the NLSE is solved with $N_b = 0$ over a distance $\Delta z/2$. The linear field $q_b^l(t, \Delta z/2)$ is multiplied by the nonlinear phase shift and amplified. The resulting field is propagated over a distance $\Delta z/2$ with $N_b = 0$. It may appear that the

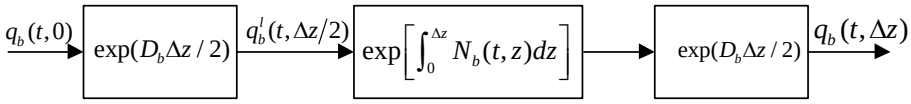

Figure 3.4: Symmetric split-step Fourier scheme for a single step Δz.

computational effort for the symmetric SSFS is twice that of unsymmetric SSFS. But the computation efforts are roughly same when the step size is much smaller than the fiber length. This can be understood from the propagation of the field from 0 to $2\Delta z$, as shown in Fig. 3.5. The linear propagation operator, $e^{D_b \Delta z/2}$ shown in the

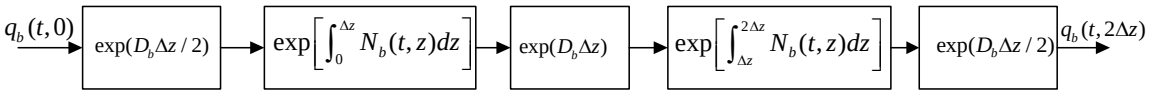

Figure 3.5: Symmetric split-step Fourier scheme for the propagation from 0 to $2\Delta z$.

last block of Fig. 3.4 can be combined with $e^{D_b \Delta z/2}$ corresponding to the first block of the propagation from Δz to $2\Delta z$, leading to a linear propagation operator $e^{D_b \Delta z}$, as indicated by the third block in Fig. 3.5. For the given step-size, the symmetric SSFS gives a more accurate results than the unsymmetric SSFS. This is because the error in the case of symmetric SSFS scales as Δz^3 whereas it scales as Δz^2 for unsymmetric

SSFS [3]. Alternatively, for the given accuracy, a larger step size could be chosen in the case of symmetric SSFS.

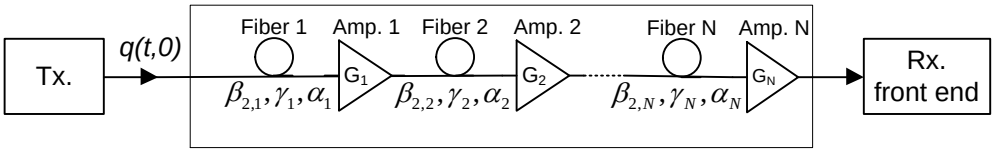

Figure 3.6: Propagation in a N-span fiber optic system. Tx: transmitter, Rx: receiver.

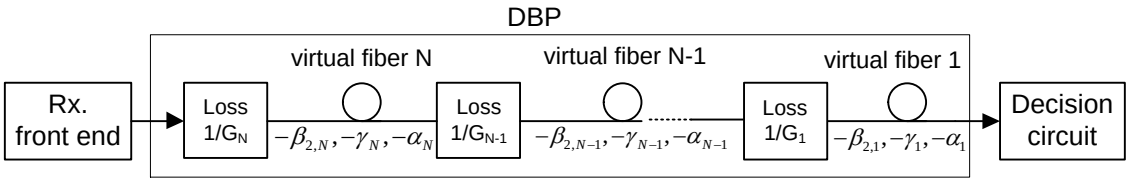

Figure 3.7: Digital back propagation for a N-span fiber-optic system. Rx: receiver.

For multi-span systems, Fig. 3.6 shows the propagation in a N-span fiber-optic system. To undo the propagation effect, amplifiers with gain G_n are substituted by loss elements $1/G_n$ in the digital domain and a real fiber with parameters (β_{2n}, γ_n, α_n), $n = 1, 2, ..., N$ are replaced by a virtual fiber having parameters ($-\beta_{2n}$, $-\gamma_n$, $-\alpha_n$), as shown in Fig. 3.7. Note that the signal distortions due to the last fiber in the fiber-optic link is compensated first in the digital domain. Although the digital back propagation can compensate for deterministic (and bit-pattern dependent) nonlinear effects, it can not undo the impact of ASE and nonlinearity-ASE coupling such as Gordon-Mollenauer phase noise [10].

3.3 DBP with optimal step sizes

In polarization division multiplexing (PDM) systems, the evolution of the electric field in the fiber can be described by the vector NLSE

$$\frac{\partial A_x}{\partial z} = -\beta_{1x}\frac{\partial A_x}{\partial t} - \frac{i\beta_2}{2}\frac{\partial^2 A_x}{\partial t^2} - \frac{\alpha}{2}A_x + i\gamma\left(|A_x|^2 + \frac{2}{3}|A_y|^2\right)A_x, \tag{3.29a}$$

$$\frac{\partial A_y}{\partial z} = -\beta_{1y}\frac{\partial A_y}{\partial t} - \frac{i\beta_2}{2}\frac{\partial^2 A_x}{\partial t^2} - \frac{\alpha}{2}A_y + i\gamma\left(|A_y|^2 + \frac{2}{3}|A_x|^2\right)A_y, \tag{3.29b}$$

where A_x and A_y are the electric field in x- and y- polarization, respectively; β_{1x}, β_{1y}, β_2, γ and α are inverse group velocities for x- and y- polarization components, dispersion, nonlinear and loss coefficients, respectively. To model polarization mode dispersion (PMD) in the fiber, we employed the method of [79, 80] in which fibers with randomly varying birefringence are approximated by multiple short fiber sections with constant birefringence in each fiber section. The power transfer between the polarization components and the random phase changes due to refractive index fluctuations are accounted for by introducing a matrix

$$F = \begin{bmatrix} \cos\theta & \sin\theta e^{i\phi} \\ -\sin\theta e^{i\phi} & \cos\theta \end{bmatrix} \tag{3.30}$$

between the fiber sections. Here, θ and ϕ are the random variables with uniform distribution in the interval $-\pi < \theta < \pi$, $-\pi/2 < \phi < \pi/2$.

Since the residual birefringence in the transmission fiber changes randomly much faster than the nonlinear interaction, by averaging the vector NLSE over the Poincare

sphere, Manakov equations are obtained as

$$\frac{\partial A_r}{\partial z} = -\frac{i\beta_2}{2}\frac{\partial^2 A_r}{\partial t^2} - \frac{\alpha}{2}A_r + \frac{i8\gamma}{9}\left(|A_x|^2 + \frac{2}{3}|A_y|^2\right)A_r, \quad r = x, y. \tag{3.31}$$

Consider a single span of a transmission fiber of length L_a. The output field of the fiber in two orthogonal polarizations may be written as [3]

$$A_r(t, L_a) = \exp\left\{i\int_0^{L_a}\left[D(t) + N(t,z)\right]dz\right\}A_r(t,0), \quad r = x, y. \tag{3.32}$$

where

$$D(t) = -\frac{\beta_2}{2}\frac{\partial^2}{\partial t^2}, \tag{3.33}$$

$$N(t,z) = \frac{8}{9}\gamma\left(|A_x(t,z)|^2 + |A_y(t,z)|^2\right) + i\frac{\alpha}{2}. \tag{3.34}$$

After coherent detection and analog to digital conversion, the distorted field passes through the virtual fiber in digital domain. The virtual fiber in DBP has loss, dispersion and nonlinear coefficients with the opposite sign of the transmission fiber, i.e.,

$$D_{DBP}(t) = \frac{\beta_2}{2}\frac{\partial^2}{\partial t^2} = -D(t), \tag{3.35}$$

$$N_{DBP}(t,z) = -\frac{8}{9}\gamma\left(|A_x(t,z)|^2 + |A_y(t,z)|^2\right) - i\frac{\alpha}{2} = -N(t,z). \tag{3.36}$$

Then, the digital signal after the DBP may be written as

$$\begin{aligned} A_{r,out}(t) &= e^{i\int_0^{La}[D_{DBP}(t)+N_{DBP}(t,z)]dz} \cdot e^{i\int_0^{La}[D(t)+N(t,z)]dz}A_r(t,0) \\ &= e^{-i\int_0^{La}[D(t)+N(t,z)]dz} \cdot e^{i\int_0^{La}[D(t)+N(t,z)]dz}A_r(t,0) \\ &= A_r(t,0). \qquad (r = x, y) \end{aligned} \tag{3.37}$$

Thus, the transmitted electric field can be fully recovered after the DBP if there is no noise. Eq. (3.37) can also be expressed in the following form

$$\frac{\partial A_{r,b}}{\partial z} = i\left[D_{DBP} + N_{DBP}\right] A_{r,b} = -i\left[D + N\right] A_{r,b}, \tag{3.38}$$

with $A_{r,b}(t,0) = A_r(t, L_a)$. Using $A_{r,b} = e^{\alpha z/2} u_{r,b}$, Eq. (3.38) can be written as

$$i\frac{\partial u_{r,b}}{\partial z} - \frac{\beta_2}{2}\frac{\partial^2 u_{r,b}}{\partial t^2} + \frac{8\gamma'(z)}{9}\left(|u_{x,b}|^2 + |u_{y,b}|^2\right) u_{r,b} = 0, \quad r = x, y, \tag{3.39}$$

where $\gamma'(z) = \gamma e^{\alpha z}$ is the effective nonlinear coefficient. In DBP, if the step size is small enough such that the effective nonlinear coefficient has an exponential profile, it provides the ideal compensation of dispersion and nonlinearity. However, this ideal case is unfeasible due to the enormous computational cost. One realistic method to implement DBP is to divide the virtual fiber into M cascaded sections, which can compensate for the signal distortion from the transmission fiber by solving Manakov equations using SSFS [3]

$$\begin{aligned} u_{r,b}(t, z_{j-1} + l_j) \approx & e^{-iD(t)l_j/2} \cdot e^{-i\frac{8}{9}\left(|u_{x,b}(t,z_{j-1})|^2 + |u_{y,b}(t,z_{j-1})|^2\right)\int_{z_{j-1}}^{z_{j-1}+l_j}\gamma'(z)dz} \\ & \times e^{-iD(t)l_j/2} u_{r,b}(t, z_{j-1}), \end{aligned} \tag{3.40}$$

where $r = x, y$, l_j is the length of the section of the virtual fiber, and $z_j = \sum_{k=1}^{j} l_k$, $z_0 = 0$ and $z_M = L_a$. In this chapter, we investigate the DBP scheme by optimizing the accumulated dispersion and nonlinear phase shift of each section, and compare its performance with that of the uniform spacing scheme.

For the uniform spacing case, the virtual fiber is divided into M sections with equal length $l_j = L_a/M$, $j = 1, 2, , M$ (see Fig. 3.8a). The accumulated dispersion of

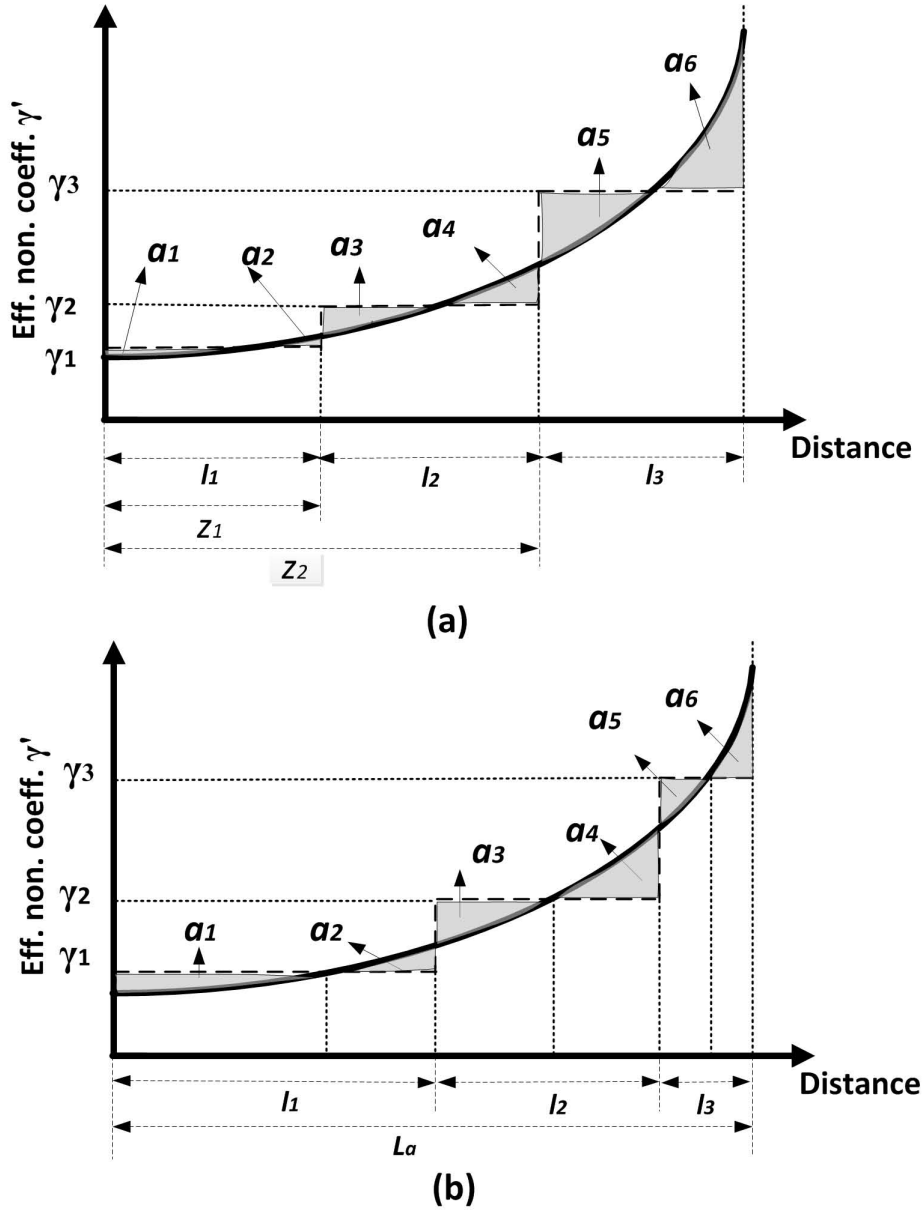

Figure 3.8: Effective nonlinear coefficient and its stepwise approximation for the number of sections $M = 3$. (a) Uniform spacing, (b) MAM.

each section is $\xi_j = \beta_2 l_j$, and the nonlinear phase shift imparted by the jth section is

$$\varphi_j = \frac{8}{9\alpha}\gamma\left(|u_{x,b}|^2 + |u_{y,b}|^2\right)e^{\alpha z_{j-1}}\left(e^{\alpha L_a/M} - 1\right). \tag{3.41}$$

It is easy to see from Fig. 3.8a that because of the limited number of steps in DBP, there is a mismatch between the area under the exponential curve (solid line) and its stepwise approximation (dashed line) and the total absolute area mismatch is $\Delta = \sum_{j=1}^{6} a_j$. If the area mismatch is minimized, the stepwise curve is expected to provide the closest approximation to the ideal exponential curve. A similar idea was investigated in the context of soliton communications to approximate the exponentially decreasing dispersion profile by stepwise decreasing profile with an additional constraint of soliton average condition [81]. The technique of MAM has been used in Ref. [21] for the scalar NLSE in the context of optical back propagation (OBP). Let $M = 3$. In this case, we have 5 unknowns, $l_1, l_2, \gamma_1, \gamma_2,$ and γ_3. The DBP can compensate the linear and nonlinear distortions if it satisfies the following conditions,

$$l_1 + l_2 + l_3 = L_a, \qquad \sum_{j=1}^{3}\gamma_j l_j = \gamma\int_0^{L_a} e^{\alpha z}dz = \gamma\left(\frac{e^{\alpha L_a - 1}}{\alpha}\right). \tag{3.42}$$

We construct a Lagrange function

$$L(l_1, l_2, \gamma_1, \gamma_2, \gamma_3, \lambda) = \sum_{j=1}^{6} a_j + \lambda\left[\sum_{j=1}^{3}\gamma_j l_j - \gamma\left(\frac{e^{\alpha L_a - 1}}{\alpha}\right)\right], \tag{3.43}$$

where λ is the Lagrange multiplier. Setting the derivative of L with respect to each of its arguments, we obtain a set of nonlinear equations and their solutions yield the

optimum values of $l_1, l_2, \gamma_1, \gamma_2,$ and γ_3. Then the dispersion in the jth section is

$$\xi_j = \beta_2 l_j, \tag{3.44}$$

and the nonlinear phase shift in the jth section is

$$\varphi_j = \frac{8}{9}\gamma_j l_j \left(|u_{x,b}(t, z_{j-1})|^2 + |u_{y,b}(t, z_{j-1})|^2\right). \tag{3.45}$$

The Lagarange multiplier method is effective when the number of unknown parameters is not too many. For the case of a large number of steps, the number of unknown parameters become large and the least squares method (LSM) together with the steepest descent method is used to optimized the lengths and nonlinear coefficients [82]. The detailed derivation of LSM has been given in Chapter 2 for the optimization of Gaussian function coefficients. Table 3.1 shows the optimum section lengths and their nonlinear coefficients for various M.

Table 3.1: Optimum values of the parameters in DBP

M	l_1	l_2	l_3	l_4	γ_1	γ_2	γ_3	γ_4
2	55.8	24.2	—	—	5.13	26.3	—	—
3	43.7	21.8	14.5	—	3.54	14.17	31.94	—
4	36.3	19.8	13.6	10.4	2.84	9.53	20.2	34.8

Parameters: α=0.2 dB/km, γ=1.1 $\mathrm{W^{-1}km^{-1}}$, and L_a=80 km. l_j has the unit of km and γ_j has the unit of $\mathrm{W^{-1}km^{-1}}$. $(j = 1, 2, 3, 4)$

So far we considered a single span system. Fig. 3.9 shows a fiber optic transmission system consisting of K spans with an amplifier in each span. At the receiver, the DBP consists of K spans of virtual fibers. It is followed by a least mean square (LMS) equalizer to compensate for PMD.

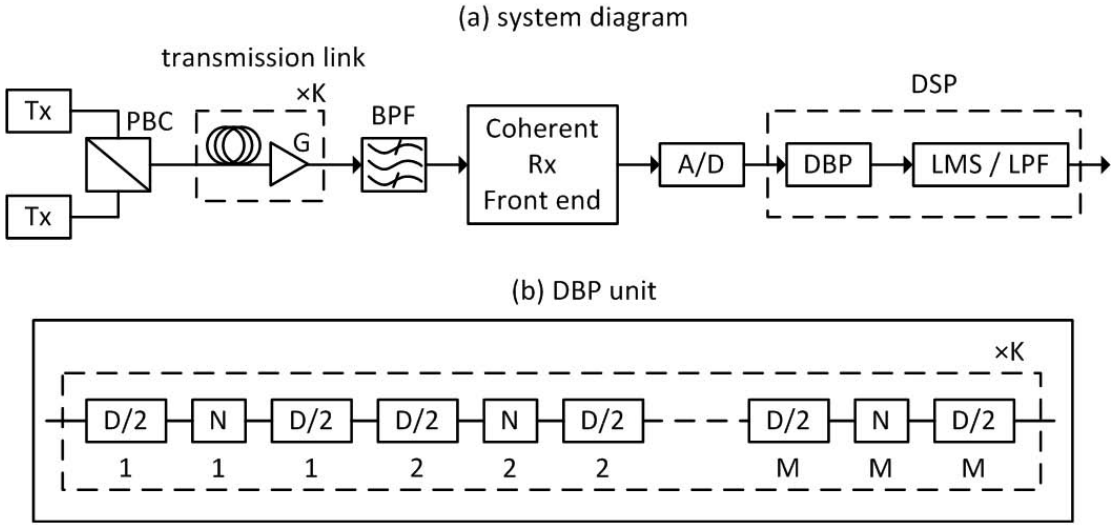

Figure 3.9: (a) Block diagram of a fiber-optic link with DBP; (b) The dispersion and nonlinear operator in DBP. PBC: polarization beam combiner, BPF: band pass filter, LMS: least mean square equalizer, LPF: low pass filter.

3.4 Simulation results and discussions

Monte-Carlo simulations of a single-channel dual-polarization fiber optic system with DBP at the receiver are carried out. 25 Gbaud per polarization and 16-quadrature amplitude modulation (16-QAM) signal is used in the simulation. Total number of symbols is 32768 symbols per polarization. Standard single mode fiber (SSMF) is used as the transmission fiber with following parameters, $\alpha = 0.046$ km^{-1}, $\beta_2 = -21$ ps^2/km, $\gamma = 1.1$ W^{-1}km^{-1}, and the PMD parameter $D_p = 0.04$ ps/$\sqrt{\text{km}}$. The amplifier spacing L_a is 80 km, the gain of the amplifier is 16 dB and the spontaneous emission noise factor n_{sp} is 1.5. Eight and two samples per symbol are used for optical forward propagation and digital processing, respectively, unless otherwise specified. A second order Gaussian filter with 50 GHz bandwidth (BPF in Fig. 3.9a) is used before the coherent receiver. The polarization diversity coherent receiver provides

four outputs I and Q components of each polarization. These outputs after DBP pass through an adaptive equalizer based on decision-directed LMS algorithm. The adaptive equalizer calculates the inverse Jones matrix adaptively and compensates for the polarization rotation, phase shift and delay between polarization components [28]. Number of taps of the LMS equalizer is 12 and the number of training symbols per polarization is 15360. The symbol sequence after the equalizer is compared with the symbol sequence at the transmitter and those symbols which have crossed the boundaries are counted as error symbols.

The forward propagation is simulated in two different ways with vector NLSE and random rotational matrix between fiber sections (case 1), and with Manakov equations (case 2). For case 2, LMS equalizer is not required since there is no PMD in the system. Instead a second order Gaussian low pass filter (LPF) with 20 GHz bandwidth is used to limit the noise.

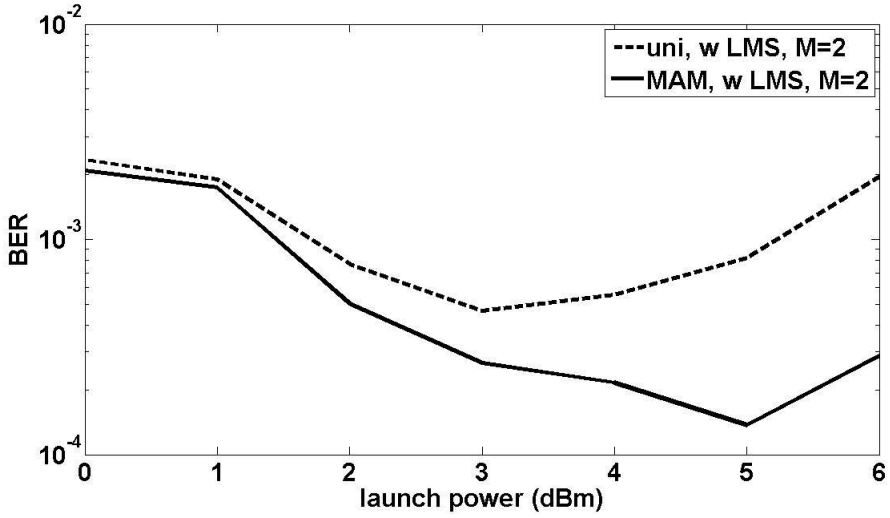

Figure 3.10: BER versus launch power when vector NLSE is used for forward propagation and LMS adaptive equalizer is introduced to remove PMD after DBP. Transmission distance = 2800 km. 2 samples/symbol is used.

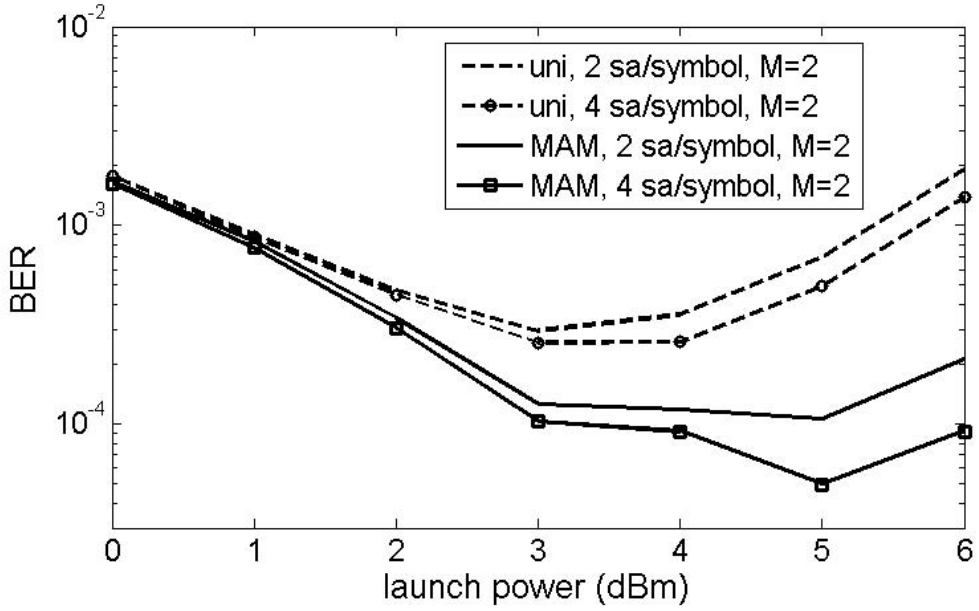

Figure 3.11: BER versus launch power when Manakov equation is used for forward propagation. Transmission distance = 2800 km. Optical signal-to-noise ratio (OSNR) is 24.2 dB when launch power is 3 dBm.

Let us first consider case 1. Fig. 3.10 shows the bit error ratio (BER) as a function of the launch power to the SSMF at 2800 km transmission distance. The number of steps per span M is 2 in DBP. The solid line and dashed line show BER versus launch power when the MAM and uniform spacing methods are used in DBP, respectively. As can be seen, the DBP with MAM method outperforms that using uniform spacing method at the same computational cost. When the launch power is less than 1 dBm, the performance of the two techniques are almost the same, but DBP with MAM is better when launch power is large and nonlinearity becomes dominant. Fig. 3.11 shows BER as a function of launch power at the same transmission distance except that the Manakov equations are solved in the forward propagation (case 2). Although the LMS equalizer can effectively mitigate linear PMD impairments, neither LMS nor DBP compensates for the PMD-nonlinearity interactions. Hence, comparing

Fig. 3.10 and Fig. 3.11, with 2 samples per symbol, we see that the performance is slightly worse at larger launch power for case 1, for both uniform spacing and MAM techniques. When 4 samples per symbol are used, the Q-factor is improved by 0.1 dB and 0.4 dB for uniform and MAM schemes, respectively (as compared with 2 samples per symbol).

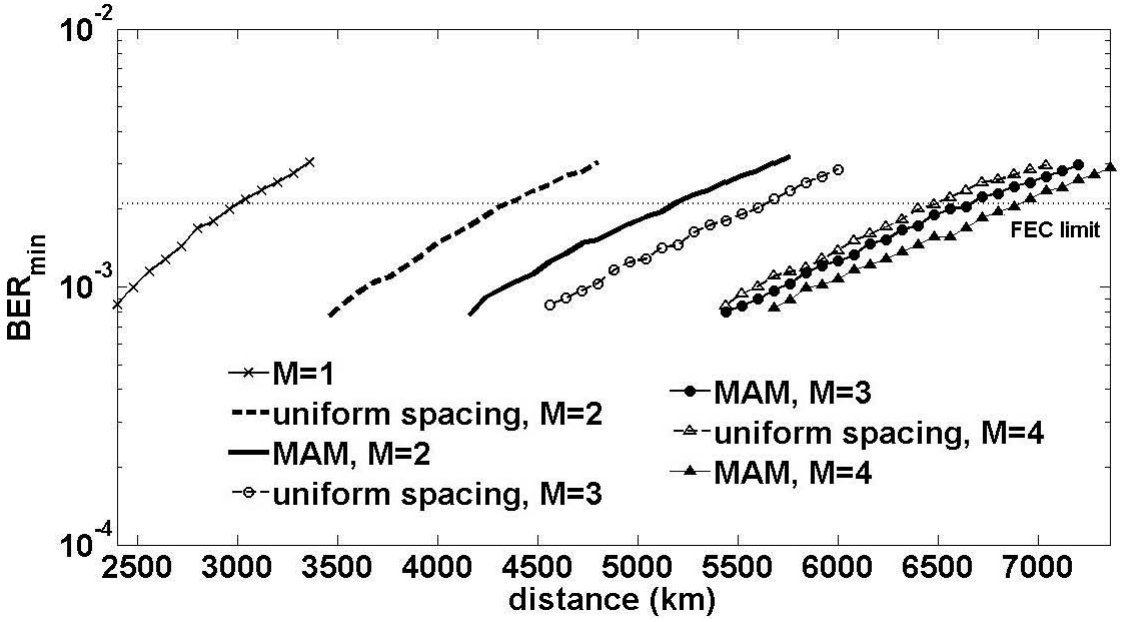

Figure 3.12: BER versus transmission distance. Manakov equation is used for forward propagation. 2 samples/symbol is used.

The minimum BER (such as the minimum point in Fig. 3.11) is plotted as a function of the transmission reach in Fig. 3.12 with different M. As M increases, the maximum reach increases. The MAM technique has a longer reach than that of the uniform spacing case. When $M = 2$, the maximum transmission distance at the forward error correction (FEC) limit of BER $= 2.1 \times 10^{-3}$ is limited to 4300 km for the uniform spacing, which can be extended to 5200 km with the MAM technique. Also, the transmission reach of the uniform spacing case is 5600 km and 6480 km

when $M = 3$ and $M = 4$, respectively, which can be increased to 6640 km and 6880 km, respectively, by using the MAM method. So, only optimizing the parameters of DBP without additional computational cost and system complexity, MAM technique can make a better compensation of the fiber dispersion and nonlinearity compared with the uniform spacing method.

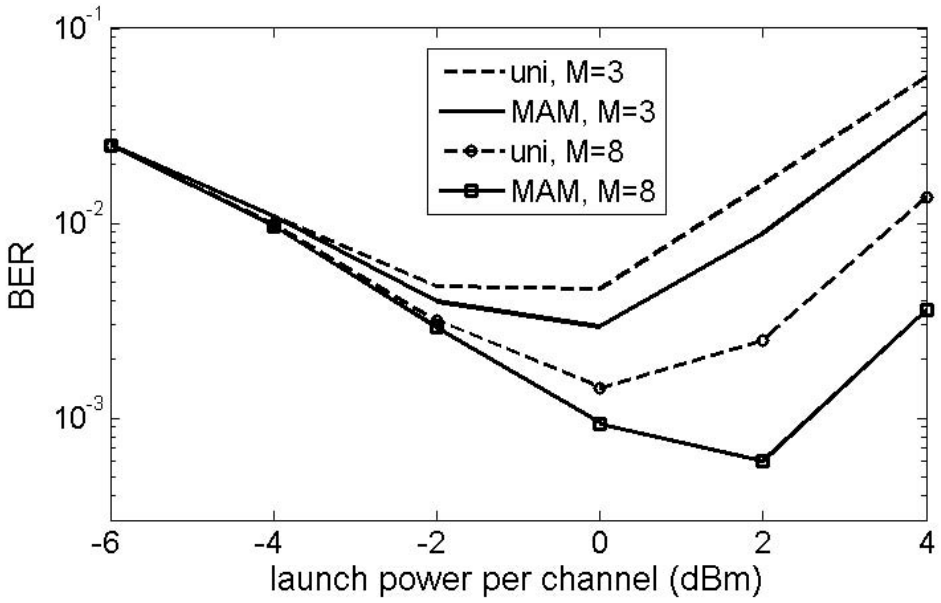

Figure 3.13: BER versus launch power per channel for a WDM system. Transmission distance = 2000 km. 2 samples/symbol is used. OSNR is 22.5 dB when launch power is 0 dBm.

Next, we consider a wavelength division multiplexing (WDM) system with the following additional parameters: number of channels = 5, channel spacing = 100 GHz, a second order Gaussian filter with a bandwidth of 50 GHz is used to demultiplex channels. Coupled vector NLSEs [42] without four-wave mixing (FWM) are solved in digital domain with 2 samples per symbol. As pointed out in [35], the step size of a WDM system has to be really small (of the order of 3 km for uniform spacing). Therefore, we considered a relatively larger M in our WDM simulation. Fig. 3.13

shows the BER versus launch power per channel. As can be seen, the performance improvement is larger with MAM, $M = 8$ as compared to the case of $M = 3$. Relatively smaller improvement for $M = 3$ with MAM is due to the fact that WDM nonlinear impairments are much stronger when the step sizes are larger and both uniform and MAM schemes do not provide substantial improvements.

For the content presented in this chapter, my contribution includes: (i) deriving equations and building a numerical tool to optimize the step sizes; (ii) implementing Matlab codes to simulate the entire fiber optic systems including single-channel and WDM systems; (ii) compiling and analyzing simulation results and plotting result figures of Fig. 3.11 and Fig. 3.13.

3.5 Conclusions

We have investigated a DBP scheme to compensate for the dispersion and nonlinearity of the transmission fibers. By optimizing the step size of each section through minimizing the area mismatch between the exponential profile of the effective nonlinear coefficient and its stepwise approximation, a better system performance can be obtained without additional computational cost and system complexity. The optical forward propagation is simulated in two different ways: (i) vector NLSE with random polarization rotation. (ii) Manakov equations. An adaptive LMS equalizer is employed after the DBP to compensate for the randomly changing birefringence when the vector NLSE is used for forward propagation. The simulation results show that the two approaches have almost the same performance, except that PMD-nonlinearity interaction results in a slight degradation for case (i). In both the approaches, DBP

with uniform spacing and MAM are simulated and results show that the MAM technique can increase the system reach significantly as compared to the uniform spacing.

Chapter 4

Digital compensation of XPM distortions using perturbation technique for dispersion-managed systems

4.1 Introduction

The performance of fiber-optic transmission systems is mainly limited by intra-channel [44, 83, 84] and inter-channel [48, 55, 57, 60] nonlinear impairments. Digital/optical back propagation [20, 21, 33, 34] based on split-step Fourier scheme (SSFS) is an effective method to compensate for intra-channel nonlinear impairments. Digital back propagation (DBP) requires computations of multiple fast Fourier transforms (FFTs) and two or more samples per symbol. Alternatively, perturbation techniques can be

implemented either at the transmitter [49] or at the receiver [50, 85] for the compensation of the intra-channel nonlinear impairments. For quasi-linear systems, the fiber-optic channel is considered to be linear to the leading order. The nonlinear interaction among signal pulses leads to distortions in the first and higher orders, which can be calculated using the perturbation theory. In transmitter side perturbation theory based compensation technique, the signal field is distorted by subtracting the first order field from the signal field at the transmitter. The fiber-optic system generates the first order field which cancels the distortion introduced at the transmitter. However, if the first order field is large, nonlinear interaction between this field and signal field causes additional distortions. In order to calculate the first order field, double summations have to be performed and the number of terms in the double summation grows quickly with accumulated dispersion. An interesting fact is that by employing symmetric electronic dispersion compensation (EDC), complex multiplications in the double summation become real multiplications which leads to significant reduction in computational complexity [51, 86].

In a wavelength division multiplexing (WDM) system, a signal pulse in the given symbol slot interacts nonlinearly not only with the neighboring symbols of the same channel, but also with the symbols of the other channels due to cross phase modulation (XPM). The distortion due to XPM can be compensated for using the DBP [35], in which coupled NLSEs are solved using SSFS. This scheme is quite effective; however, it requires huge computational resources since the step size should be about 3 km. The step size can be increased by factorizing the walk-off effect [43], however, the computational cost is still large. In [45, 47, 48, 70], inter-channel nonlinear distortion due to XPM is calculated using a perturbation theory. In this chapter, we

make use of the analytical expressions for the first order fields developed in Chapter 2 to compensate the distortion at the receiver [87]. We first compensated for the intra-channel as well as inter-channel nonlinear distortions using the perturbation theory and the results showed that this compensation scheme brought only 0.5 dB improvement in Q-factor as compared to the case of linear compensation. Next, we investigated the possibility of compensating inter-channel distortions using the low-complexity intra-channel DBP (with a step size of 40 km) and inter-channel distortions using the perturbation technique. In this case, we found that the Q-factor improvement is 2.4 dB as compared to the case of linear compensation for 2-channel WDM systems. Constellation diagram revealed the existence of small islands drifting away from the constellation points. These islands do not behave like amplified spontaneous emission (ASE) noise and they result from the wrong estimations in the hard-decision unit. Instead of choosing the closest constellation points for the received signal, we replaced the decision with the second-closest constellation point. Using the corrected hard-decision data, XPM distortion compensation is done again and now the Q-factor improvement over the linear compensation scheme is 3.2 dB. We note that this method is applicable not only for WDM systems, but also for superchannel systems with multiple carriers [88]. The digital signal processing (DSP) technique for superchannel systems is discussed in [88–90]. For simplicity, we have ignored the polarization dependence of the signals and limited our study to single-polarization WDM systems.

4.2 Perturbation technique for compensating XPM distortions

The nonlinear distortions of signals propagating in fiber-optic links can be calculated using a perturbation theory, as discusses in Chapter 2. When there is a single pulse at 0th symbol slot at the channel of interest (channel 1) and multiple pulses at the interfering channel (channel 2), the intra-channel nonlinear distortion and the XPM distortion can be respectively written as (see Eq. 2.42 in Chapter 2)

$$\Delta u_1^{intra,NG}(t) = i\gamma_0 P^{3/2} a_0 \sum_{m=-N_{sym}}^{N_{sym}} \sum_{n=-N_{sym}}^{N_{sym}} a_m a_n^* Y_{mn}(L_{tot}, t), \tag{4.1}$$

and

$$\Delta u_1^{XPM,NG}(t) = 2i\gamma_0 P^{3/2} a_0 \sum_{m=-N_{sym}}^{N_{sym}} \sum_{n=-N_{sym}}^{N_{sym}} b_m b_n^* Y_{mn}(L_{tot}, t), \tag{4.2}$$

where a_n and b_n are the random data, Y_{mn} is the perturbation coefficient matrix. When there are multiple pulses at the channel 1, the nonlinear interaction between a neighboring pulse of channel 1 (e.g. pulse at symbol slot 1) and the multiple pulses of channel 2 leads to distortion on the pulse at the symbol slot 0 of channel 1. This is because the neighboring pulses as well as XPM fields broaden due to dispersion and walk-off effects such that they could appear at symbol slot 0 at various propagation distances, leading to additional XPM distortions. Therefore, Eq. (4.2) is modified as

$$\Delta u_1^{XPM,NG}(t) = 2i\gamma_0 P^{3/2} \sum_{l=-M}^{M} a_l \sum_{m=-N_{sym}}^{N_{sym}} \sum_{n=-N_{sym}}^{N_{sym}} b_m b_n^* Y_{mn}^{(l)}(L_{tot}, t), \tag{4.3}$$

where a_l is the random data on channel 1, $Y_{mn}^{(l)}$ is the matrix which corresponds to the nonlinear interaction between the pulse at the symbol slot l of channel 1 and multiple pulses of channel 2. M is the number of neighboring symbols up to which the nonlinear distortion is significant. Similarly, for intra-channel distortions, Eq. (4.1) is modified as

$$\Delta u_1^{intra,NG}(t) = i\gamma_0 P^{3/2} \sum_{l=-M}^{M} a_l \sum_{m=-N_{sym}}^{N_{sym}} \sum_{n=-N_{sym}}^{N_{sym}} a_m a_n^* Y_{mn}^{(l)}(L_{tot}, t). \tag{4.4}$$

So far we considered the XPM distortion due to a single neighboring channel. If there are N_{nb} neighboring channels, total nonlinear distortion due to XPM is

$$\Delta u_{XPM} = \sum_{k=1}^{N_{nb}} \Delta u_{1,k}^{XPM,NG}, \tag{4.5}$$

where $\Delta u_{1,k}^{XPM,NG}$ represents the XPM distortion due to the neighboring channel k and is calculated using Eq. (4.3).

Using the perturbation technique, the distorted output signal of a fiber-optic link can be written as

$$u_{out} = u_{in} + \Delta u_{intra} + \Delta u_{XPM} + \Delta u_H, \tag{4.6}$$

where u_{out} and u_{in} are the input and output signals, respectively; Δu_{intra} and Δu_{XPM} are the first order intra-channel and XPM distortions calculated by Eqs. (4.4) and (4.5), respectively; Δu_H is the high-order component that is neglected by the first-order perturbation theory [45]. To the first-order accuracy, the fiber nonlinearity can

be compensated by

$$u_{comp} = u_{out} - u_{in} - \Delta u_{intra} - \Delta u_{XPM}. \tag{4.7}$$

Perturbation-based nonlinearity compensation can be implemented at the transmitter side and/or at the receiver side [49, 50, 85]. In the transmitter side perturbation scheme, the accurate input data (a_n, b_n) is available for the perturbation calculation of nonlinear distortions. However, due to the limitations of first-order theory, the high-order component Δu_H will co-propagate and interact with signals in the fiber-optic link which will introduce additional distortions. In the receiver side perturbation scheme, the high-order component does not propagate; but the input data is not available so that perturbation calculation has to be done based on estimated data from the distorted signals. In single channel systems, transmitter side and receiver side perturbation schemes have almost the same performance [50].

4.3 Simulation results and discussions

As the first case, we investigated a receiver side compensation scheme that mitigates both intra-channel and XPM distortions using the perturbation technique. To reduce computational complexity (i.e., the value of M and the size of the matrix Y_{mn}), we consider a dispersion-managed (DM) fiber-optic system, as shown in Fig. 4.1. Unless otherwise specified, the system configuration is as follows: symbol rate per channel = 28 Gbaud, modulation = 16-quadrature amplitude modulation (16-QAM), channel spacing = 50 GHz, Tx and local oscillator (LO) laser linewidth = 100 kHz, amplifier spacing = 80 km, number of fiber spans = 20, number of symbols simulated = 32768

per channel. The dispersion, loss, and nonlinear coefficients of the transmission fiber are D_{TF} = 16.5 ps/nm/km, α_{TF} = 0.2 dB/km, and γ_{TF} = 1.1 $W^{-1}km^{-1}$, respectively. For dispersion compensating fiber (DCF), D_{DCF} = -117.7 ps/nm/km, α_{DCF} = 0.5dB/km, and γ_{DCF} = 4.4 $W^{-1}km^{-1}$. Gain of the first and second stages of the amplifiers are G_1 = 13.0 dB and G_2 = 8.4 dB, respectively. The residual dispersion per span (= $D_{TF}L_{TF} + D_{DCF}L_{DCF}$) is 50 ps/nm. The standard split-step Fourier scheme (SSFS) is used to simulate the signal propagation in the fiber-optic link. The computational bandwidths are 0.22 THz and 0.45 THz for the cases of 2-channel and 5-channel WDM systems, respectively; and the maximum nonlinear phase shift per step is 0.0005 radians. A Nyquist pulse with a roll-off factor $\alpha = 0.6$ is used, defined as

$$x(t) = \text{sinc}\left(\frac{t}{T_s}\right)\frac{\cos(a\pi t/T_s)}{1-(2at/T_s)^2}. \tag{4.8}$$

Six time-shifted Gaussian pulses are used to fit the Nyquist pulse, with the parameters optimized by the least squares method (LSM) given in Table. 2.1 [70]. As the roll-off factor decreases, the number of pulses required increases. However, this does not increase the computational complexity of the compensation scheme, as the calculation of Y_{mn} matrixes are done off-line and stored as look-up tables.

At the output of the fiber-optic link, a demultiplxer (DMUX) separates signals into different channels. Second order Gaussian band pass filters (BPFs) centered at each channel with 3-dB bandwidth of 42 GHz are used as demultiplexing filters. The output signals from the coherent receivers are then converted into the digital domain using analog-to-digital convertors (ADCs). In the receiver digital signal processing (DSP) block, two samples per symbol are used for the compensation of residual dispersion. The output of dispersion compensator (DC) is down-sampled to one

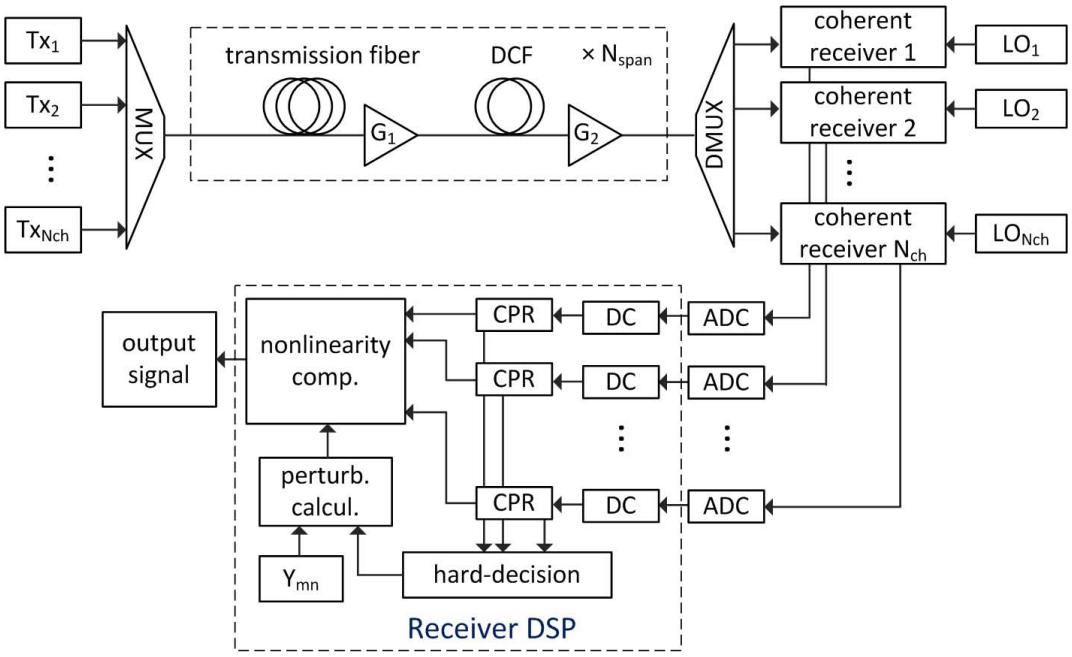

Figure 4.1: Schematic of a dispersion-managed fiber-optic WDM system using perturbation-based nonlinearity compensation. Tx: transmitter, MUX: multiplexer, DCF: dispersion compensating fiber, G_1, G_2: amplifier gains, DMUX: demultiplexer, LO: local oscillator, ADC: analog-to-digital convertor, DC: dispersion compensator, CPR: carrier phase recovery, Y_{mn}: coefficient matrix stored in a lookup table, DSP: digital signal processing.

sample per symbol. After that, carrier phase recovery (CPR) is implemented using the feed-forward method [91]. The output signal of CPR is used for hard decision which uses a threshold device to make decisions based on the proximity of the signal to the complex amplitude levels of 16-QAM. The rectangular regions about the constellation points are used for hard decision. Perturbation calculations for both intra-channel and XPM distortions are carried out using the hard-decision data, which approximate the input data sequences a_n and b_n required for perturbation calculation in Eqs. (4.3) and (4.4). The coefficient matrix Y_{mn} are stored in a lookup table. When the channel separations between the probe and the pump channel are 50 GHz, 100 GHz, 150 GHz, and 200 GHz, the numbers of neighboring symbols included (i.e., M in Eq. (4.3)) are 2, 1, 1, and 0, respectively. Then intra-channel and XPM distortions are compensated using Eq. (4.7) and the output of CPR is used as u_{out}.

For simplicity, we first consider a 2-channel WDM system. Figures 4.2(a) and 4.2(b) show the constellations of recovered signals by dispersion compensation only and by nonlinear compensation of both intra-channel and XPM distortions using the perturbation technique, respectively. We note that in simulations the signal constellation becomes enlarged after nonlinearity compensation. Before calculating bit error rate ratio (BER), the power of the compensated signal is normalized to that of the input signal. The BER is calculated by error counting. Figure 4.3 shows the Q-factor as a function of average launch power per channel P_{ave}. The Q-factor is converted from the BER using $Q = \sqrt{2}\text{erfc}^{-1}(2 \times \text{BER})$ and $Q(\text{dB}) = 20\log_{10}Q$. Perturbation-based nonlinearity compensation brings 0.5 dB Q-factor improvement. The relatively smaller improvement is mostly due to the inaccurate data after the hard decision.

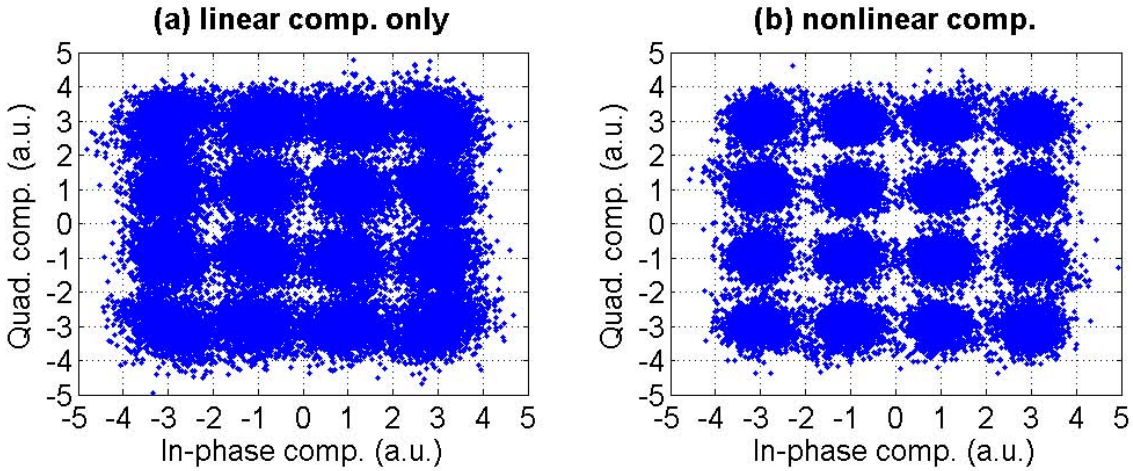

Figure 4.2: Constellations of recovered signals in a 2-channel WDM system: (a) linear compensation only, (b) nonlinear compensation of both intra-channel and XPM distortions using the perturbation technique. (average power per channel P_{ave} = -6 dBm)

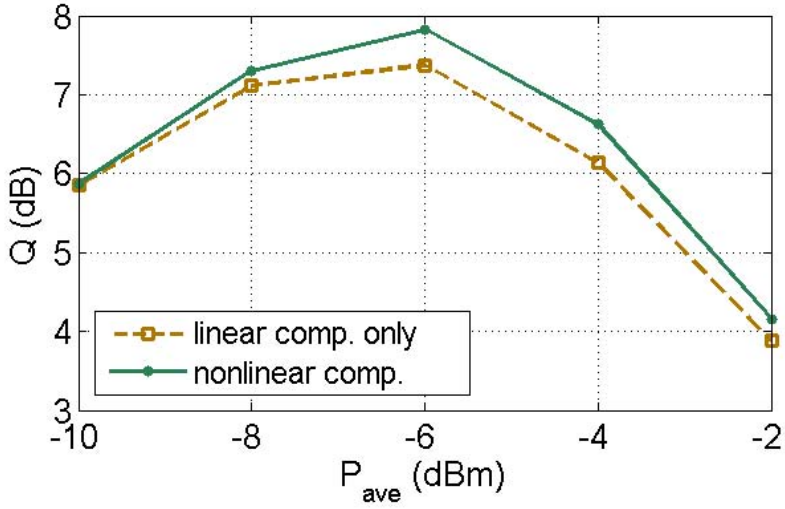

Figure 4.3: Q-factor versus average launch power per channel in a 2-channel WDM system. (Optical signal-to-noise ratio (OSNR) is 20.8 dB when P_{ave} is -6 dBm. Transmission distance is 1600 km.)

As an alternative scheme, we choose to compensate for intra-channel nonlinearities using intra-channel DBP based on SSFS [33], since the intra-channel DBP has high accuracy and moderate computational cost. However, for XPM compensation, the computational cost of inter-channel DBP is very large. The required step size is as small as a few kilometers [35]. Perturbation-based XPM compensation requires much less computational cost, since it only requires one-stage compensation and symbol-rate signal processing. Therefore, we investigated a hybrid nonlinearity compensation scheme, which compensates for dispersion and intra-channel nonlinearities using intra-channel DBP and compensates for XPM distortions using the perturbation technique. The scheme diagram is shown in Fig. 4.4. The ADC outputs with two samples per symbol are launched into the intra-channel DBP units to compensate for intra-channel nonlinear distortions. After that, second order Gaussian low pass filters (LPFs) with 3-dB bandwidth of 19 GHz are used as noise limiting filters. Then, CPR and hard decision are implemented using one sample per symbol. XPM perturbation calculation and compensation are carried out based on the hard-decision data.

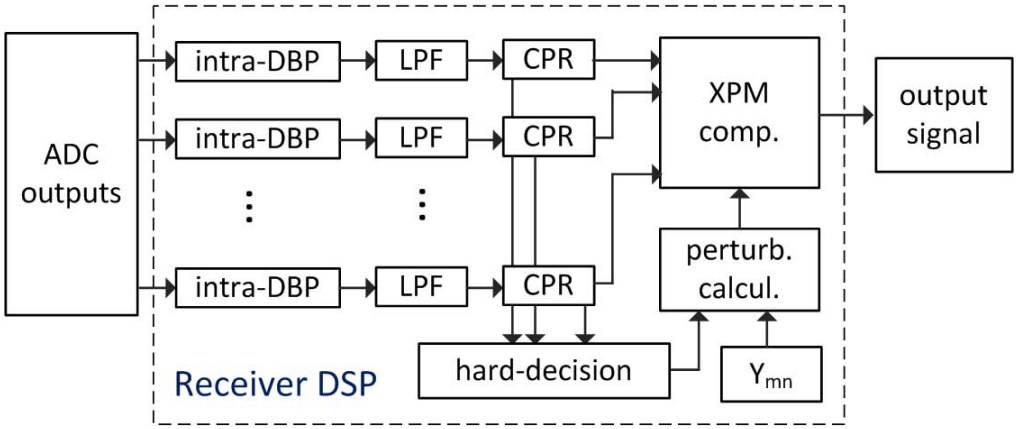

Figure 4.4: Diagram of a hybrid nonlinearity compensation scheme using DBP for intra-channel impairments compensation and the perturbation technique for XPM compensation. LPF: low pass filter.

As intra-channel DBP provides more accurate compensation of intra-channel nonlinear distortions than the perturbation technique, the hard-decision unit provides more accurate estimation of the input data. As a result, the XPM perturbation calculation and compensation becomes more accurate than the aforementioned scheme. Figure 4.5 shows the constellations of recovered signals. Comparing Fig. 4.5(c) with Fig. 4.5(b), we see that the perturbation technique is effective to compensate XPM distortions. However, the improvement in Q-factor by XPM compensation using the perturbation technique is still relatively smaller (see Fig. 4.8). The main reason is that the presence of XPM distortions results in wrong estimations in the hard-decision unit. From Fig. 4.5(c), we see that in addition to 16 constellation points (enlarged due to ASE noise), there exist small islands drifting away from the 16 constellation points. The drifting islands do not behave as ASE noise and we found that they result from the wrong estimations in the hard-decision unit. We employed a hard-decision correction method (as shown in Fig. 4.6) to correct the wrong decisions and re-compensated XPM distortions using the perturbation technique based on the corrected data. The drifting islands were mostly removed by the hard-decision correction method, as shown in Fig. 4.5(d).

Figure 4.6 shows the hard-decision correction method. The first step is to locate the wrong decisions. This is realized by finding the drifting islands in the constellation (Fig. 4.5(c)) of the output signals of the XPM compensation unit. We assume that a wrong decision occurred if the distance between an output signal point and its closet constellation point is larger than a certain threshold distance, that is

$$|sig_{out} - sig_{constel}| > r, \tag{4.9}$$

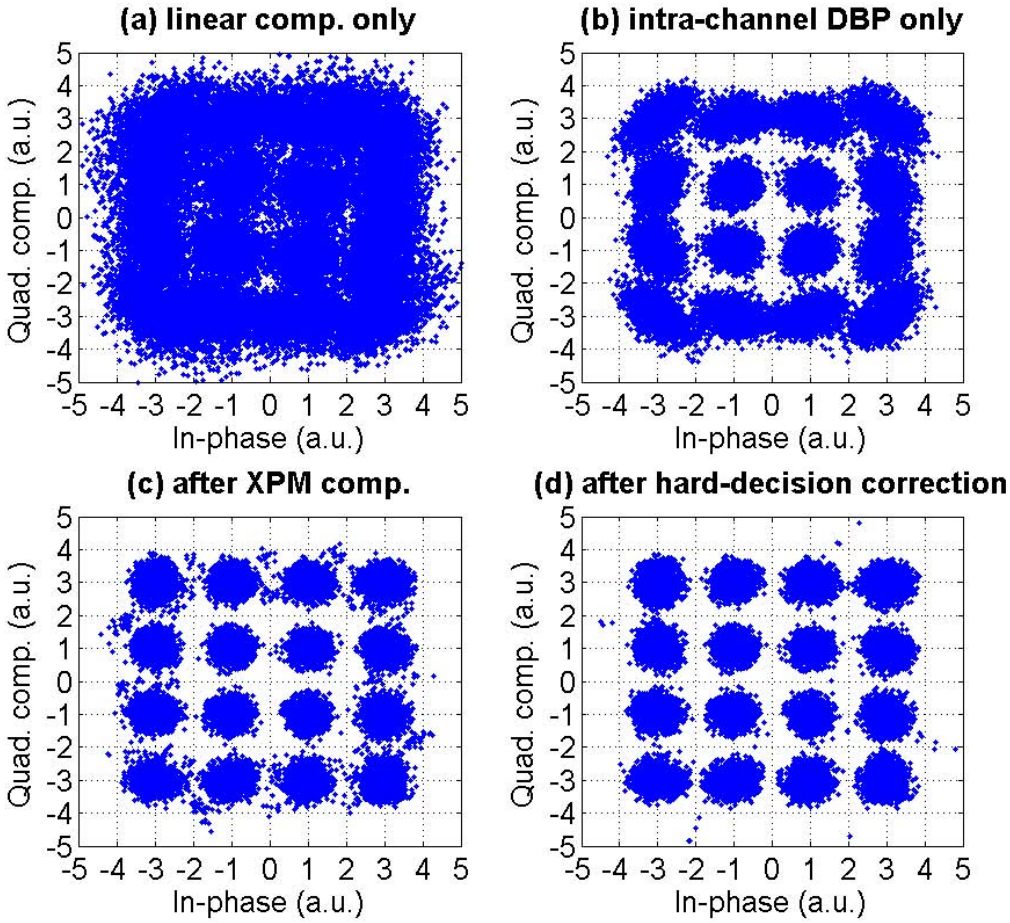

Figure 4.5: Constellations of recovered signals in a 2-channel WDM system: (a) linear compensation only, (b) nonlinearity compensation using intra-channel DBP only (step size = 40 km), (c) nonlinearity compensation using intra-channel DBP and the perturbation technique for XPM, (d) after hard-decision correction. (average power per channel P_{ave} = -3 dBm)

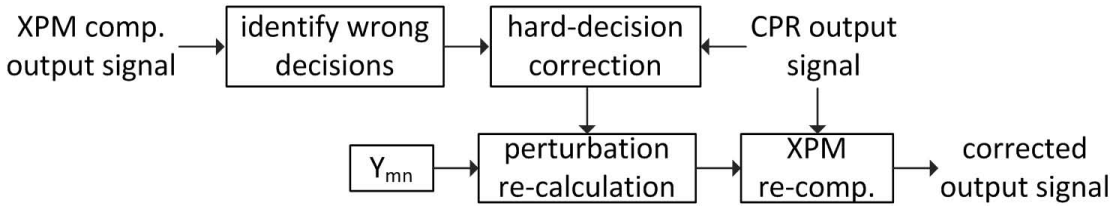

Figure 4.6: Diagram of a nonlinearity compensation scheme using hard-decision correction.

where sig_{out} and $sig_{constel}$ are the normalized output signal and its closest constellation point, respectively; r is the threshold distance. The circular regions about constellation points are used for hard-decision correction. Then we trace back to the hard-decision unit and replace the decision with the second-closest constellation point (rather than the closest one) of that CPR output signal point. Using the corrected hard-decision data, the perturbation calculation and compensation for XPM distortions are implemented for a second time. In the second round XPM compensation, corrected data from hard-decision correction is used to re-calculate the XPM distortion (Δu_{XPM}) using Eqs. (4.3) and (4.5), i.e., the input data sequence a_n and b_n appearing in Eqs. (4.3) and (4.5) are approximated by the corrected data from the hard-decision correction unit. Then, the XPM distortion is removed using $u_{comp} = u_{out}\Delta u_{XPM}$, where the CPR output is used as u_{out}. In the hard-decision correction unit, both the CPR output (u_{out}) and the decisions of first-stage XPM compensation are used as inputs to find the corrected data. The matrix Y_{mn} calculated before is re-used in the second-stage compensation. In simulations, the optimal threshold distances are obtained by sweeping the range [0 1]. The distance between the nearest constellation points is normalized to 2. Figure 4.7 shows the Q-factor as a function of the normalized threshold distance. It shows that the optimum threshold distance is dependent on launch power and system configuration. In practical systems, the optimal threshold values can be pre-determined by numerical simulations and then built into the DSP for transmission systems.

Figure 4.8 compares the Q-factors of different compensation schemes. The Q-factor improvement is defined as the difference between maximum Q-factors of different schemes. Figure 4.8(a) shows the case when the step size of intra-channel DBP

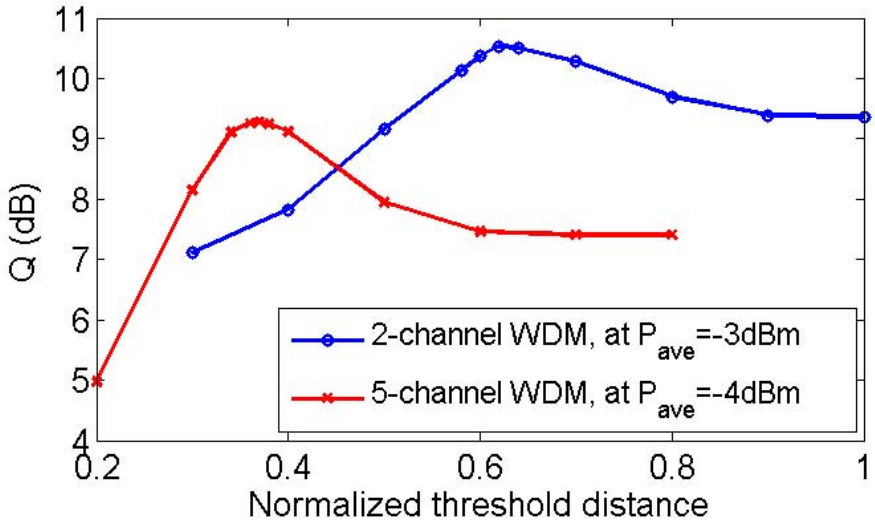

Figure 4.7: Q-factor versus normalized threshold distance.

is 2 km. Intra-channel DBP (line with 'x') brings 2.0 dB Q-factor improvement as compared with linear compensation only. Using the perturbation technique to compensate for XPM distortions (line with dots), an additional 0.7 dB improvement is obtained. Using the hard-decision correction method (line with triangles), the Q-factor improvements are 3.7 dB and 1.7 dB as compared with linear compensation and intra-channel DBP, respectively. We also investigated the case when a large step size is used for intra-channel DBP. Figure 4.8(b) shows slight performance degradation when the step size is 40 km. The scheme with hard-decision correction shows 3.2 dB and 1.4 dB Q-factor improvements as compared with linear compensation and intra-channel DBP, respectively. When the correct symbols are artificially used (instead of the output of the hard-decision correction unit), the BER becomes very small ($< 10^{-6}$). This implies that the first-order perturbation based compensation technique is able to effectively remove the XPM distortions and the performance degradation is due to hard-decision error. This can be seen by the few islands in Fig.

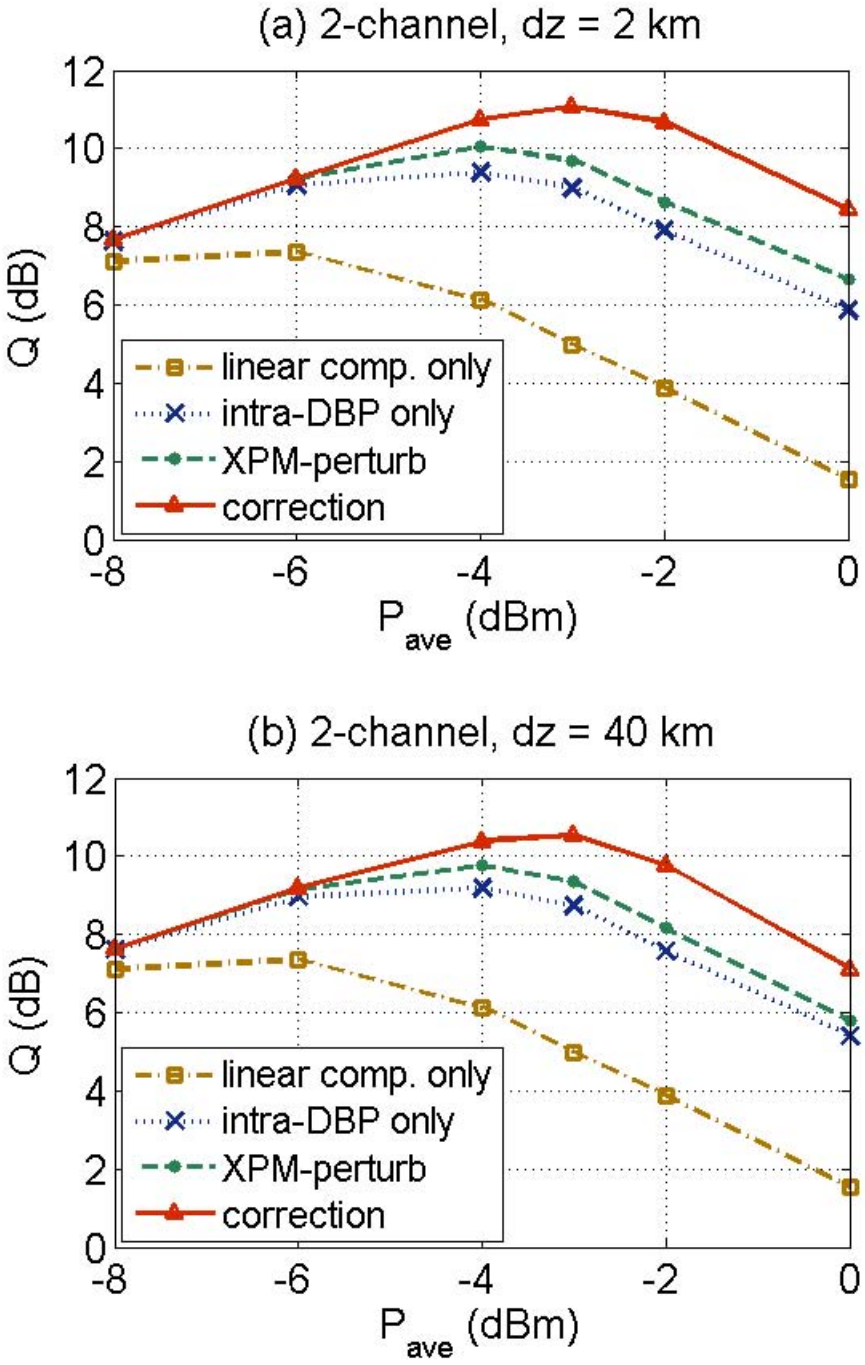

Figure 4.8: Q-factor versus average launch power per channel in a 2-channel WDM system: (a) intra-channel DBP step size = 2 km, (b) intra-channel DBP step size = 40 km. (OSNR is 23.8 dB when P_{ave} is -3 dBm. Transmission distance is 1600 km.)

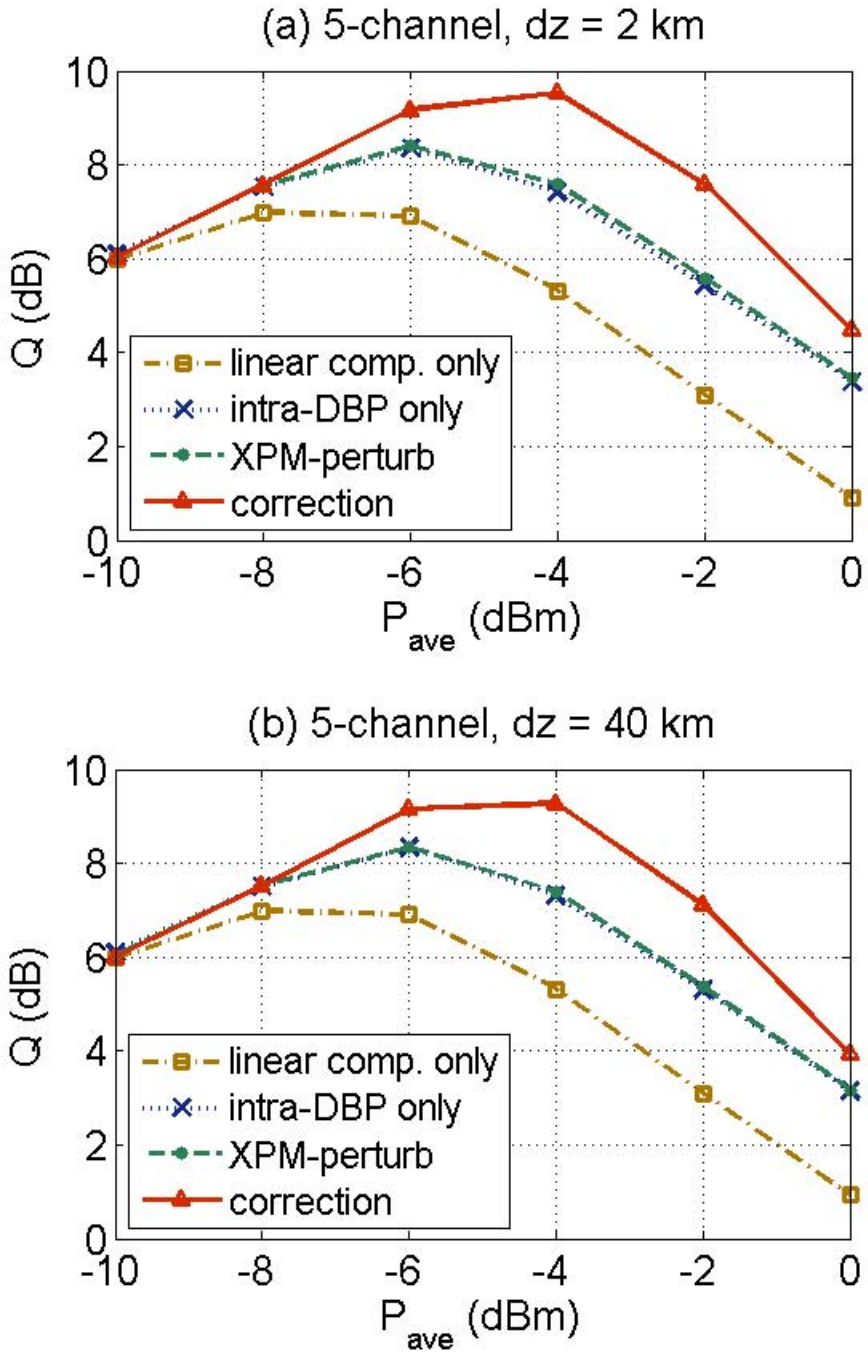

Figure 4.9: Q-factor versus average launch power per channel in a 5-channel WDM system: (a) intra-channel DBP step size = 2 km, (b) intra-channel DBP step size = 40 km. (OSNR is 22.9 dB when P_{ave} is -4 dBm. Transmission distance is 1600 km.)

4.5(d) even after hard-decision correction.

For a more general case, we investigated a 5-channel WDM system with the channel spacing of 50 GHz. Figure 4.9 shows the Q-factors of different schemes. In this case, the perturbation technique for XPM leads only to a slight performance improvement. However, with hard-decision correction, the additional Q-factor improvements are 1.2 dB and 1.0 dB as compared to intra-channel DBP only, for the cases of 2 km and 40 km step sizes, respectively. Total Q-factor improvements as compared to the case of linear compensation are 2.5 dB and 2.3 dB for the cases of 2 km and 40 km step sizes, respectively.

4.4 Conclusions

We have investigated a digital compensation scheme based on a perturbation theory to compensate for fiber nonlinearities in dispersion-managed fiber-optic systems. The scheme uses the data obtained from a hard-decision unit at the receiver to do perturbation calculation. In the scheme that uses perturbation technique to compensate for both intra-channel and XPM distortions, the performance improvement is small due to the inaccurate data after the hard-decision unit and the limitations of the first-order theory. We then considered a hybrid scheme, where the intra-channel distortions are removed by intra-channel DBP and the XPM distortions are compensated by the perturbation technique. Better performance improvement is obtained since intra-channel DBP provides more accurate compensation for intra-channel distortions which results in more accurate data in the hard-decision process. We also studied a hard-decision correction method to correct the wrong estimations in the hard-decision unit. We located the wrong estimated signals from the constellation of

the recovered signal and then traced back to replace the hard-decision data of those wrong estimations with the second-closest constellation point (rather than the closest one). Numerical simulations show that the hybrid scheme brings up to 3.7 dB and 1.7 dB Q-factor improvements as compared with the schemes of linear compensation only and intra-channel DBP, respectively. The perturbation technique for XPM compensation requires only one-stage (or two-stage when hard-decision correction is applied) compensation and symbol-rate signal processing. The results are also applicable to superchannel systems with multiple carriers.

Chapter 5

A multi-stage perturbation technique for compensating intra-channel nonlinear effects

5.1 Introduction

One of the dominant impairments in fiber-optic systems is caused by fiber intra-channel nonlinear effects. A number of techniques have been proposed to mitigate intra-channel nonlinear impairments such as digital back propagation (DBP) [2, 33, 34, 38, 75, 76, 78, 92] and perturbation techniques [49–53, 85, 86]. In DBP, typically split-step Fourier scheme (SSFS) is used to solve the NLSE in digital domain and it provides significant performance improvement if the step size is sufficiently small. In contrast, the existing perturbation-based compensation schemes use single-stage compensation, in which the dispersive and nonlinear distortions of the entire link are compensated all together at one step. Perturbation techniques have drawn significant

attention for modeling the fiber-optic systems [44, 45, 47, 48, 69, 70, 84, 93–96] as well as for compensation [49–53, 85–87]. In a first order perturbation theory, the signal field propagating in a fiber is divided into two parts: (i) signal field due to fiber dispersion and loss in the absence of nonlinearity, which is the unperturbed solution; (ii) the first order field due to nonlinear distortions, which is the perturbation correction to the unperturbed solution. The first order correction of a given symbol is calculated by considering its nonlinear interaction with neighboring symbols, where single and double summations involving the perturbation coefficient matrix X_{mn} have to be carried out. For a symbol at 0th time slot, X_{mn} indicates the coefficient for the nonlinear interaction between the mth, nth, and $(m+n)$th symbols. Generally, triple summation is required to calculate the first order field. The phase matching condition is usually applied to reduce the triple summation to double summation [44, 48, 94]. The single-stage compensation technique based on the first order perturbation theory has the following disadvantages: (i) the computational complexity is large in dispersion noncompensated links since the size of perturbation matrix X_{mn} is huge due to large accumulated dispersion; (ii) first order perturbation theory becomes inaccurate as the product of the transmission distance and launch power increases [45] and hence, the compensation performance decreases. In [97], a multi-stage nonlinear compensation technique based on a logarithmic perturbation analysis was shown to allow significant complexity reduction without sacrificing performance.

In this chapter, we develop a novel recursive perturbation theory to model a fiber-optic link. Suppose the fiber-optic link consisting of N_{tot} spans is divided into N_{stg} stages so that $N_{tot} = N_{stg} \times N_{spn}$, where N_{spn} is the number of spans per stage. The first order field due to the kth stage is calculated using the conventional perturbation

theory and it is added to the linear field at the end of the kth stage. The combined field is used as the input to the $(k+1)$th stage. However, dispersive effect as well as the addition of the first order field alters the pulse shape of the signal field and hence the perturbation coefficients of the kth stage cannot be used for $(k+1)$th stage without adjusting the pulse shape. For this purpose, we project the signal field on the basis of suitably chosen sampling functions. At the end of each stage, weights of the combined field (i.e., linear field + nonlinear distortion) on the basis of the sampling functions are computed. The distorted output signal of the kth stage can be expressed in the same form as the fiber input, except that the input data a_n^{in} is modified as a_n^k, so that perturbation coefficient matrix X_{mn} is the same for all the stages. We investigate a multi-stage compensation scheme based on the recursive perturbation theory [98]. The multi-stage technique has the following advantages: (i) the size of the matrix X_{mn} and hence the implementation complexity is significantly reduced since the size of X_{mn} is determined by the accumulated dispersion in each stage rather than that of the entire fiber-optic link; (ii) the accuracy of the perturbation technique is enhanced, resulting in better performance. This is because, in each stage the first order theory is used to calculate the nonlinear distortions occurring in a shorter distance, which improves the accuracy and the summation of the signal field and the first order field of the previous stage is used as the unperturbed solution for the next stage, which further improves the accuracy. We investigated a 28 Gbaud single channel system with 32-quadrature amplitude modulation (32-QAM) format and 3,200 km transmission distance. With 2 samples per symbol, the multi-stage scheme with $N_{stg} = 8$ increases the Q-factor as compared with linear compensation by 4.5 dB; as compared with single-stage compensation, the computational complexity is reduced

by a factor of 1.3 and the required memory for storing matrix X_{mn} is decreased by a factor of 13. For systems with quadrature phase-shift keying (QPSK) or 16-QAM, we expect similar performance improvements using the multi-stage perturbation technique. In this chapter, the multi-stage perturbation technique is implemented at the receiver; however, this technique can also be deployed at the transmitter and similar performance improvements are expected. The simulations in this chapter are based on single-polarization systems; however, the multi-stage perturbation technique can be properly modified to apply to dual-polarization systems and similar performance improvement is expected.

For DBP, increasing the number of stages (or steps) increases the computational complexity (and improves the performance, too). In contrast, for multi-stage perturbation technique, it is the opposite unless the number of stages is too large. This is because a given pulse interacts nonlinearly with K neighboring pulses over a distance L and K is roughly proportional to L. Total number of nonlinear interactions (and hence the number of complex multiplications) scales as $\sim K^2 N_p$ (or $\sim L^2 N_p$), where N_p is the number of signal pulses. If L is divided into N_{stg} equal segments, total number of nonlinear interactions scales as $\sim N_{stg}(L/N_{stg})^2 N_p$.

5.2 Recursive perturbation theory

In this chapter, we develop a recursive perturbation theory to model the evolution of optical signals propagating in fiber-optic links. A fiber-optic link is divided into multiple stages and the dispersive and nonlinear effects of each stage are calculated using a first order perturbation technique. The input and output signals of different

stages are expressed using the same basis functions such that the perturbation calculations of different stages can be done in a similar way using an identical perturbation coefficient matrix X_{mn}. Perturbation calculations are implemented recursively, that is, the output signal of the kth perturbation stage is used as the input signal of the $(k+1)$th perturbation stage. The optical signal propagation is described by the NLSE (see Eq. 2.3 in Chapter 2):

$$i\frac{\partial u}{\partial z} - \frac{\beta_2}{2}\frac{\partial^2 u}{\partial t^2} = -\gamma|u|^2 u, \tag{5.1}$$

where $\gamma = \gamma_0 e^{-w(z)}$. Let the input signal be

$$u(0,t) = \sqrt{P}\sum_{n=-N_{sym}}^{N_{sym}} d_n p(0, t-nT_0), \tag{5.2}$$

where P is the signal power, d_n is the data, $p(0,t)$ is the pulse shape function, T_0 is the symbol period, and $N_s(=2N_{sym}+1)$ is the number of symbols. Using the Nyquist sampling theorem, we express the input signal as

$$u(0,t) = \sqrt{P}\sum_{n=-N/2+1}^{N/2} a_n g(0, t-nT_s), \tag{5.3}$$

where N is the number of samples, a_n is the data sample, $g(0,t)$ is a sampling function, and T_s is the sampling period. In this chapter, we choose an inter-symbol interference (ISI)-free sampling pulse $g(0,t) = \mathrm{sinc}(t/T_s)$, so that a_n is simply the data sample at $t = nT_s$. Here $g(0,t)$ is the sampling function, not necessarily the same as the symbol pulse shape $p(0,t)$. The symbol pulse shape can be arbitrary. Also, the mathematical derivation can be applied to the cases of multiple samples per symbol by properly

choosing the sampling period T_s. For example, if T_s equals to half the symbol period, the perturbation calculations will be carried out with two samples per symbol. Using the perturbation technique, we assume that the leading order solution of Eq. (5.1) is linear and treat the nonlinear terms on the right-hand side as perturbations. We expand the optical field into a series [45, 93]

$$u = u^{(0)} + \gamma_0 u^{(1)} + \gamma_0^2 u^{(2)} + ..., \tag{5.4}$$

where $u^{(m)}$ denotes the mth-order solution. The linear solution is found as

$$u^{(0)}(z,t) = \sqrt{P}\sum_n a_n g(z, t - nT_s), \tag{5.5}$$

where

$$g(z,t) = \frac{T_s}{2\pi}\int_{-\pi/T_s}^{\pi/T_s} \exp[iS(z)\omega^2/2 - i\omega t]d\omega, \tag{5.6}$$

and $S(z) = \int_0^z \beta_2(s)ds$. Substituting Eq. (5.4) into Eq. (5.1), we find the governing equation for the first order correction as

$$i\frac{\partial u^{(1)}}{\partial z} - \frac{\beta_2}{2}\frac{\partial^2 u^{(1)}}{\partial t^2} = -e^{-w(z)}|u^{(0)}|^2 u^{(0)}, \tag{5.7}$$

Taking the Fourier transform of Eq. (5.7), we find

$$\frac{\partial \widetilde{u}^{(1)}}{\partial z} - i\frac{\beta_2}{2}\omega^2 \widetilde{u}^{(1)} = \widetilde{G}(z,\omega), \tag{5.8}$$

where $\widetilde{u}^{(1)}(z,\omega) = F\{u^{(1)}(z,t)\}$, $\widetilde{G}(z,\omega) = F\{G(z,t)\}$, $G(z,t) = ie^{-w(z)}|u^{(0)}|^2 u^{(0)}$, and F is the Fourier transform operator. The solution to Eq. (5.8) with the initial

condition $\widetilde{u}^{(1)}(0,\omega)=0$ is

$$\widetilde{u}^{(1)}(z,\omega)=\int_0^z \widetilde{G}(s,\omega)\exp\{i[S(z)-S(s)]\omega^2/2\}ds. \tag{5.9}$$

The first order nonlinear distortion is found as

$$\Delta u(z,t)=\gamma_0 u^{(1)}(z,t)=\gamma_0 F^{-1}\{\widetilde{u}^{(1)}(z,\omega)\}, \tag{5.10}$$

where F^{-1} is the inverse Fourier transform operator. Using the orthogonality of the linear output waveforms $g(z,t-nT_s)$ [47], we rewrite the nonlinear distortion as

$$\Delta u(z,t)=\gamma_0\sqrt{P}\sum_n a_n^{(1)}g(z,t-nT_s), \tag{5.11}$$

where the modification to the input data due to nonlinear effects is found as [47, 48, 96]

$$\begin{aligned} a_n^{(1)} &= \int_{-\infty}^{\infty}\frac{\Delta u(z,t)}{T_s\gamma_0\sqrt{P}}g^*(z,t-nT_s)dt \\ &= \frac{i}{T_s\sqrt{P}}\int_0^z ds e^{-w(s)}\int_{-\infty}^{\infty}dt g^*(s,t-nT_s)|u^{(0)}(s,t)|^2u^{(0)}(s,t). \end{aligned} \tag{5.12}$$

Consider the pulse at symbol slot j. Substituting Eq. (5.5) into Eq. (5.12) and using the phase matching condition $m+n-l=j$, where m, n, and l are sample indices, we obtain [47, 48, 52, 96]

$$a_j^{(1)}=iP\sum_{m=-K/2}^{K/2}\sum_{n=-K/2}^{K/2}a_{m+j}a_{n+j}a_{m+n+j}^*X_{mn}, \tag{5.13}$$

$$X_{mn} = \frac{1}{T_s}\int_0^z dse^{-w(s)}\int_{-\infty}^{\infty} dtg^*(s,t)g(s,t-mT_s)g(s,t-nTs)g^*(s,t-(m+n)T_s), \tag{5.14}$$

where K is the number of neighboring samples that interacts nonlinearly with the jth sample, X_{mn} is the perturbation coefficient matrix. The integration in Eq. (5.14) is evaluated numerically using Simpsons 1/3 rule with step sizes $dt = T_s/8$ and $ds = 0.1$ km. Including the nonlinear distortions, the output signal of the first perturbation stage can be written as

$$u(L,t) = \sqrt{P}\sum_n a'_n g(L, t-nT_s), \tag{5.15}$$

where the modified data is given as $a'_n = a_n + \gamma_0 a_n^{(1)}$, and L is the fiber length of the first perturbation stage.

To make the perturbation coefficient matrix X_{mn} independent of the stages, we express the output signal of the first stage on the basis $g(0, t-nT_s)$ rather than $g(L, t-nT_s)$. We rewrite the output signal of the first stage as

$$u(L,t) = \sqrt{P}\sum_m b_m g(0, t-mT_s), \tag{5.16}$$

where b_m is the weight under the basis $g(0, t-mT_s)$. Since $g(0, t-mT_s)$ is a sinc function centered at mT_s, $b_m\sqrt{P}$ is simply the sample of $u(L,t)$ at mT_s. Using Eq. (5.15), we find

$$\begin{aligned} b_m &= u(L, t=mT_s)/\sqrt{P} \\ &= \sum_n a'_n g(L, (m-n)T_s). \end{aligned} \tag{5.17}$$

Let

$$c_{m-n} = g(L, (m-n)T_s). \tag{5.18}$$

Using Eq. (5.6), c_n is calculated by

$$c_n = \frac{T_s}{2\pi} \int_{-\pi/T_s}^{\pi/T_s} \exp[iS(L)\omega^2/2 - i\omega n T_s] d\omega. \tag{5.19}$$

Substituting Eq. (5.18) in Eq. (5.17), we obtain

$$b_m = \sum_n a'_n c_{m-n}. \tag{5.20}$$

The convolution in Eq. (5.20) can be conveniently computed using discrete Fourier transforms as

$$b_n = \text{IDFT}\left\{\text{DFT}\{a'_n\} \times \text{DFT}\{c_n\}\right\}, \tag{5.21}$$

where DFT and IDFT indicate the discrete Fourier transform and the inverse discrete Fourier transform, respectively. Now, the output signal (Eq. (5.16)) of the first perturbation stage is expressed in the same form as the input signal (Eq. (5.3)), so the output signal of the second perturbation stage can be calculated recursively by using the output data of the first stage as its input data.

So far, we considered an additive perturbation model, where the nonlinear distortion is added to the linear field (i.e., $a'_n = a_n + \gamma_0 a_n^{(1)}$). Equation (5.13) shows that the nonlinear distortion $a_n^{(1)}$ includes self-phase modulation (SPM), intra-channel cross-phase modulation (IXPM) and intra-channel four wave mixing (IFWM) effects. In order to accurately model the phase noise characteristics of SPM and IXPM effects, it is useful to introduce a multiplicative model for the SPM and IXPM effects while

keeping the additive model for IFWM effect [99]. At symbol slot 0, we expand Eq. (5.13) as

$$a_{n=0}^{(1)} = iPa_0 \left[|a_0|^2 X_{m=0,n=0} + 2\sum_{n\neq 0} |a_n|^2 X_{m=0,n} \right] + iP \sum_{m\neq 0} \sum_{n\neq 0} a_m a_n a_{m+n}^* X_{mn}, \quad (5.22)$$

where the first, second and third terms account for SPM, IXPM and IFWM effects, respectively. Using the following definitions,

$$\phi_{nl} = \gamma_0 P \left(|a_0|^2 X_{m=0,n=0} + 2\sum_{n\neq 0} |a_n|^2 X_{m=0,n} \right), \quad (5.23)$$

$$\Delta a_{IFWM} = i\gamma_0 P \sum_{m\neq 0} \sum_{n\neq 0} a_m a_n a_{m+n}^* X_{mn}, \quad (5.24)$$

we find the modified data at symbol slot 0 as

$$a'_{n=0} = a_0 + \gamma_0 a_0^{(1)}, \quad (5.25)$$

$$= a_0(1 + i\phi_{nl}) + \Delta a_{IFWM} \quad (5.26)$$

$$\approx a_0 \exp(i\phi_{nl}) + \Delta a_{IFWM}. \quad (5.27)$$

Equation (5.26) represents the additive perturbation model, while Eq. (5.27) corresponds to an additive-multiplicative (A-M) model where the phase noise characteristics of SPM and IXPM effects are included. The sample at time slot j can be calculated similarly using Eqs. (5.26) and (5.27) with the time window shifted by jT_s.

The difference between the regular additive perturbation model and the A-M perturbation model can be understood by considering the power conservation. Let's

consider a simple case with loss and dispersion coefficients to be zero and the NLSE becomes

$$i\frac{\partial u}{\partial z} = -\gamma|u|^2 u. \tag{5.28}$$

The exact solution is given as

$$u(L,t) = u(0,t)\exp\left[i\gamma\int_0^L |u(z,t)|^2 dz\right]. \tag{5.29}$$

We see that the power is conserved since $|u(L,t)|^2 = |u(0,t)|^2$. In the case of $\alpha = 0$ and $\beta_2 = 0$, the linear solution is the same as the input field,

$$u^{(0)}(L,t) = u(0,t). \tag{5.30}$$

Using the regular additive perturbation model, the output field may be written as

$$u(L,t) = u^{(0)}(L,t) + \gamma u^{(1)}(L,t) = [1 + i\gamma PL]\, u(0,t), \tag{5.31}$$

where

$$P = |u(0,t)|^2. \tag{5.32}$$

This output signal has higher power than the input signal since $|u(L,t)|^2 > |u(0,t)|^2$. However, if we use the A-M model, the output field may be written as

$$u(L,t) = u(0,t)\exp\left[i\phi(t)\right], \tag{5.33}$$

where $\phi(t)$ is a nonlinear phase shift. We see that in the A-M model, the signal power is conserved, since $|u(L,t)|^2 = |u(0,t)|^2$.

5.3 Multi-stage compensation scheme based on recursive perturbation theory

A multi-stage compensation scheme is developed based on the recursive perturbation theory. Consider a fiber-optic link consisting of N_{tot} spans. We divide the compensation process into N_{stg} stages, and the number of fiber spans of each perturbation stage is $N_{spn} = N_{tot}/N_{stg}$. At the receiver, the data samples r_n of the distorted signal are used as the input to the first compensation stage. The signal impairments due to propagating in the last N_{spn} spans of transmission fibers are removed in the first compensation stage based on the A-M model, using the following steps:

$$h_n = \text{IDFT}\left\{\text{DFT}\{r_n\} \times \text{DFT}\{c'_n\}\right\}, \tag{5.34}$$

$$c'_n = \frac{T_s}{2\pi}\int_{-\pi/T_s}^{\pi/T_s} \exp[-iS(L)\omega^2/2 - i\omega nT_s]d\omega, \tag{5.35}$$

$$v_n = (h_n - \Delta a_{IFWM})\exp(-i\phi_{nl}), \tag{5.36}$$

where ϕ_{nl} and Δa_{IFWM} are respectively calculated using Eqs. (5.23) and (5.24), with the data a_n replaced by h_n. In the next compensation stage, the output data of the previous stage is used as the input data, and the same compensation procedures are implemented using an identical perturbation coefficient matrix X_{mn} as the first stage. In the multi-stage perturbation technique, the propagation of signal field is reversed in a multi-stage flow where dispersion and nonlinearity are removed in each stage, similar to the DBP scheme. The difference between the two algorithms is that the multi-stage perturbation technique provides a better approximation of the nonlinear operation in each stage. The multi-stage perturbation technique employs

a perturbation analysis and calculates the nonlinear distortions by summing over multiple triplets (using the perturbation coefficient matrix X_{mn}, as shown in Eqs. (5.23) and (5.24)), while DBP involves only a phase rotation that is proportional to the energy of each sample.

5.4 Simulation results and discussions

First we compare the additive perturbation model with the additive-multiplicative (A-M) perturbation model for optical signals propagating in a dispersion noncompensated fiber-optic link. The input signal is 28 Gbaud, modulated with 32-QAM format using a raised cosine pulse with a roll-off factor of 0.1. The launch power is 2 dBm. The fiber-optic link consists of 40 spans of standard single mode fiber (SSMF) with 80 km amplifier spacing. The loss, dispersion, and nonlinear coefficients of the SSMF are 0.2 dB/km, -21 ps^2/km, and 1.1 $W^{-1}km^{-1}$, respectively. An in-line amplifier is used after each fiber span to fully compensate the fiber loss. The output signals calculated using the additive model and the A-M model are compared with the numerical simulation result based on SSFS. The amplifier noise is turned off to obtain the results in Fig. 5.1. Figure 5.1(a) shows that the result of the A-M model agrees well with the numerical result, while the result of the additive model shows the overestimated signal amplitude which has been observed in [87]. Figure 5.1(b) shows the signal power differences of the two models. The signal power difference is calculated using $|q_{model}|^2 - |q_{SSFS}|^2$, where q_{model} and q_{SSFS} are the output signal fields obtained using the additive or A-M models and the SSFS simulation, respectively. The mean power differences are 0.72 mW and -0.06 mW for the additive model and the A-M model, respectively. Figure 5.1(c) shows the signal power as a function of the number

of perturbation stages, where each stage includes one fiber span. It shows that the over-estimation of signal power in the additive model accumulates over perturbation stages. This power over-estimation is due to the neglecting of phase noise characteristics of SPM and IXPM effects. Comparing Eqs. (5.26) and (5.27), we note that the power is conserved in the A-M model since $|a_0 \exp(i\phi_{nl})|^2 = |a_0|^2$, while for the additive model, $|a_0(1 + i\phi_{nl})|^2 > |a_0|^2$, which is the reason of power over-estimation.

Enhanced regular perturbation (ERP) in [93] is an interesting technique to remove the average nonlinear phase before applying the perturbative analysis. ERP is an alternative technique that could help to partially cope with the energy divergence problem. Both A-M and ERP techniques are expected to provide similar results.

We investigated a single-channel fiber-optic system to study the performance of the multi-stage compensation scheme based on the recursive perturbation theory, as shown in Fig. 5.2. The system configuration is as follows: symbol rate = 28 Gbaud, modulation format = 32-QAM, amplifier spacing = 80 km, total number of fiber spans $N_{tot} = 40$, transmission fiber = SSMF, linewidth of transmitter and local oscillator lasers = 100 kHz. In each Monte-Carlo simulation, 65,536 symbols are transmitted all together. The optical signal is modulated using a raised cosine pulse with a roll-off factor of 0.1. A second order Gaussian band pass filter (BPF) with 3-dB bandwidth of 40 GHz is used before the coherent receiver. After multi-stage perturbation-based compensation, a second order Gaussian low pass filter (LPF) with 3-dB bandwidth of 15 GHz is used to limit out-of-band noise. Carrier phase recovery (CPR) is then implemented using the feedforward method [91]. Bit error rate (BER) is calculated by counting the number of error bits, and Q-factor is converted from BER using $Q = \sqrt{2}\text{erfc}^{-1}(2 \times \text{BER})$.

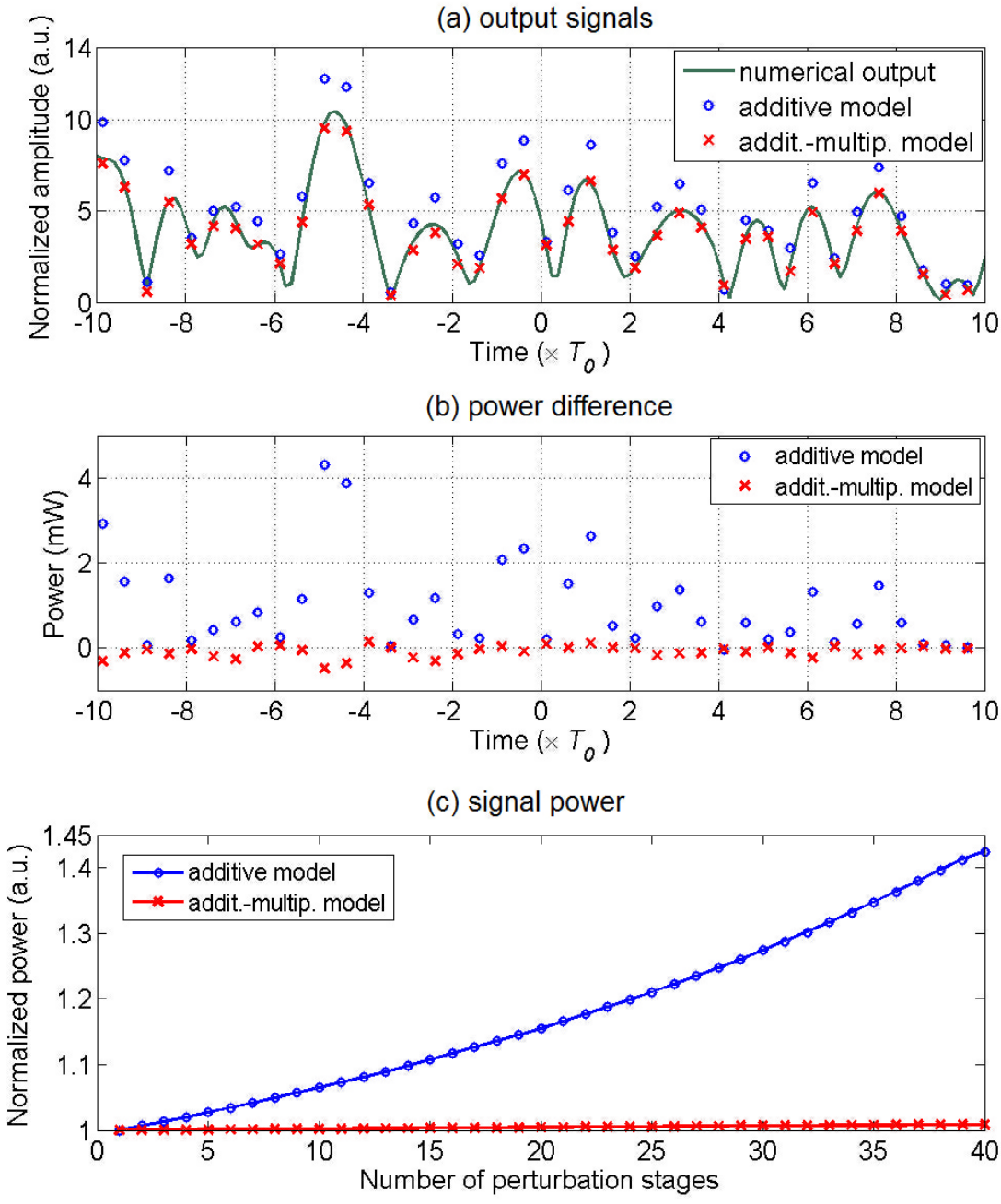

Figure 5.1: Comparisons of the additive perturbation model and the additive-multiplicative perturbation model (40-span SSMFs, power = 2dBm): (a) output signals versus time, (b) power difference versus time, and (c) signal power versus number of perturbation stages.

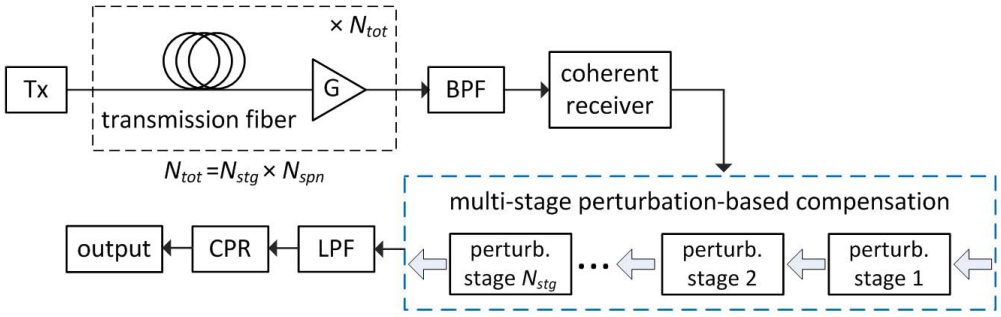

Figure 5.2: Schematic of a single-channel fiber-optic system with multi-stage perturbation-based compensation. Tx: transmitter, BPF: band-pass filter, LPF: low-pass filter, CPR: carrier phase recovery.

We studied compensation schemes with different number of stages. The signal impairments of $N_{spn}(= N_{tot}/N_{stg})$ fiber spans is compensated in one stage. The computational complexity of the perturbation-based compensation scheme is proportional to the size of the coefficient matrix X_{mn} (as shown in Eqs. (5.23) and (5.24)), which is dependent on N_{stg}. In practical implementations, the insignificant components in the matrix X_{mn} are truncated to reduce the computational complexity. We use the following truncation criterion: $20\log_{10}|X_{mn}/X_{m=0,n=0}| > xdB$, where x is a truncation threshold [49]. Figure 5.3 shows the perturbation coefficient matrices for different values of N_{stg}, where 2 samples/symbol are used (i.e., T_s equals half the symbol period). At -40 dB truncation threshold, the numbers of significant terms in X_{mn} are 173, 6193, and 23289 for the cases when N_{stg} is 40, 8, and 1, respectively. Due to the reduced dispersive effect within one stage, the matrix size and hence the required memory in DSP for storing X_{mn} are significantly reduced in multi-stage schemes. Also, the number of neighboring samples required for perturbation calculation is reduced. Figure 5.3 shows that the required numbers of neighboring samples are 28, 194, and 1544 for the cases when N_{stg} is 40, 8, and 1, respectively.

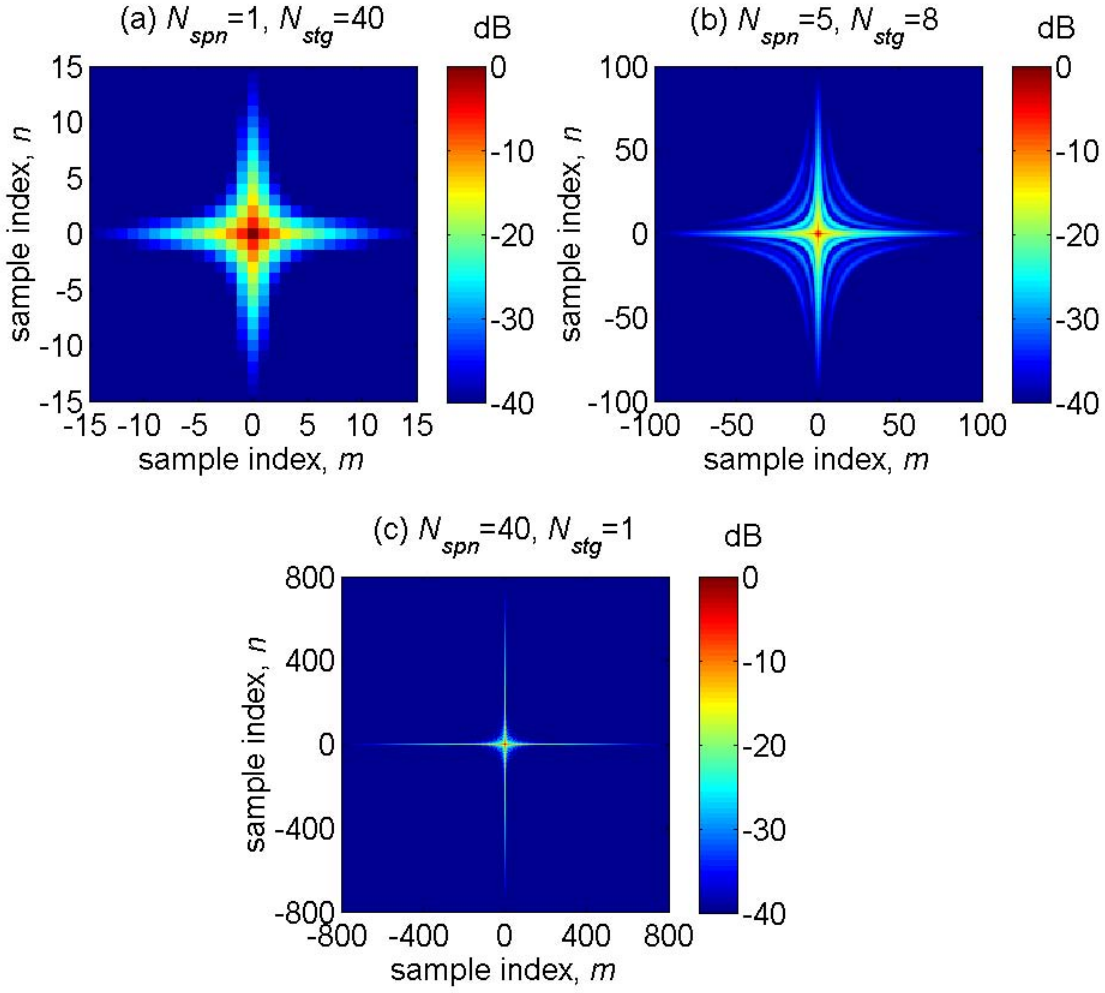

Figure 5.3: Perturbation coefficient matrices, $20\log_{10}|X_{mn}|$: (a) $N_{stg} = 40$, (b) $N_{stg} = 8$, (c) $N_{stg} = 1$.

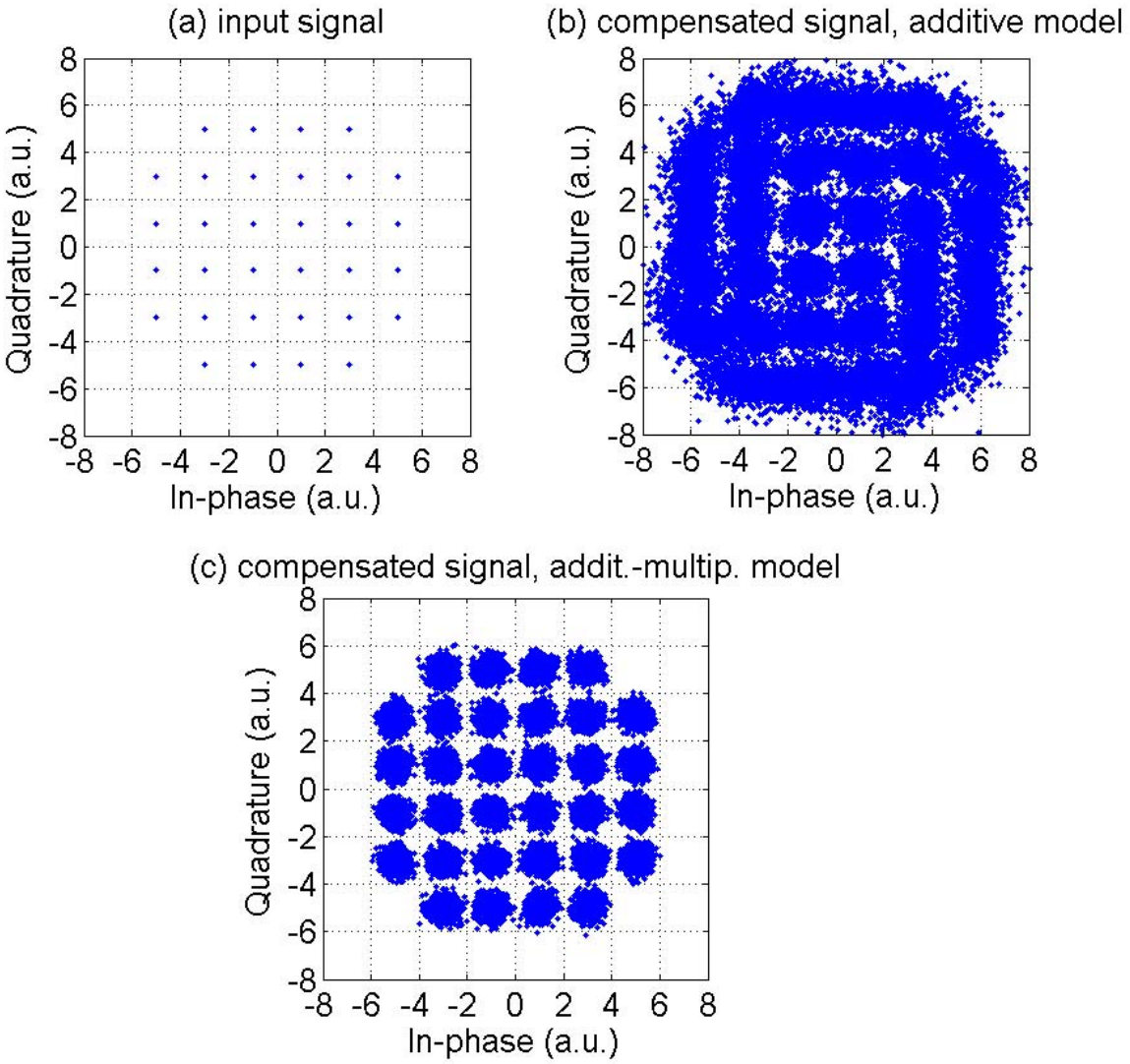

Figure 5.4: Signal constellations: (a) input signal, (b) compensated signal using the additive model, (c) compensated signal using the additive-multiplicative model.

Figure 5.4 shows the compensated signal constellations, in comparison with the input signal constellation. The launch power is 2 dBm and $N_{stg} = 8$. The constellation of the compensated signal obtained using the additive model is expanded, indicating over-estimation of signal power, while the power of the compensated signal using the A-M model is conserved, which is consistent with the previous discussion about power conversation.

Figures (5.5) and (5.6) show the compensation performance of the A-M model, where 1 sample/symbol and 2 samples/symbol are used, respectively. In the case of 1 sample/symbol, Fig. 5.5(a) shows that Q-factor improvements over the linear compensation scheme are 1.9, 2.0, 2.3, 2.5, and 2.6 dB, when N_{stg} is 1, 2, 4, 8 and 40, respectively. In the case of 2 samples/symbol, Fig. 5.6(a) shows that the Q-factor improvements are 2.9, 3.6, 4.0, 4.5, and 5.3 dB, when N_{stg} is 1, 2, 4, 8 and 40, respectively. In this chapter, we have simulated a single-channel transmission system. In the case of wavelength division multiplexing (WDM) systems, the performance improvements are expected to be significantly lower unless inter-channel impairments due to cross-phase modulation (XPM) are mitigated [87]. The compensation schemes using 2 samples/symbol bring 1.0 $\sim$ 2.7 dB improvements in Q-factor as compared with 1 sample/symbol cases, due to the fact that the nonlinear effects broaden the signal spectrum and hence the sampling rate should exceed the symbol rate which roughly equals the bandwidth of the linear signal. As compared with single-stage compensation schemes, multi-stage schemes with $N_{stg} = 8$ bring 0.6 and 1.6 dB improvements in Q-factor for the cases of 1 sample/symbol and 2 samples/symbol, respectively; multi-stage schemes with $N_{stg} = 40$ bring 0.7 and 2.4 dB improvements in Q-factor for the cases of 1 sample/symbol and 2 samples/symbol, respectively. Figures 5.5(b)

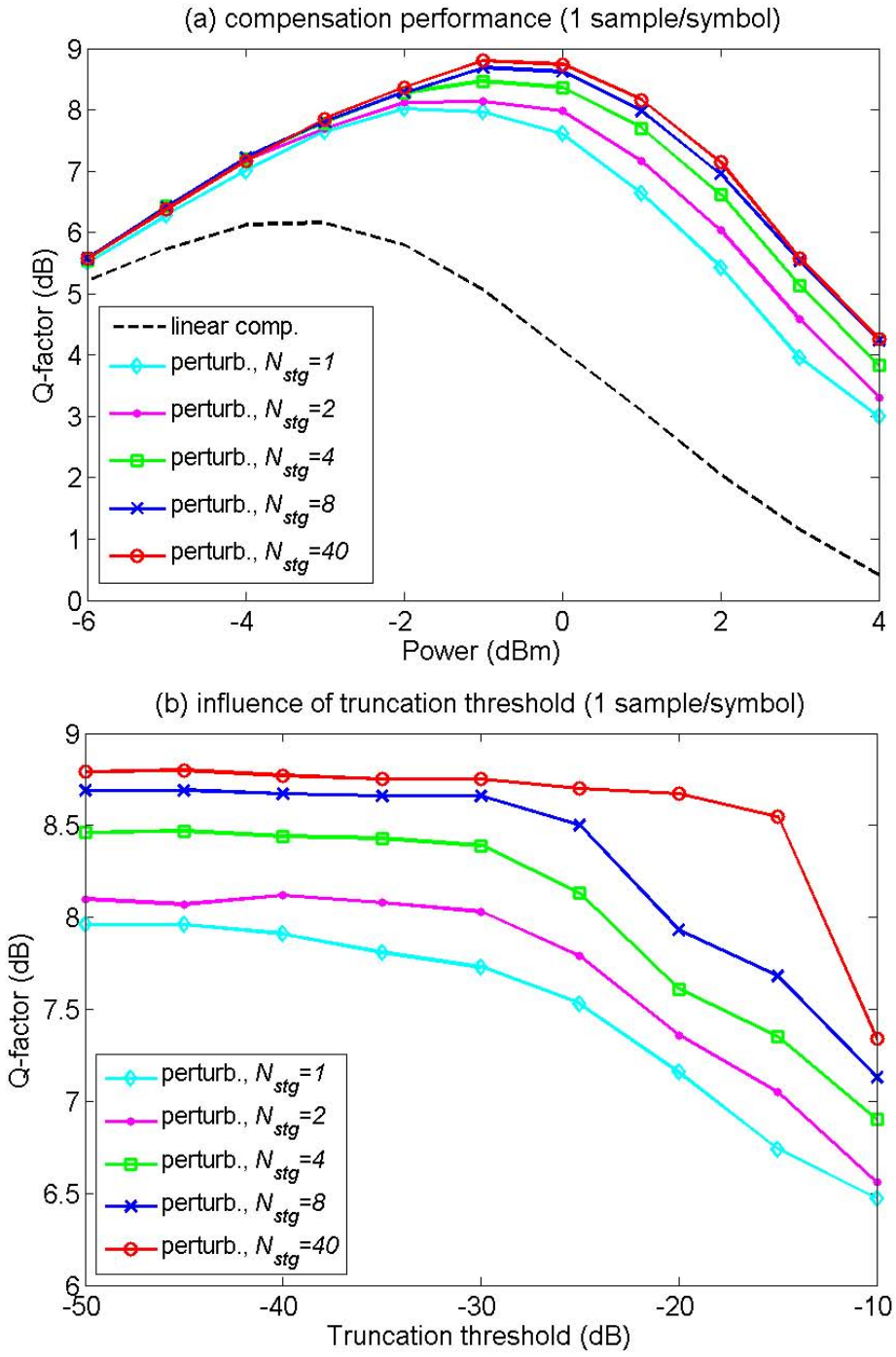

Figure 5.5: Q-factor versus (a) launch power and (b) truncation threshold, 1 sample/symbol is used. (Optical signal-to-noise ratio (OSNR) is 23.3 dB when average launch power is -1 dBm. Transmission distance is 3200 km.)

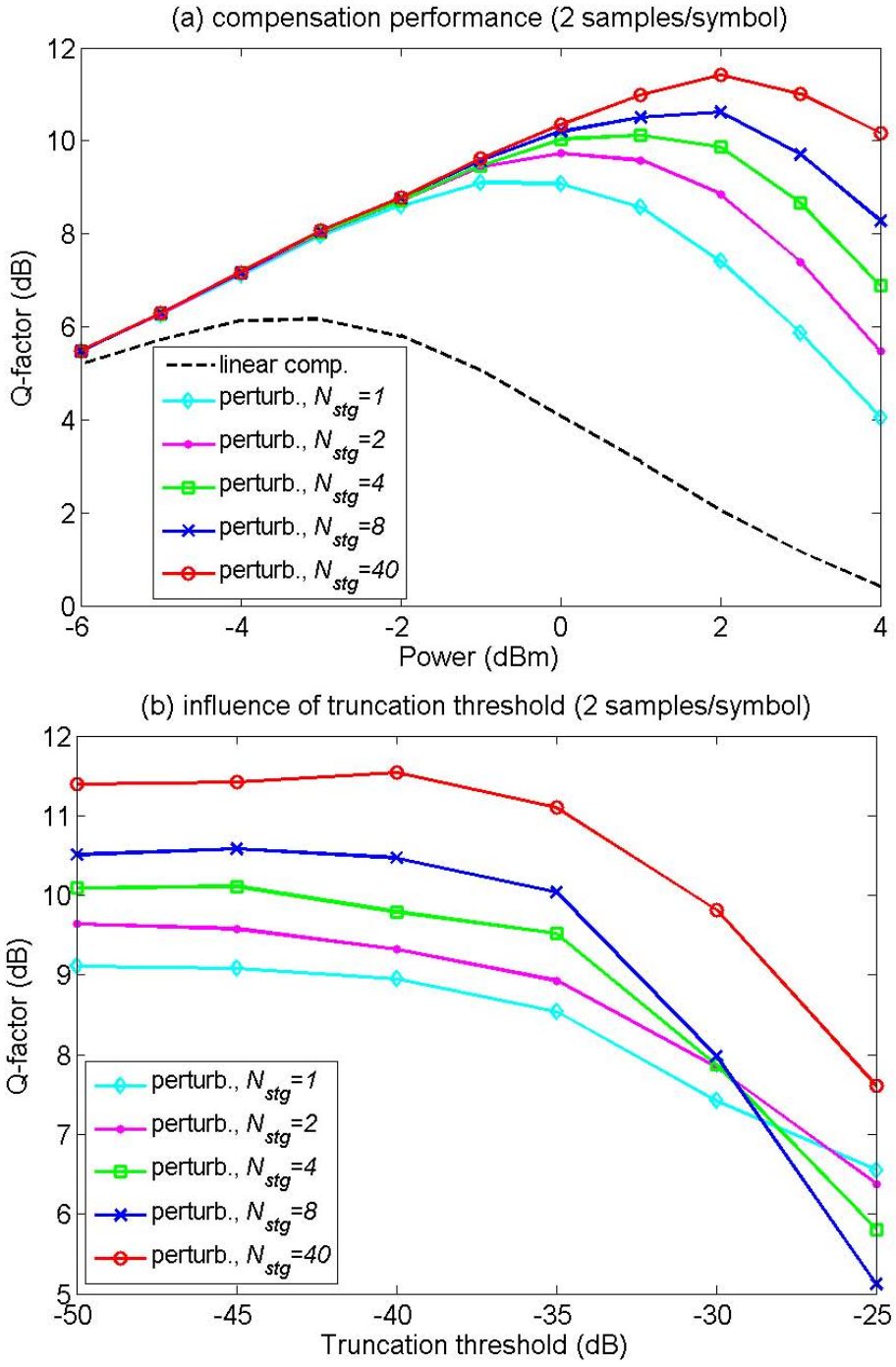

Figure 5.6: Q-factor versus (a) launch power and (b) truncation threshold, 2 samples/symbol are used. (OSNR is 26.3 dB when average launch power is 2 dBm. Transmission distance is 3200 km.)

and 5.6(b) show that compensation performance degrades as the truncation threshold increases. The optimal launch powers that maximize Q-factors, obtained from Figs. 5.5(a) and 5.6(a) are chosen as the launch powers for Figs. 5.5(b) and 5.6(b), respectively. When the truncation threshold is too high (> -30 dB), the number of coefficients in X_{mn} is not adequate to provide an accurate estimation of nonlinear distortions. This inaccuracy will accumulate with the number of perturbation stages. The build-up of uncompensated nonlinear distortions in a multi-stage scheme could be larger than that in a single-stage in some cases, as shown in Fig. 5.6(b) at high truncation thresholds.

Table 5.1: Q-factor improvement (ΔQ), number of complex multiplications per symbol (M_c), and required memory for storing X_{mn}. Reference Q-factor = 6.2 dB.

N_{stg}		1	2	4	8	40
1 sample per symbol	$\Delta Q(dB)$	1.8	1.9	2.2	2.4	2.5
	M_c	32,227	10,478	9,820	7,736	2,200
	memory	10,737	1,741	813	317	13
2 samples per symbol	$\Delta Q(dB)$	2.8	3.5	3.9	4.4	5.2
	M_c	248,089	392,306	326,836	148,904	22,120
	memory	82,685	65,373	27,225	6,193	173

Table 5.2: Comparison of scheme complexity to achieve ΔQ=2.0 dB. Reference Q-factor = 6.2 dB.

N_{stg}		1	2	4	8	40
1 sample per symbol	M_c	—	—	6,028	3,032	1,240
	memory	—	—	497	121	5
2 samples per symbol	M_c	55,477	45,986	39,220	33,320	8,680
	memory	18,481	7,653	3,257	1,377	61

Table 5.3: Comparison of scheme complexity to achieve ΔQ=3.0 dB. Reference Q-factor = 6.2 dB.

N_{stg}		1	2	4	8	40
1 sample per symbol	M_c	—	—	—	—	—
	memory	—	—	—	—	—
2 samples per symbol	M_c	—	104,258	56,836	50,120	10,120
	memory	—	17,365	4,725	2,077	73

In order to reduce the implementation complexity, we select the truncation threshold based on a criterion that the reduction of Q-factor from its value at -50 dB truncation threshold is within 0.1 dB. To estimate the computational complexity, the numbers of complex multiplications per symbol is found as $M_c = N_{stg}[3M+(N\log_2 N)/N_s]$, where M is the number of significant perturbation coefficient in X_{mn} for one compensation stage, N is the number of samples, $N_s = (2N_{sym} + 1)$ is the number of symbols, the factor 3 accounts for the three multiplications for each coefficient in X_{mn}, as shown in Eq. (5.24), and the logarithm terms correspond to the fast Fourier transforms (FFTs) in Eq. (5.34). Table. 5.1 compares the Q-factor improvement over the linear compensation scheme, computational complexity, and required memory for multi-stage compensation schemes with different N_{stg}. As compared with single-stage schemes, in case of 1 sample/symbol and $N_{stg} = 8$, the computational complexity and the required memory of storing X_{mn} are reduced by factors of 4.2 and 34, respectively; in case of 2 samples/symbol and $N_{stg} = 8$, the computational complexity and the required memory are reduced by factors of 1.3 and 13, respectively. The reference Q-factor corresponds to the value obtained by using only the linear compensation at the receiver. Table. 5.2 and Table. 5.3 compare the implementation complexities of schemes with different values of N_{stg} to achieve Q-factor improvements of 2.0 dB and 3.0 dB over the scheme consisting of linear compensation only, respectively. The "—"

sign indicate that the given Q-factor is not achievable by the scheme. The required memory is related with the number of samples per symbol, the accumulated dispersion within one perturbation stage, and the truncation threshold. When we increases from 1 sample/symbol to 2 samples/symbol, the pulse width of the sampling function ($g(0,t)$ in Eq. (5.3)) decreases by half, and as a result, the broadening in the pulse width of $g(z,t)$ is increased for a given transmission distance, which increases the required memory.

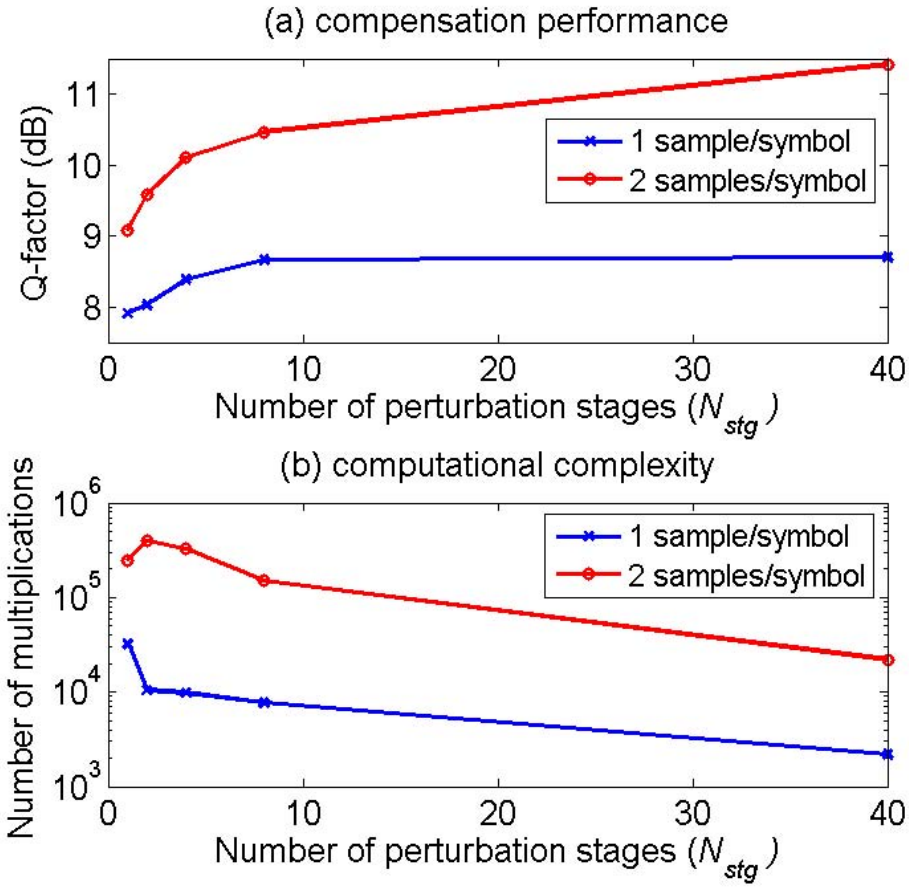

Figure 5.7: Comparisons of multi-stage perturbation-based compensation scheme with different number of stages: (a) compensation performance, (b) computational complexity. (Transmission distance is 3200 km.)

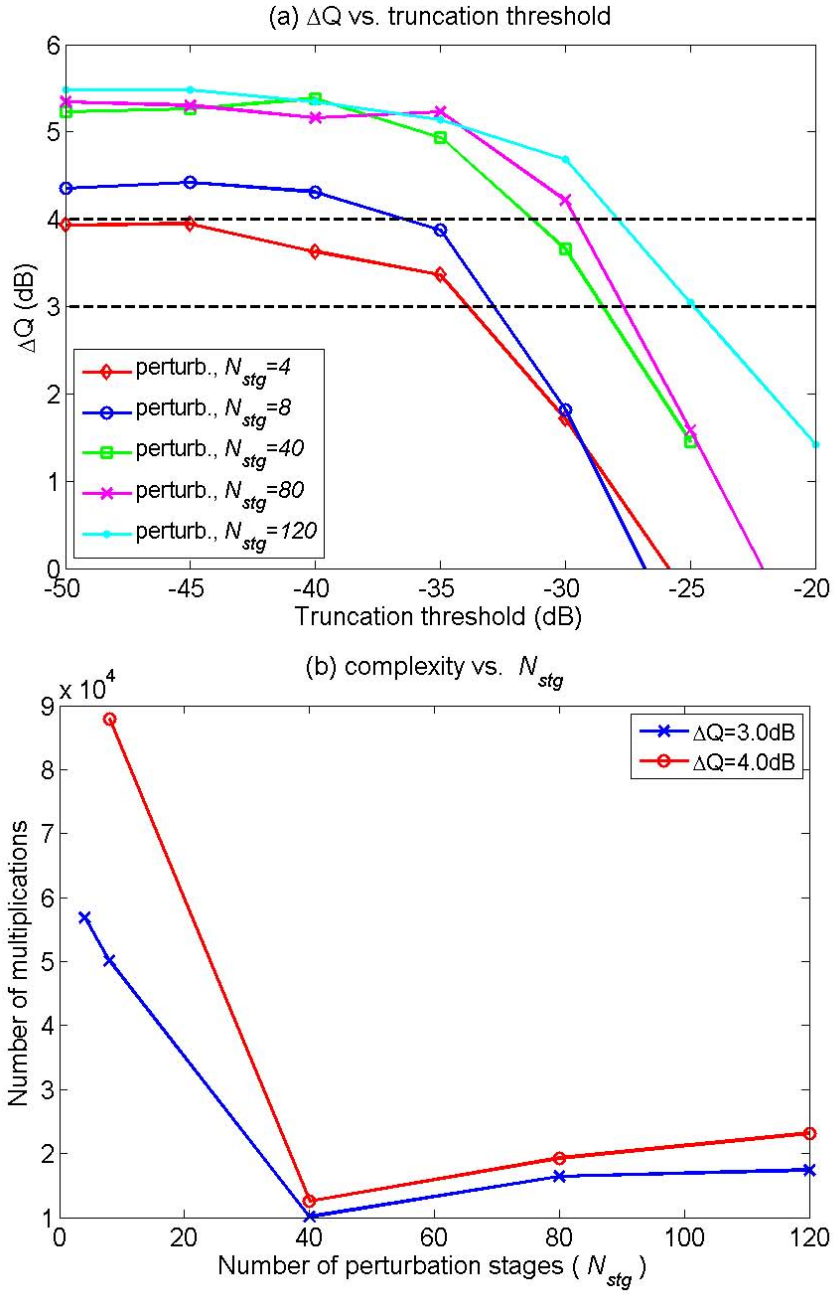

Figure 5.8: (a) Q-factor gain versus truncation threshold, (b) number of complex multiplications per symbol versus number of perturbation stages for given Q-factor gains. (2 samples/symbol are used. Reference Q-factor is 6.2 dB. Transmission distance is 3200 km.)

Figures 5.7(a) and 5.7(b) show that as the number of perturbation stage increases, the compensation performance increases and also the computational complexity decreases. Compared with the conventional single-stage compensation scheme with 1 sample/symbol, the multi-stage scheme with $N_{stg} = 8$ and 2 samples/symbol enhances the Q-factor improvement by 2.6 dB. To determine the optimum number of stages in terms of computational complexity for the given Q-factor gain, we first calculated the truncation threshold for the fixed Q-factor gain for various number of perturbation stages, as shown in Fig. 5.8(a). Since the computational complexity depends on both the truncation threshold and the number of perturbation stages, we calculate the number of complex multiplications per symbol as a function of number of perturbation stages for the fixed Q-factor gains of 3.0 dB and 4.0 dB, which is shown in Fig. 5.8(b). As can be seen, the number of multiplications per symbol decreases initially and then it increases when the number of stages is large. In this example, the optimum number of stages is 40, which is the same as the number of amplification stages. However, this optimal value may depend on the system configuration.

5.5 Conclusions

We have investigated a multi-stage scheme based on a recursive perturbation theory to compensate for intra-channel nonlinear impairments. The input signals of different compensation stages are expressed using the same basis functions so that the perturbation coefficient matrix X_{mn} is the same for all stages. The multi-stage compensation is implemented recursively. In each stage the first order theory is used to calculate the nonlinear distortions occurring in a distance much shorter than the entire fiber-optic link, which improves the accuracy and the summation of the signal

field and the first order field of the previous stage is used as the unperturbed solution for the next stage, which further improves the accuracy. Moreover, the accumulated dispersion in one compensation stage is much smaller than that of the entire link which significantly reduces the size of the matrix X_{mn}, leading to reductions both in computational complexity and the required memory for storing X_{mn}. Numerical simulations of a 28 Gbaud single-polarization single-channel fiber-optic system with 32-QAM and 40 $\times$ 80 km transmission distance show that, with 2 samples per symbol, the multi-stage scheme with eight compensation stages increases the Q-factor as compared with the linear compensation scheme by 4.5 dB; as compared with single-stage compensation, the computational complexity is reduced by a factor of 1.3 and the required memory for storing perturbation coefficients is decreased by a factor of 13.

Chapter 6

Ideal optical back propagation using dispersion-decreasing fiber

6.1 Introduction

The maximum reach of a long haul fiber optic system with advanced modulation formats is mainly limited by fiber nonlinear impairments. The back propagation techniques can be used to compensate for dispersion and nonlinear effects of the transmission fiber (TF). The compensation schemes can be divided into three types: digital [33–35, 37, 38, 74–77, 92, 100], optical [19–21, 101–105], and the combination of both [106]. The optical back propagation (OBP) has the following advantages/disadvantages over digital back propagation (DBP). (i) A very large bandwidth ($\sim$ 4 THz) is available for OBP while the bandwidth of the DBP is limited by the bandwidth of the coherent receiver. (ii) DBP requires significant computational resources, especially for wavelength division multiplexing (WDM) system and hence it

is currently limited to off-line signal processing. In contrast, OBP provides compensation in real time and it can compensate for nonlinear impairments in WDM systems. (iii) Number of samples per symbol available for DBP is limited by the sampling rate of the analog-to-digital converter (ADC). Although it is possible to do upsampling on the digital signal processor (DSP), it leads to additional computational complexity. However, for OBP, the signal processing is done on the analog optical waveform. (iv) OBP requires a real fiber which has loss. So, amplifiers are needed to compensate for fiber loss in the OBP section which increases the noise in the system.

In [20, 21], an OBP scheme consisting of optical phase conjugation (OPC), dispersion compensation fiber (DCF)/fiber Bragg grating (FBG), and highly nonlinear fiber (HNLF) is investigated. DCF/FBG is used to compensate for dispersion, and HNLF is used to compensate for nonlinearity. The dispersion and nonlinear effects are compensated in a split-step fashion analogous to split-step Fourier scheme (SSFS) used to solve the NLSE. Although this technique is quite effective for a single channel, for a WDM system, small step size is required and hence the insertion losses due to DCF/FBG and HNLF increase which limit the transmission performance. In this chapter, we investigate the possibility of introducing a single optical device which can exactly compensate for dispersion and nonlinearity. A dispersion-decreasing fiber (DDF) with a specific dispersion profile is found to meet our requirements [107].

In the proposed scheme, an OPC is placed at the end of the transmission link which is followed by N spans of DDFs where N is the number of TF spans. The DDFs introduce a small amount of losses which are compensated by amplifiers placed in the OBP section. Numerical simulation results show that the OBP with DDF outperforms DBP and midpoint-OPC schemes. The transmission reach of a WDM

system can be significantly enhanced using the proposed scheme as compared to linear compensation in the receiver or DBP. We found that the DBP is limited mainly by the sampling rate of the ADC.

Existing digital compensation schemes including DBP and perturbation-based techniques compensate for fiber nonlinear effects based on the information of signal propagation path and link parameters such as dispersion profiles and nonlinear coefficient. Such compensation schemes can be easily implemented in a point-to-point link. However, in the case of network communications, the implementations of DBP and perturbation-based techniques become difficult since the signal propagation path and link parameters become much complicated due to the complex network mesh and the presence of add/drop multiplexers. The OBP scheme with DDF is a potential compensation scheme for the network communication systems. If the compensation block with a DDF and amplifier is placed after the transmission fiber in each span (other than at the receiver only), the signal impairments of the transmission fiber will be fully compensated by the following compensation block. As a result, the compensation of a certain signal channel becomes independent of its propagation path and independent of the added/dropped channels within the propagation path.

6.2 Optical back propagation theory

The evolution of the optical field envelope in a fiber optic link is described by the NLSE (see Eq. 2.1 in Chapter 2):

$$\frac{\partial q}{\partial z} = i[D(t) + N(t,z)]q(t,z), \tag{6.1}$$

$$D(t) = -\frac{\beta_2(z)}{2}\frac{\partial^2}{\partial t^2}, \quad N(t,z) = \gamma|q(t,z)|^2 + i\frac{\alpha}{2}, \tag{6.2}$$

where β_2, γ and α are dispersion, nonlinear and loss coefficients of TF, respectively. The formal solution of Eq. (6.1) for a single span of TF is

$$q(t,L_a) = \exp\left\{i\int_0^{L_a}[D(t)+N(t,z)]dz\right\}q(t,0). \tag{6.3}$$

Here L_a is the fiber length. Let the output signal field of the fiber pass through an OPC, as shown in Fig. 6.1(a). The output of the OPC is

$$q^*(t,L_a) = \exp\left\{-i\int_0^{L_a}[D(t)+N^*(t,z)]dz\right\}q^*(t,0). \tag{6.4}$$

Let the output of OPC propagate through an ideal optical back propagation fiber

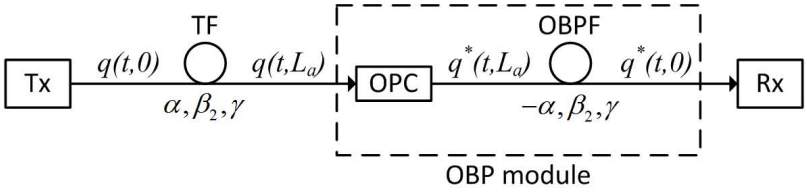

(a)

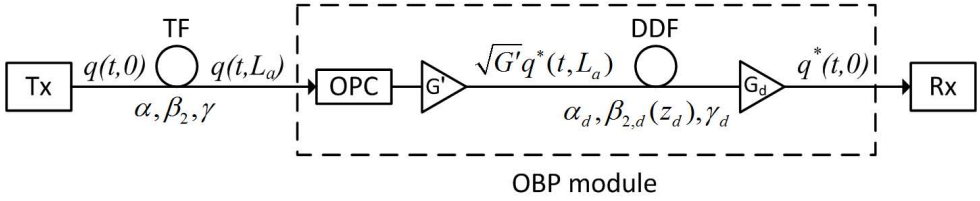

(b)

Figure 6.1: A single-span fiber optic system with (a) OBP using an ideal optical back propagation fiber with negative loss coefficient, (b) OBP using a DDF and amplifiers. Tx: transmitter, TF: transmission fiber, OPC: optical phase conjugator, OBPF: optical back propagation fiber, DDF: dispersion-decreasing fiber, Rx: receiver.

(OBPF) that is identical to the TF except that the sign of the loss coefficient of OBPF is inverted. In this case, from Eq. (6.2), we see that the nonlinear operator corresponding to OBPF is $N^*(t,z)$. Using Eq. (6.4), the output of the OBPF is

$$q_{OBPF,out}(t) = e^{i\int_0^{La}[D(t)+N^*(t,z)]dz} q^*(t,L_a) \tag{6.5}$$

$$\begin{aligned} &= e^{i\int_0^{La}[D(t)+N^*(t,z)]dz} e^{-i\int_0^{La}[D(t)+N^*(t,z)]dz} q^*(t,0) \\ &= q^*(t,0). \end{aligned} \tag{6.6}$$

Thus, the input field envelope can be recovered by performing a phase conjugation in the electrical domain at the receiver. Eq. (6.5) is equivalent to

$$\frac{\partial q_b}{\partial z_b} = i[D(t) + N^*(t,z_b)]q_b(t,z_b), \tag{6.7}$$

with $q_b(t,0) = q^*(t,L_a)$, and z_b is the distance in OBPF. Using

$$q_b = \sqrt{P_{in}} e^{-\alpha(L_a - z_b)/2} u_b, \tag{6.8}$$

and

$$dz_b' = \beta_2 dz_b, \tag{6.9}$$

Eq. (6.7) can be rewritten as

$$i\frac{\partial u_b}{\partial z_b'} - \frac{1}{2}\frac{\partial^2 u_b}{\partial t^2} + \frac{\gamma P_{in}}{\beta_2} e^{-\alpha(L_a - z_b)} |u_b|^2 u_b = 0, \tag{6.10}$$

where P_{in} is the power launched to the TF. Eq. (6.10) describes the field propagation in an ideal fiber with a constant β_2 and a negative loss coefficient (or equivalently the

power increasing with distance) that exactly compensates for dispersion and nonlinearity of the TF. However, it is hard to realize such a fiber in practice. For an ideal OBP, we like to have a short length of a fiber (so that its insertion loss is small) which provides the same response as that of the ideal OBPF given by Eq. (6.10). Here, we derive an equivalent way of realizing Eq. (6.10) by using amplifiers and a DDF with positive loss coefficient α_d and a dispersion profile $\beta_{2,d}(z_d)$ [see Fig. 6.1(b)]. The optical field envelope in the DDF is described by

$$i\frac{\partial q_b}{\partial z_d} - \frac{\beta_{2,d}(z_d)}{2}\frac{\partial^2 q_b}{\partial t^2} + \gamma_d|q_b|^2 q_b + i\frac{\alpha_d}{2}q_d = 0, \tag{6.11}$$

where α_d and γ_d are the loss and nonlinear coefficients of DDF, respectively, z_d is the distance in the DDF, $q_b(t,0) = \sqrt{G'}q^*(t,L_a)$, and G' is the gain of the amplifier preceding DDF. Using transformations

$$q_d = \sqrt{P_d}e^{-\alpha_d z_d/2}u_b, \tag{6.12}$$

and

$$dz'_d = \beta_{2,d}(z_d)dz_d, \tag{6.13}$$

Eq. (6.11) can be rewritten as

$$i\frac{\partial u_b}{\partial z'_b} - \frac{1}{2}\frac{\partial^2 u_b}{\partial t^2} + \frac{\gamma_d P_d e^{-\alpha_d z_d}}{\beta_{2,d}(z_d)}|u_b|^2 u_b = 0, \tag{6.14}$$

where $P_d = GP_{in} = G'e^{-\alpha L_a}P_{in}$ is the input power of the DDF. Eqs. (6.10) and (6.14) are identical only if

$$dz'_b = dz'_d, \tag{6.15}$$

and

$$\frac{\gamma P_{in}}{\beta_2} e^{-\alpha(L_a - z_b)} = \frac{\gamma_d P_d e^{-\alpha_d z_d}}{\beta_{2,d}(z_d)}. \tag{6.16}$$

Substituting Eqs. (6.9) and (6.13) in Eq. (6.15), we find

$$\beta_2 \frac{dz_b}{dz_d} = \beta_{2,d}(z_d), \tag{6.17}$$

$$w \equiv \beta_2 z_b = \int_0^{z_d} \beta_{2,d}(z_d) dz_d, \tag{6.18}$$

$$\frac{dw}{dz_d} = \beta_{2,d}(z_d), \tag{6.19}$$

Substituting Eqs. (6.18) and (6.19) in Eq. (6.16), we obtain

$$\frac{dw}{dz_d} e^{\alpha w/\beta_2} = \left(\frac{\gamma_d P_d \beta_2}{\gamma P_{in}}\right) e^{\alpha L_a} e^{-\alpha_d z_d}. \tag{6.20}$$

Integrating Eq. (6.20), we find

$$\frac{\beta_2}{\alpha}\left(e^{\frac{\alpha}{\beta_2} w(z_d)} - 1\right) = \left(\frac{\gamma_d P_d}{\gamma P_{in}}\right) e^{\alpha L_a} \frac{1 - e^{-\alpha_d z_d}}{\alpha_d}. \tag{6.21}$$

Simplifying Eq. (6.21), we obtain

$$w(z_d) = \frac{\beta_2}{\alpha} \ln\left(1 + \frac{\gamma_d G \alpha}{\gamma e^{-\alpha L_a}} \frac{1 - e^{-\alpha_d z_d}}{\alpha_d}\right), \tag{6.22}$$

$$\beta_{2,d} = \frac{e^{-\alpha_d z_d}}{\frac{\gamma e^{-\alpha L_a}}{\gamma_d G} + \alpha\left(\frac{1 - e^{-\alpha_d z_d}}{\alpha_d}\right)} \beta_2. \tag{6.23}$$

The length of DDF L_d is found as follows. Total accumulated dispersion of the ideal OBPF [Fig. 6.1(a)] should be the same as that of the DDF, i.e.,

$$\beta_2 L_a = w(L_d) = \int_0^{L_d} \beta_{2,d}(z_d) dz_d, \tag{6.24}$$

or

$$L_d = -\frac{1}{\alpha_d} \ln \left[1 - \frac{\alpha_d \gamma e^{-\alpha L_a}}{\gamma_d G \alpha} \left(e^{\alpha L_a} - 1 \right) \right]. \tag{6.25}$$

If the dispersion profile of the DDF is tailored to satisfy Eq. (6.23), the combination of the amplifiers and DDF provides the ideal response described by Eq. (6.10), and hence, signal-signal nonlinear interactions can be exactly compensated. The amplifier with gain $G_d = e^{\alpha_d L_d}$ is introduced after the DDF [see Fig. 6.1(b)] to compensate for the loss of DDF. Fig. 6.2 shows the dispersion profiles of DDF that satisfy Eq. (6.23). As can be seen, relatively shorter length of DDF can compensate for the dispersion and nonlinear effects of the TF.

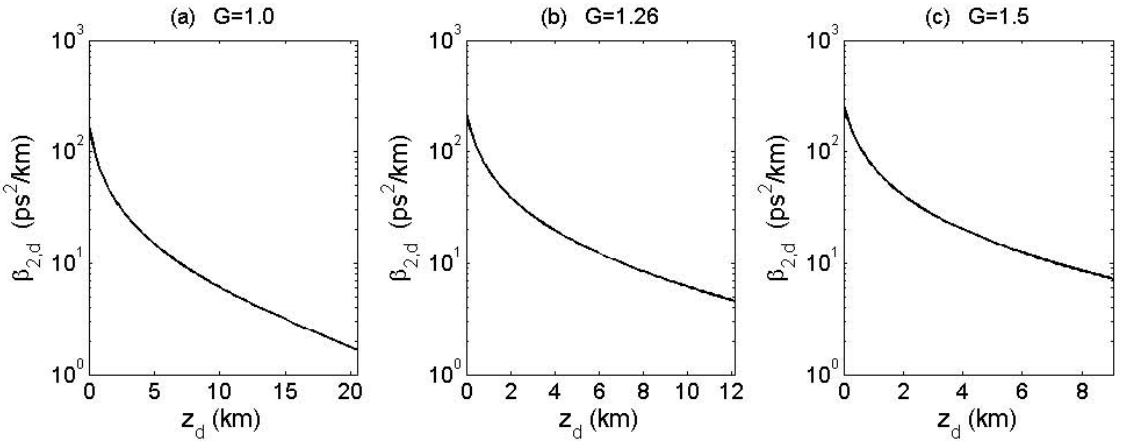

Figure 6.2: Dispersion profiles of DDF. TF parameters: α=0.2 dB/km, β_2=5 ps^2/km, γ=2.2 W^{-1}km^{-1}, L_a=60 km. DDF parameters: α_d=0.4 dB/km, γ_d=4.86 W^{-1}km^{-1}. (a) G=1.0: $\beta_{2,d}(0)$=175.1 ps^2/km, L_d=20.5 km, (b) G=1.26: $\beta_{2,d}(0)$=220.6 ps^2/km, L_d=12.1 km, (c) G=1.5: $\beta_{2,d}(0)$=262.6 ps^2/km, L_d=9.0 km.

So far we considered the compensation of dispersion and nonlinearity of a single-span fiber optic link. For a multiple-span transmission system, Fig. 6.3 shows the schematic of a WDM fiber optic transmission system consisting of M transmitters, N spans of TFs, the OBP module, and M coherent receivers. The OBP is applied at the end of the transmission link. A pre-amplifier with gain G is introduced so that the required dispersion profile and length of the DDF can be adjusted according to Eqs. (6.23) and (6.25), respectively. A band pass filter (BPF) is introduced to remove the out of band amplified spontaneous emission (ASE) noise. During back propagation, amplifiers with gain G_d are used to fully compensate for the loss of each span of DDF.

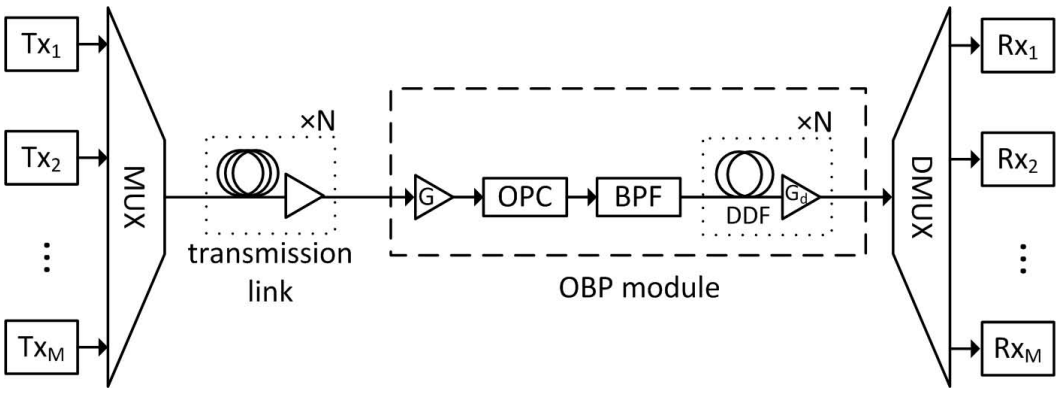

Figure 6.3: Schematic diagram of a WDM fiber optic transmission system with OBP. MUX: multiplexer, BPF: band pass filter, DMUX: demultiplexer.

In DBP, the compensation of fiber dispersion and nonlinearity is implemented in a step-wise manner and the performance is usually limited by the step size which has to be traded off against computational cost or system complexity. In WDM systems, the required computational load may prevent DBP from real time implementation. In the OBP with DDF, the compensation of dispersion and nonlinearity is realized by a gradually decreasing dispersion profile, which inherently has a very small step

size. The DDF with exponentially dispersion decreasing fibers have been fabricated before [108, 109]. The step size of the order of a few meters in DDF can be realized and hence, nearly ideal OBP can be realized using DDF. The DDF can be fabricated by tapering the fiber during drawing process which alters the waveguide contribution to the dispersion [108]. The maximum dispersion required for OBP fiber is of the same order as the commercially available dispersion compensation fiber and of the same sign.

DBP compensates for fiber nonlinear effects based on the information of signal propagation path and link parameters such as dispersion profiles and nonlinear coefficient, which can be easily implemented in a point-to-point link. However, in the case of network communications, the implementation of DBP becomes difficult since the signal propagation path and link parameters become much complicated due to the complex network mesh and the presence of add/drop multiplexers. The OBP scheme with DDF is a potential compensation scheme for network communication systems. If the OBP compensation module is placed after the transmission fiber in each span (other than at the receiver only), the signal impairments of the transmission fiber will be fully compensated by the following OBP module. As a result, the compensation of a certain signal channel becomes independent of its propagation path and independent of the added/dropped channels within the propagation path.

6.3 Simulation results and discussions

We simulate a WDM fiber optic transmission system with OBP at the receiver with the following parameters: number of WDM channels = 5, channel spacing = 100

GHz, symbol rate per channel = 25 Gsymbols/s, modulation = 32 quadrature amplitude modulation (QAM), number of symbols simulated = 32768 per channel. The linewidths of the transmitter and local oscillator lasers are 100 kHz each. The dispersion, loss, and nonlinear coefficients of the TF are $\beta_2 = 5$ ps^2/km, $\alpha = 0.2$ dB/km, and $\gamma = 2.2$ W^{-1}km^{-1}, respectively. This type of fiber has been fabricated before and it is known as negative dispersion fiber (NDF) [110, 111]. Typically, standard single mode fiber (SSMF) is used as transmission fiber in optic communication systems. We choose NDF (with a negative dispersion) as the transmission fiber so that the required dispersion profile of corresponding DDFs is easier to fabricate in practice. We note that a large negative dispersion fiber is easy to make than one with a large positive dispersion coefficient. The amplifier spacing is 60 km, and the spontaneous emission noise factor is $n_{sp} = 1.5$. The BPF shown in Fig. 6.3 is a second order Gaussian filter with full bandwidth of 450 GHz. For the DDF, $\alpha_d = 0.4$ dB/km, $\gamma_d = 4.86$ W^{-1}km^{-1}, and $L_d = 12.1$ km [see Fig. 6.2(b)]. The corresponding amplifier gain for compensating the DDF loss is 4.84 dB. In all the simulations, 32 samples per symbol are used in the transmission link so as to obtain a frequency window covering all the WDM channels. In DBP simulations, 2 samples per symbol are used after the ADC unless otherwise specified, while in OBP simulations, back propagation is in the optical domain and 32 samples per symbol are used. Using the method of [35], the coupled NLSE is used to compensate for the inter-channel nonlinear impairments ignoring four-wave mixing (FWM). However, the OBP scheme compensates for both cross-phase modulation (XPM) and FWM simultaneously. The central channel is demultiplexed using a second order Gaussian filter with full bandwidth of 50 GHz. In the coherent receiver, for OBP, two samples per symbol are used after the ADC and

phase noise compensation is done using the approach of Ref. [91]. A low pass filter (LPF) of bandwidth 25 GHz is used prior to phase noise compensation. For the DBP scheme, coupled NLSE is solved in digital domain prior to phase noise compensation. The optical and electrical filter bandwidths are optimized in both OBP and DBP schemes.

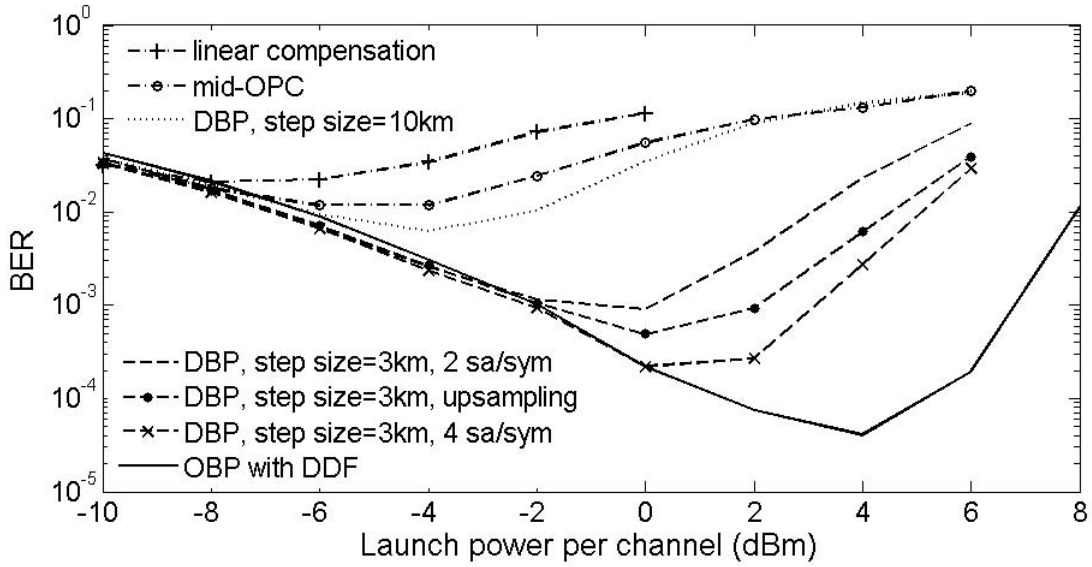

Figure 6.4: BER versus launch power per WDM channel. (Number of WDM channels = 5, transmission distance = 1200 km.)

Fig. 6.4 shows the bit error ratio (BER) as a function of the launch power per WDM channel when the transmission distance is 1200 km. The solid curve represents the BER of OBP using DDFs, and the dashed and dotted curves represent the BER of DBP with 3 km and 10 km step sizes, respectively. The DBP step size of the simulated WDM system is limited by the walk-off length [35], which is 3.2 km. We found that there is no obvious performance improvement when a step size smaller than 3 km is chosen for DBP, consistent with the results of Ref. [35]. Also, Fig. 6.4 shows the simulation results of DBP with 4 samples/symbol ADC sampling rate and

DBP with DSP upsampling [33] from 2 to 4 samples/symbol. The DBP performance can be improved by increasing ADC sampling rate or DSP upsampling, at the cost of increased system complexity and computational cost. The OBP outperforms DBP (2 samples/symbol, step size = 3 km) by 2.0 dB in Q-factor. The relatively poor performance of DBP as compared to OBP is mainly due to the down sampling penalty and the lack of FWM compensation. The performance of midpoint OPC is worse than DBP, because the power profile is unsymmetrical with respect to the location of OPC. The performance of OBP is worse than that of DBP (with step size = 3 km) when the launch power is less than -2 dBm which is due to the optical signal to noise ratio (OSNR) penalty resulting from OBP amplifiers. The OSNR penalty due to OBP amplifiers is found to be 0.56 dB. From Fig. 6.4, it can also be seen that the DBP with a step size of 10 km performs worse than the DBP with a step size of 3 km even at lower launch powers (-10 dBm to -6 dBm) due to residual nonlinearity. The curve with "+" shows the case where no OBP (or DBP) is applied and fiber dispersion and laser phase noise are compensated in the receiver. As can be seen, the performance of this system is much worse than the system with DBP or OBP.

Fig. 6.5 shows the minimum BER as a function of transmission distance. The BER_{min} is obtained by optimizing the launch power for each distance. At the BER of 2.1×10^{-3}, the transmission reaches of linear compensation only and midpoint OPC are 300 km and 360 km, respectively. For DBP with a 10 km step size and 2 samples/symbol sampling rate, the reach is 760 km, which can be increased to 1600 km by using a 3 km step size at the cost of more than tripling the computational effort. The transmission reach of OBP with DDF is 2460 km. Although the OBP fully compensates for signal-signal nonlinear interactions, it neither compensates for

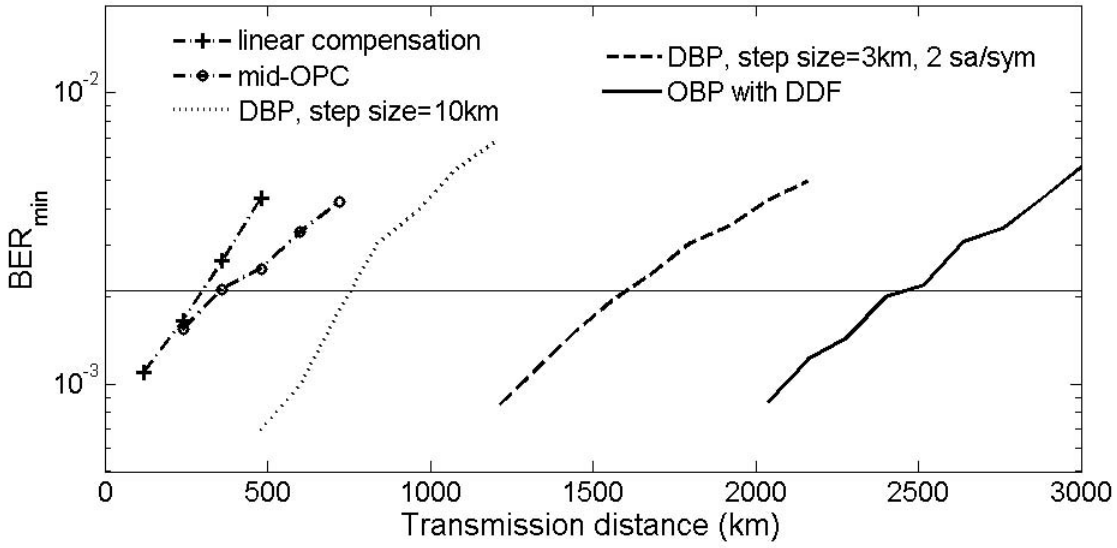

Figure 6.5: BER_{min} versus transmission distance. OSNR is 30.5 dB at the output of the fiber-optic link when launch power per channel is 0 dBm.

signal-ASE nonlinear interactions [10, 94, 112] nor mitigates nonlinear polarization mode dispersion (PMD) [9], which are the limiting factors to enhance the reach in systems based on OBP. Instead of placing the OBP module at the receiver, it can be placed at each of the amplifier location. In such a scheme, signal-ASE nonlinear interactions can be compensated and better performance is expected.

6.4 Conclusions

We have investigated the performance of an OBP scheme consisting of an OPC and N spans of DDFs followed by amplifiers to compensate for dispersion and nonlinear effects of an N-span fiber optic WDM system. We have identified the conditions under which the nonlinear effects (both intra- and inter-channel nonlinearities) can be fully compensated and obtained an analytical expression for the novel dispersion

profile of the DDF which provides the exact compensation of intra- and inter-channel signal-signal nonlinear impairments. The performance of the proposed OBP scheme is compared with DBP and midpoint OPC and simulation results show that the transmission reach can be significantly enhanced using the OBP with DDF. The OBP scheme with DDF is also potential for applications in network communication systems by placing the OBP module after the transmission fiber in each span.

Chapter 7

Impulse response of nonlinear Schrödinger equation and its implications for pre-dispersed fiber-optic communication systems

7.1 Introduction

The propagation dynamics of the pulse in a cubically nonlinear dispersive medium such as an optical fiber is described by the nonlinear Schrödinger equation (NLSE) [113, 114]. Optical soliton is a normal mode of the nonlinear system described by the NLSE, which can be integrated by means of inverse scattering transform (IST) [115, 116]. Zakharov and Shabat [114] solved the NLSE using IST and obtained soliton and breather solutions. The breathers or higher order solitons undergo periodic

compression and expansion with a soliton period. Impulse response approach to nonlinear dispersive propagation in fiber has been studied in the past [117, 118]. In Ref. [117] , the impulse response approach of linear system is extended to nonlinear system using a self-consistent time-transformation. In Ref. [118], an impulse response approach is used to calculate the multiplicative correction due to the interplay between chromatic dispersion and Kerr nonlinearity. In this chapter, we obtain an exact solution of the NLSE for an impulse input [119]. However, we found that there is a singularity in the phase. To remove this singularity, we introduced pre-dispersion which can be added either in electrical domain at the transmitter or in optical domain prior to transmission. The exact solution in this case has a phase factor which is described by the exponential integral. Next, we investigated the nonlinear interaction among pulses in a fiber due to periodically placed impulses at the input and analyzed the conditions under which they propagate over long distances without exchanging energy among them [119].

When a cluster of continuous wave (CW) beams of different frequencies propagate in optical fiber, they exchange energy through the process known as four wave mixing (FWM). Eventually the amplitudes of CW beams reach an equilibrium in which there is no exchange of energy among them and they take secant-hyperbolic shape corresponding to soliton spectrum. There exists an alternate explanation in time domain. The dual of classical FWM is time-domain FWM or intra-channel FWM (IFWM) [44, 83, 120, 121] and the dual of CW signal is a Dirac delta function in time domain (CW signal is an impulse function in frequency domain). When a cluster of closely spaced impulses propagate in fiber, they exchange energy through IFWM. However, if the weights of the impulses have secent-hyperbolic shapes, they do not

exchange energy and propagate stably as solitons over long distances. In order to have soliton propagation, the impulses have to be infinitesimally closer. In this chapter, we have investigated if it is possible to propagate a large number of periodically placed impulses over large distances without exchanging energy among them. We found that if the impulse weights at the input have a secant-hyperbolic shape and a proper chirp factor, they propagate without change in shape over long distances just like the soliton of NLSE [119]. The amplitude of the soliton solution depends on system parameters such as pre-accumulated dispersion, separation between the impulses and the dispersion of the transmission fiber. When the impulses are infinitesimally closer, this solution becomes the classical soliton of the continuous NLSE. We have derived a discrete NLSE which describes the evolution of the discrete Fourier transform of the product of the impulse weights and a chirp factor. We note that the discrete NLSE can be easily obtained by discretizing the continuous NLSE. In such a discrete NLSE, the dispersion term would be directly proportional to fiber dispersion coefficient. However, in the discrete NLSE derived here, the effective dispersion term is inversely proportional to the square of the accumulated dispersion and the effective nonlinear term is inversely proportional to the absolute accumulated dispersion. It is not yet known if the discrete NLSE derived here can be integrated by IST. However, we have numerically found that the discrete NLSE admits higher order soliton solutions which undergo periodic compression and expansion with a certain period, similar to its continuous analogue.

In the context of discrete NLSE, if the effective dispersion length is much longer than the effective nonlinear length, the equation becomes significantly simplified. In this case, intra-channel cross-phase modulation (IXPM) and IFWM [2, 44, 83,

120, 121] vanish in the transformed system. We have obtained nonlinear eigenmodes which form the natural basis for description of signal propagation and signal and noise nonlinear interaction in highly pre-dispersed fiber-optic systems.

7.2 Impulse response

The evolution of optical field envelope is described by NLSE (see Eq. 2.3 in Chapter 2)

$$i\frac{\partial u}{\partial z} - \frac{\beta_2}{2}\frac{\partial^2 u}{\partial t^2} + \gamma_0 e^{-\alpha z}|u|^2 u = 0, \tag{7.1}$$

where α, β_2, and γ_0 are the loss, dispersion and nonlinear coefficients, respectively. In a linear fiber ($\gamma_0 = 0$), when an impluse is launched,

$$u(t,0) = A\delta(t), \tag{7.2}$$

the optical field in the fiber is

$$u(t,z) = \frac{A}{\sqrt{-i2\pi\beta_2 z}} e^{-i\frac{t^2}{2\beta_2 z}}. \tag{7.3}$$

In the presence of nonlinearity, we look for a solution of Eq. (7.1) in the form,

$$u(t,z) = \frac{A}{\sqrt{-i2\pi\beta_2 z}} e^{-i\frac{t^2}{2\beta_2 z}+iv(z)}, \tag{7.4}$$

Substituting Eq. (7.4) in Eq. (7.1), we obtain

$$\frac{A}{\sqrt{-i2\pi\beta_2 z}}\left[-\frac{i}{2z}-\frac{t^2}{2\beta_2 z^2}-\frac{dv(z)}{dz}+\frac{\beta_2}{2}\left(\frac{i}{\beta_2 z}+\frac{t^2}{\beta_2^2 z^2}\right)+\gamma_0 e^{-\alpha z}\frac{|A|^2}{2\pi|\beta_2|z}\right]=0. \tag{7.5}$$

Simplifying Eq. (7.5), we obtain

$$v(z)=\frac{\gamma_0|A|^2}{2\pi|\beta_2|}\int_0^z\frac{e^{-\alpha x}}{x}dx. \tag{7.6}$$

The integrand of Eq. (7.6) has a singularity, which should be expected due to the impulse input. The singularity can be avoided by using pre-dispersion. Suppose

$$\beta_2(z)=\begin{cases}\beta_{2-}, & \text{for } z<0\\ \beta_{2+}, & \text{for } z>0\end{cases} \tag{7.7}$$

$$\gamma=\begin{cases}0, & \text{for } z<0\\ \gamma_0, & \text{for } z>0.\end{cases} \tag{7.8}$$

Let $s_0=\int_{-L}^{0}\beta_{2-}(z)dz$ be the pre-accumulated dispersion. The pre-dispersion can be realized using a high dispersion fiber prior to transmission fiber or a digital dispersion filter in the digital signal processing (DSP) unit of the optical transmitter [2, 28]. Now for $z>0$, Eqs. (7.4) and (7.6) are modified as

$$u(t,z)=\frac{A}{\sqrt{-i2\pi s(z)}}e^{-i\frac{t^2}{2s(z)}+i\gamma_0\frac{|A|^2}{2\pi}\theta(z)}, \tag{7.9}$$

$$\theta(z)=\int_0^z\frac{e^{-\alpha x}}{s(x)}dx, \tag{7.10}$$

$$s(z) = s_0 + \beta_{2+} z. \tag{7.11}$$

$\theta(z)$ in Eq. (7.9) does not diverge only if $s_0 + \beta_{2+} z$ does not cross 0 for any z. In this chapter, we assume that pre-accumulated dispersion s_0 has the same sign as β_{2+} so that $s(z)$ does not cross 0. Under this condition, Eq. (7.10) can be written in a closed form as [122]

$$\theta(z) = e^{\alpha s_0/\beta_{2+}} \left[\mathrm{Ei}\left(\frac{-\alpha s(z)}{\beta_{2+}}\right) - \mathrm{Ei}\left(\frac{-\alpha s_0}{\beta_{2+}}\right)\right], \tag{7.12}$$

where $\mathrm{Ei}(x)$ is the exponential integral.

$$\mathrm{Ei}(x) = -\int_{-x}^{\infty} \frac{e^{-t}}{t} dt. \tag{7.13}$$

Equation (7.9) is an exact solution of the NLSE when the input (at $z = -L$) is a single impulse. Suppose the input consists of a train of impluses,

$$u_{in}(t) = \sum_{n=-N/2}^{N/2-1} A_n \delta(t - nT), \tag{7.14}$$

where N is the number of impulses, which is assumed to be large. The optical field in the transmission fiber for this input may be written as

$$u(t,z) = \sum_{n=-N/2}^{N/2-1} \frac{A_n(z) e^{-i(t-nT)^2/2s(z)}}{\sqrt{-i2\pi s(z)}}, \quad \text{for } z \geq 0. \tag{7.15}$$

In the absence of nonlinear interaction with the neighboring pulses, we have

$$A_n(z) = A_n(0) e^{i\gamma_0 |A_n(0)|^2 \theta(z)/2\pi}. \tag{7.16}$$

Equation (7.16) includes the effect of self-phase modulation (SPM) only. However, due to IXPM and IFWM, [44, 83, 120, 121] the pulses undergo amplitude/phase shifts. Substituting Eq. (7.15) in Eq. (7.1), we find

$$i\sum_n \frac{dA_n}{dz} e^{-i\frac{(t-nT)^2}{2s(z)}} + \frac{\gamma_0 e^{-\alpha z}}{2\pi|s(z)|}\sum_k\sum_l\sum_m A_k A_l A_m^* F_{klm} = 0, \tag{7.17}$$

where $F_{klm} = e^{-i\left[(t-kT)^2+(t-lT)^2-(t-mT)^2\right]/2s(z)}$. Multiplying Eq. (7.17) by $e^{i(t-jT)^2/2s(z)}$ and integrating from $-t$ to t with $t\to\infty$, we find

$$i\sum_n \frac{dA_n}{dz}\delta_{jn} + \frac{\gamma_0 e^{-\alpha z}}{2\pi|s(z)|}\sum_k\sum_l\sum_m A_k A_l A_m^* Y_{klm,j} = 0, \tag{7.18}$$

where δ_{jn} is a Kronecker delta function and

$$\begin{aligned} Y_{klm,j} &= \lim_{t\to\infty}\frac{1}{2t}\int_{-t}^{t} F_{klm} e^{i(\tau-jT)^2/2s(z)} d\tau \\ &= \lim_{t\to\infty}\frac{1}{2t} e^{-i(k^2+l^2-m^2-j^2)T^2/2s(z)}\int_{-t}^{t} e^{i(k+l-m-j)\tau T/s(z)} d\tau. \end{aligned} \tag{7.19}$$

$Y_{klm,j}$ will be non-zero only if $m = k+l-j$. In this case,

$$Y_{klj} \equiv Y_{klm,j} = e^{-i\left[k^2+l^2-(k+l-j)^2-j^2\right]T^2/2s(z)}. \tag{7.20}$$

So, now Eq. (7.18) becomes

$$i\frac{dA_j}{dz} + \frac{\gamma_0 e^{-\alpha z}}{2\pi|s(z)|}\sum_k\sum_l A_k(z) A_l(z) A_{k+l-j}^* Y_{klj} = 0. \tag{7.21}$$

In the absence of nonlinear effects ($\gamma_0 = 0$), from Eq. (7.21) we find

$$\frac{dA_j}{dz} = 0, \tag{7.22}$$

which indicates that there is no interaction among pulses in a linear medium. Let

$$U_k(z) = e^{-ik^2T^2/2s(z)}, \tag{7.23}$$

where k is an integer. Equation (7.20) may be written as

$$Y_{klj} = U_k U_l U^*_{k+l-j} e^{ij^2T^2/2s(z)}. \tag{7.24}$$

Let

$$B_k(z) = A_k(z)U_k(z). \tag{7.25}$$

Using Eqs. (7.23)-(7.25) in Eq. (7.21), we find

$$i\frac{dB_j}{dz} + \frac{j^2T^2\beta_{2+}}{2s^2(z)}B_j + \frac{\gamma_0 e^{-\alpha z}}{2\pi|s(z)|}\sum_k\sum_l B_k B_l B^*_{k+l-j} = 0. \tag{7.26}$$

The second term is similar to dispersion in NLSE. If we take the Fourier transform of Eq. (7.1), the second term would be $\beta_2\omega^2\widetilde{u}(\omega,z)/2$, where $\widetilde{u}(\omega,z) = \mathcal{F}\{u(t,z)\}$, $\mathcal{F}$ denotes the Fourier transformation. Therefore, in Eq. (7.26), $\beta_{2+}/s^2(z)$ may be interpreted as the effective dispersion. However, unlike $u(t,z)$, $B_j(z)$ is a discrete variable and hence, we consider the discrete Fourier transform,

$$\mathrm{DFT}\{B_j; j \to m\} = \widetilde{B}_m = \sum_{j=-N/2}^{N/2-1} B_j e^{-i2\pi jm/N}. \tag{7.27}$$

Taking the discrete Fourier transform of Eq. (7.26) and noting that a convolution becomes product in spectral domain (and vice versa), we find

$$i\frac{d\widetilde{B}_m}{dz} - \frac{\beta_{2+}T^2}{2s^2(z)}\sum_{k=-N/2}^{N/2-1}\widetilde{B}_{m-k}\widetilde{x}_k + \frac{\gamma e^{-\alpha z}}{2\pi|s(z)|}|\widetilde{B}_m|^2\widetilde{B}_m = 0, \tag{7.28}$$

where

$$\widetilde{x}_k = \mathrm{DFT}\{j^2; j \to k\}. \tag{7.29}$$

Equation (7.28) may be interpreted as a discrete analogue of the NLSE. Since A_n may be interpreted as signal sample at nT, a discrete NLSE can be easily obtained for A_n [123, 124]. In such a discrete NLSE, the dispersion term would be directly proportional to fiber dispersion coefficient. However, in Eq. (7.28), the effective dispersion term is inversely proportional to the square of accumulated dispersion and the effective nonlinear term is inversely proportional to the absolute accumulated dispersion. The discrete NLSE in Eq. (7.28) does not describe A_n, instead it describes the evolution of the DFT of B_n which is the product of A_n and U_n. In the absence of pre-dispersion ($s_0 = 0$), the effective dispersion term and the effective nonlinear term of Eq. (7.28) diverge at $z = 0$ and hence, pre-dispersion is essential for the solution of Eq. (7.28). In the terminology of Ref. [124], Eq. (7.28) is a discrete self-trapping (DST) equation of the form [125],

$$i\frac{d\widetilde{B}_m}{dz} + \epsilon\sum_k m_{jk}\widetilde{B}_k + \gamma|\widetilde{B}_m|^2\widetilde{B}_m = 0, \tag{7.30}$$

where $[m_{jk}]$ is a $f \times f$ coupling matrix. In Eq. (7.1), when $\alpha = 0$, dispersion and nonlinear coefficients are constants for $z > 0$ and hence, it admits soliton solutions.

However, in Eq. (7.28), the effective dispersion and nonlinear coefficients are varying with distance due to $s(z)$. If we choose the pre-dispersion such that $s_0 >> \beta_{2+} L_{tr}$ where L_{tr} is the length of the transmission fiber, we can approximate $s(z)$ as s_0. In this case with $\alpha = 0\ km^{-1}$, we look for a soliton solution of Eq. (7.28) in the form

$$\widetilde{B}_m(z) = \widetilde{B}_0 \text{sech}\left(\frac{m}{M}\right) e^{i\mu(z)}. \tag{7.31}$$

Equation (7.28) is numerically solved using the split-step Fourier method with the initial condition,

$$\widetilde{B}_m(0) = \widetilde{B}_0 \text{sech}\left(\frac{m}{M}\right). \tag{7.32}$$

Figure 7.1 shows the evolution of $|\widetilde{B}_m|^2$ in the transmission fiber. As can be seen, when $\widetilde{B}_0$ is less than a threshold $\widetilde{B}_{th}$, we see the broadening effect and when $\widetilde{B}_0 = \widetilde{B}_{th}$, the pulse shape is retained throughout. Figure 7.2 shows the evolution of $|B_n|^2$ obtained by taking the inverse discrete Fourier transform (IDFT) of $\widetilde{B}_m$. As can be seen, when $\widetilde{B}_0 < \widetilde{B}_{th}$ (Fig. 7.2a), the envelope of $|B_n|^2 (= |A_n|^2)$ becomes narrower which indicates that the pulses exchange energy among them resulting in the pulse at the center ($n = 0$) becoming stronger. When $\widetilde{B}_0 = \widetilde{B}_{th}$, pulses propagate long distances without exchanging energy among them.

Figure 7.3 shows the similar result by solving Eq. (7.1). The impulses of Eq. (7.14) are approximated by Gaussian pulses of short pulse widths,

$$A_n \delta(t - nT) \rightarrow \frac{A_n}{\sqrt{2\pi} T_0} e^{-\frac{(t-nT)^2}{2T_0^2}}, \tag{7.33}$$

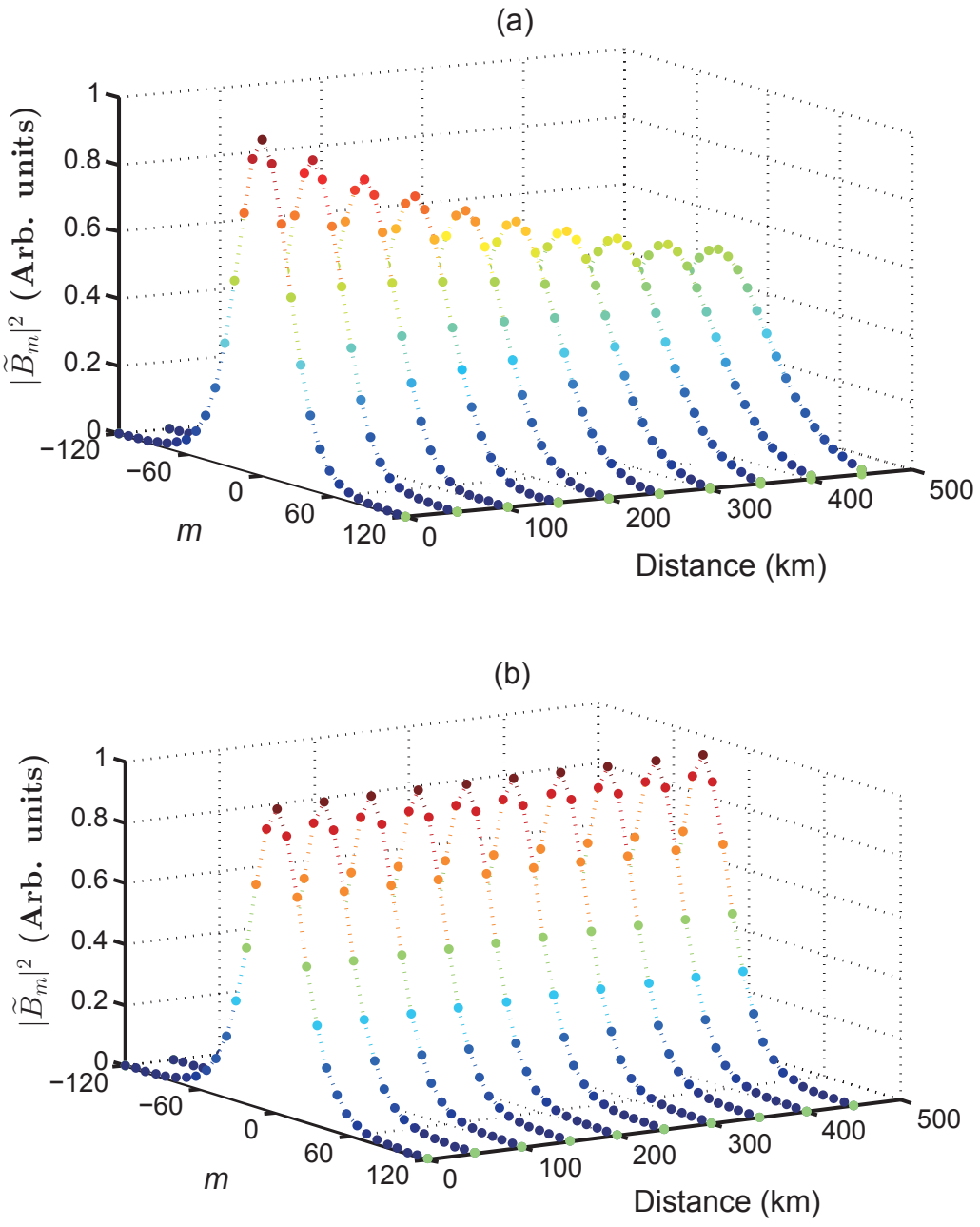

Figure 7.1: Evolution of $\widetilde{B}_m$ in the transmission fiber, (a) $\widetilde{B}_0 < \widetilde{B}_{th}$, $\widetilde{B}_0 = 10\ \sqrt{\text{mW}}\text{ps}$, (b) $\widetilde{B}_0 = \widetilde{B}_{th}$. $\widetilde{B}_{th} = 14.9\ \sqrt{\text{mW}}\text{ps}$, $M = 28$, $\alpha = 0\ \text{km}^{-1}$, $s_0 = -1.28 \times 10^4\ \text{ps}^2$, $\gamma_0 = 1.1\ \text{W}^{-1}\text{km}^{-1}$.

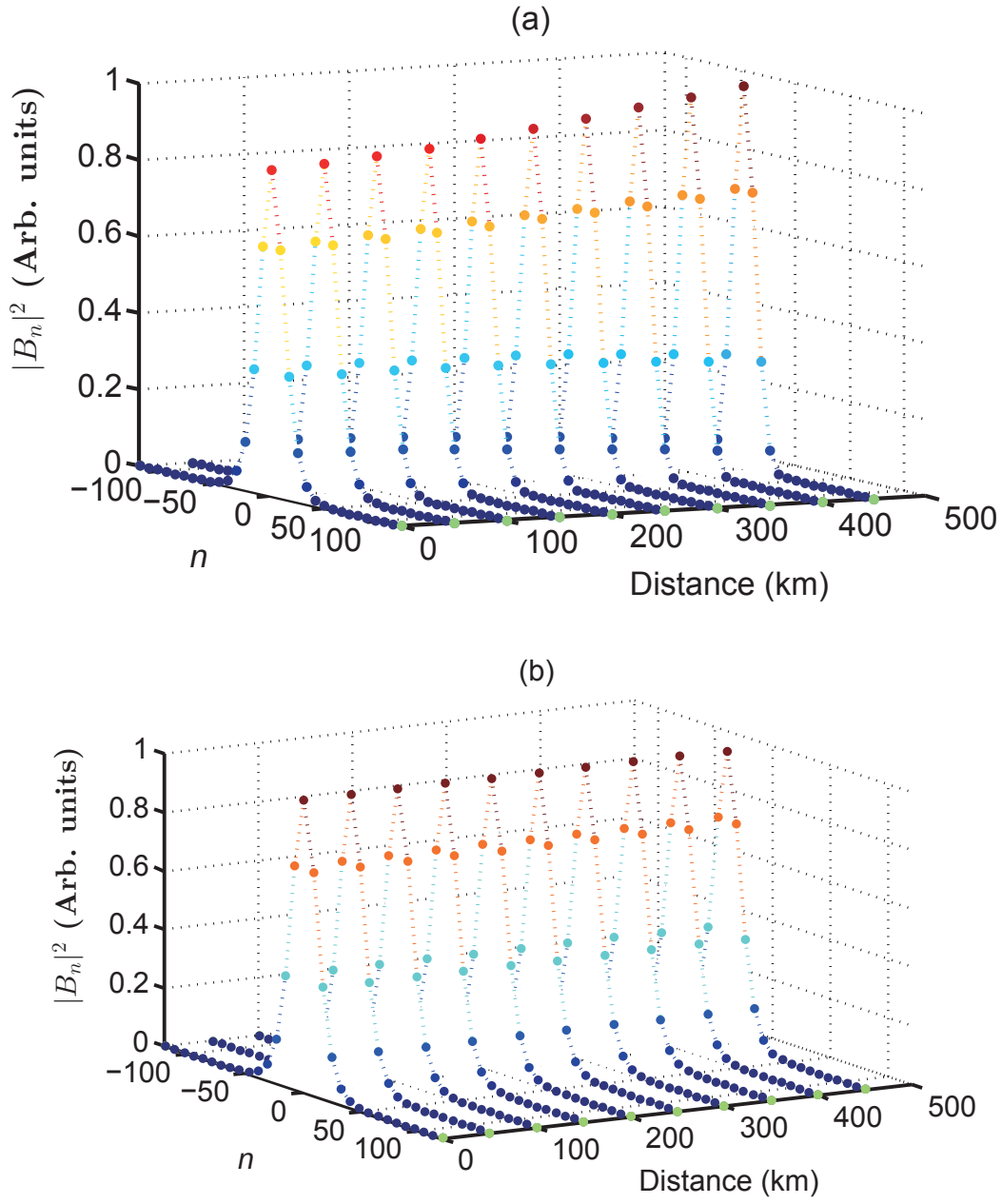

Figure 7.2: Evolution of B_m in the transmission fiber, (a) $\widetilde{B}_0 < \widetilde{B}_{th}$, (b) $\widetilde{B}_0 = \widetilde{B}_{th}$. The parameters are the same as in Fig. 7.1.

and Eq. (7.1) is solved with the following initial condition

$$u_{in}(t) = \sum_{n=-N/2}^{N/2-1} \frac{A_n(0) e^{-\frac{(t-nT)^2}{2T_0^2}}}{\sqrt{2\pi} T_0}, \tag{7.34}$$

where

$$A_n(0) = B_n(0) e^{i\frac{n^2 T^2}{2s_0}}, \tag{7.35}$$

$$B_n(0) = \text{IDFT}\left\{\widetilde{B}_m(0); m \to n\right\}, \tag{7.36}$$

and $\widetilde{B}_m(0)$ is given by Eq. (7.32). To obtain Fig. 7.3, the pre-accumulated dispersion is fully compensated at the receiver so that the pulse width of the Gaussian pulses at the output is the same as that at the input. As can be seen from Fig. 7.3, the envelope of Gaussian pulses propagate undistorted over the transmission fiber. If we had not properly chosen the input power, the nonlinear interaction among Gaussian pulses would broaden/compress the shape of the envelope. "×" in Fig. 7.3 show the power obtained by numerically solving Eq. (7.28) after converting $\widetilde{B}_m$ to A_n using Eqs. (7.23) and (7.25). The power required to form fundamental soliton is found to be

$$P_s = \frac{\beta_{2+} T^2}{4 s_0 \gamma_0 T_0^2}, \tag{7.37}$$

where T is the pulse separation and T_0 is the pulse width of the Gaussian pulses. Strictly speaking, the approximation of impulses by ultra-short Gaussian pulses is not really necessary. To test the validity of Eq. (7.28), in principle, Eq. (7.1) can be solved with the initial condition $u(t, 0)$ given by Eq. (7.15). However, the extraction of A_n from the transmission fiber output becomes hard.

As pointed in Ref. [124], DST is not typically integrable when $f > 2$. The

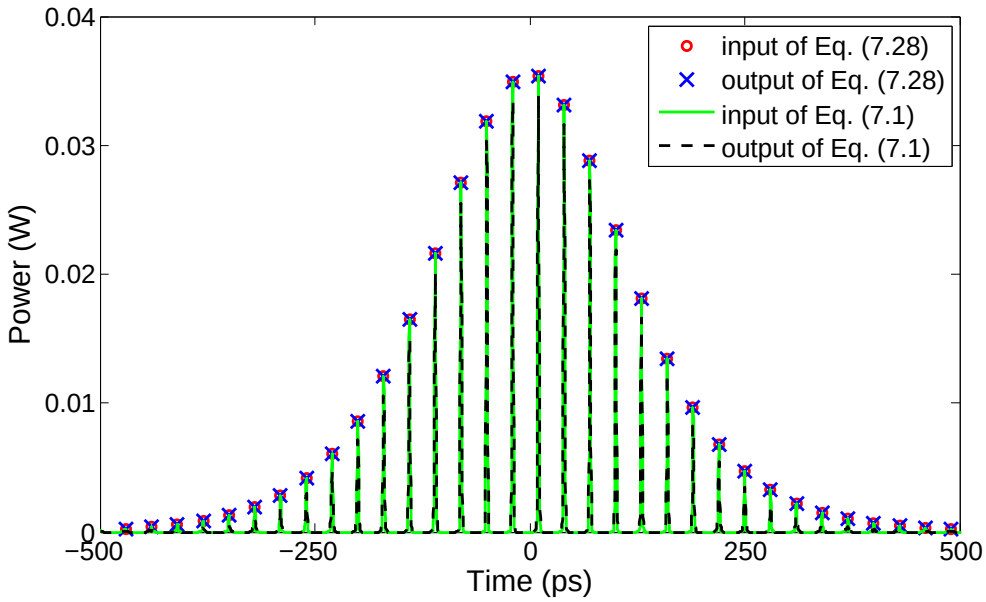

Figure 7.3: Comparison of discrete NLSE (Eq. (7.28)) and continuous NLSE (Eq. (1)). Peak power = 35.5 mw , $T = 10$ ps, $T_0 = 1$ ps, $s_0 = -1.28 \times 10^4$ ps^2, $\beta_{2+} = -20$ ps^2/km, $\gamma_0 = 1.1$ W^{-1}km^{-1}, transmission distance = 240 km.

integrability of Eq. (7.28) is not known yet, and to test if it admits high order soliton solutions, we solved Eq. (7.28) with the initial condition

$$\widetilde{B}_m(0) = 2\widetilde{B}_{th}\text{sech}\left(\frac{m}{M}\right). \tag{7.38}$$

Figure 7.4a shows the evolution of the second order soliton. As can be seen, it undergoes periodic compression just like its continuous analogue. The soliton period is found to be

$$z_0 = \frac{2s_0^2}{\pi M^2 T^2 |\beta_{2+}|}. \tag{7.39}$$

Figure 7.4b shows the evolution of $|B_n|^2$. When the envelope of $\widetilde{B}_m$ is compressed, the corresponding envelope of B_n is broadened and vice versa.

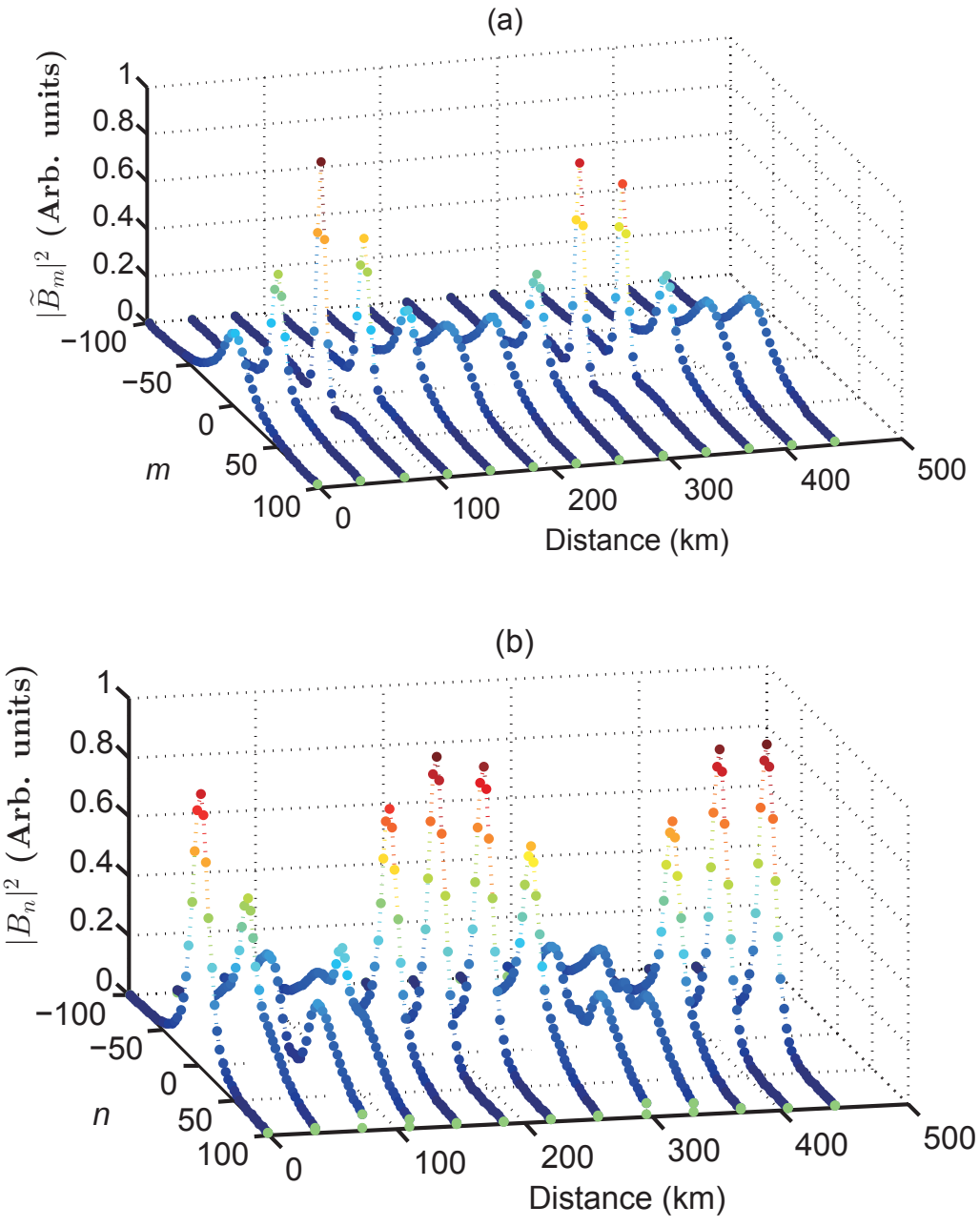

Figure 7.4: Evolution of second order soliton. $\widetilde{B}_0 = 29.8\sqrt{\text{mW}}\text{ps}$. The rest of the parameters are the same as in Fig. 7.1.

7.3 Nonlinear eigenmodes

When the effective dispersive effects are much weaker than the effective nonlinear effects in Eq. (7.28), i.e.,

$$\gamma P T_0^2/\pi >> \beta_{2+} T^2/|s(z)|, \tag{7.40}$$

where P is the peak power and T_0 is the half-width at $1/e$-intensity point of the Gaussian pulse that approximates the impulse, the second term in Eq. (7.28) can be ignored and we obtain

$$\frac{\partial \widetilde{B}_m}{\partial z} = i\frac{\gamma e^{-\alpha z}}{2\pi|s(z)|}|\widetilde{B}_m|^2 \widetilde{B}_m. \tag{7.41}$$

In Eq. (7.26), the last term is responsible for nonlinear interactions such as IXPM and IFWM among pulses. However, in Eq. (7.41), in the transformed system, these terms are absent and hence, the description of the nonlinear interactions becomes significantly simplified. Let

$$\widetilde{B}_m = Y_m e^{i\theta_m}. \tag{7.42}$$

Substituting Eq. (7.42) in Eq. (7.41), we find

$$Y_m = \text{const}, \tag{7.43}$$

$$\theta_m(z) = \theta_m(0) + \gamma|Y_m|^2 \int_0^z \frac{e^{-\alpha x}}{2\pi|s(x)|}dx. \tag{7.44}$$

The solution of Eq. (7.41) may be written as

$$\widetilde{B}_m(z) = \widetilde{B}_m(0)e^{\lambda_m z'}, \tag{7.45}$$

where

$$\lambda_m = i\gamma|\widetilde{B}_m|^2, \qquad z' = \frac{1}{2\pi}\int_0^z \frac{e^{-\alpha x}}{|s(x)|}dx. \tag{7.46}$$

When s_0 and β_{2+} have the same sign, z' can be written as

$$z' = \frac{e^{\alpha|s_0/\beta_{2+}|}}{2\pi}\left[\mathrm{Ei}\left(-\alpha\left|\frac{s(z)}{\beta_{2+}}\right|\right) - \mathrm{Ei}\left(-\alpha\left|\frac{s_0}{\beta_{2+}}\right|\right)\right]. \tag{7.47}$$

$\widetilde{B}_m$ may be interpreted as the nonlinear eigenmode of the fiber-optic system in the presence of pre-dispersion with the eigenvalue λ_m. These eigenmodes form a natural basis for the description of signal propagation, and signal and noise nonlinear interaction in highly pre-dispersed fiber-optic transmission systems. We note that using a different approach with stationary phase approximation, it has been shown that propagation equations can be considerably simplified in the presence of high pre-dispersion [65]. We found a few similarities and differences between Ref. [126] and our work. In this chapter, we introduce a transformation $B_k(z) = A_k(z)\exp\left(-ik^2T^2/2s(z)\right)$ in time domain, whereas in Ref. [126], the transformation $\hat{u}(z,\omega) \sim \hat{U}(z,\omega)\exp(-iC\omega^2/2)$ is used in frequency domain. In Ref. [126], when the system has a small value of path-average dispersion, the average dynamic of the pulse transmission is characterized only by the nonlinear phase shift. In contrast, from Eq. (7.28), it follows that when the system has a very large pre-accumulated dispersion, the pulse transmission is characterized only by the nonlinear phase shift given by Eq. (7.45). Even when the condition given by Eq. (7.40) is not met, i.e. when the pre-accumulated dispersion is moderate, the nonlinear eigenmode could serve as the unperturbed solution and a first order perturbation theory could be developed for the discrete NLSE of Eq. (7.28). An interesting fact is that the square of the accumulated dispersion appears

in the denominator of the second term in Eq. (7.28). This means that the effect of the second term becomes smaller for the fiber spans closer to receiver in a long haul system. Typically, in quasilinear fiber optic systems, dispersion length is much shorter than the nonlinear length. Hence linear solution (including dispersive effects) is treated as the unperturbed solution and first order correction due to nonlinear effects are calculated [44]. However, the computational complexity of the first order calculations scales as M^2 per sample where M is the number of neighbors with which the nonlinear interaction is significant and as a result, the digital compensation of fiber nonlinearities using first order perturbation theory is time-consuming [49, 98]. In contrast, if the nonlinear eigenmodes are treated as the unperturbed solution with the second term of Eq. (7.28) being treated as perturbation, the computational complexity is expected to be much smaller.

For the content presented in this chapter, my contribution includes: (i) theoretical study and deriving mathematical equations; (ii) running numerical simulations using codes developed by colleagues; (iii) compiling and analyzing simulation results and plotting result figures.

7.4 Conclusions

In conclusion, we have derived an exact solution of NLSE for an impulse input in the presence of pre-dispersion. The exact solution has a phase factor that is described by the exponential integral. Next, we considered the nonlinear interaction among pulses in a fiber due to periodically placed impulses at the input. We found that these pulses will propagate stably over long distances if the complex weights of impulses at the input has a secant-hyperbolic envelope and a proper chirp factor. We have derived the

discrete version of the NLSE under the condition that the input of an optical fiber is a periodic train of impluses. When the accumulated pre-dispersion is large, the discrete NLSE admits soliton and breather solutions similar to its continuous analogue. In the discrete NLSE derived here, the effective dispersion term is inversely proportional to the square of the accumulated dispersion and the effect nonlinear term is inversely proportional to absolute of accumulated dispersion. The derived discrete NLSE has a solution only if the pre-accumulated dispersion is non-zero. In the context of discrete NLSE, if the effective dispersion length is much longer than the effective nonlinear length, we have obtained the nonlinear eigenmodes of the highly pre-dispersed fiber-optic system which may be useful for the description of signal propagation, and signal and noise interaction.

Chapter 8

Conclusions and future work

8.1 Conclusions

This thesis deals with the signal impairments due to fiber dispersive and nonlinear effects in fiber-optic communication systems. Analytical models for fiber nonlinear effects, including SPM, XPM and IFWM, are obtained based on the perturbation theory. Digital and optical compensation schemes are investigated for mitigating signal impairments so as to enhance transmission performance, spectral efficiency and system capacity.

In Chapter 2, an analytical model is developed for the XPM variance in coherent WDM fiber-optic systems [69]. A first order perturbation technique is used to calculate the XPM distortion and then statistical analysis is carried out to calculate XPM variance for systems based on QAM. For arbitrary pulse shapes, the XPM variance cannot be calculated analytically, due to the difficulty in evaluating integrals explicitly. We introduced a method of using the summation of time-shifted Gaussian pulses to fit arbitrary pulse shapes, which not only provides a good approximation of the

non-Gaussian pulse but also allows explicit derivation of the XPM variance [70]. The analytically estimated XPM variance is found to be in good agreement with numerical simulations.

In Chapter 3, a digital back propagation (DBP) scheme with optimal step sizes is investigated to compensate for the dispersion and nonlinearity in fiber-optic communication systems [78]. By optimizing the step size of each section through minimizing the area mismatch between the exponential profile of the effective nonlinear coefficient and its stepwise approximation, a better system performance can be obtained without additional computational cost and system complexity. In simulations of polarization multiplexed systems, the vector NLSE or Manakov equations are used for forward propagation and Manakov equations are used for backward propagation. An adaptive least mean squares (LMS) equalizer is employed after the DBP to compensate for the randomly changing birefringence when the vector NLSE is used for forward propagation. In both the approaches, DBP with uniform spacing and minimum area mismatch (MAM) are simulated and results show that the MAM technique can increase the system reach significantly as compared to the uniform spacing at the same computational cost.

In Chapter 4, a digital compensation scheme based on the perturbation theory for mitigation of XPM distortions is developed for dispersion-managed fiber-optic communication systems [87]. It is a receiver-side scheme that uses a hard-decision unit to estimate data for the calculation of XPM fields using the perturbation technique. The intra-channel nonlinear distortions are removed by intra-channel DBP based on split-step Fourier scheme before the hard-decision unit. The perturbation technique is shown to be effective in mitigating XPM distortions. However, wrong estimations

in the hard-decision unit result in performance degradation. A hard-decision correction method is proposed to correct the wrong estimations. Numerical simulations of coherent WDM fiber-optic systems show that the perturbation-based XPM compensation scheme brings significant performance improvements. The perturbation-based XPM compensation scheme requires much less computational cost as compared with conventional DBP based on the coupled NLSE, since it only requires one-stage (or two-stage when hard-decision correction is applied) compensation and symbol-rate signal processing.

In Chapter 5, a recursive perturbation theory to model the fiber-optic system is developed [98]. Using this perturbation theory, a multi-stage compensation technique to mitigate the intra-channel nonlinear impairments is investigated. The input signals of different compensation stages are expressed using the same basis functions so that the coefficient matrix X_{mn} for perturbation calculation is the same for all stages. The multi-stage compensation is implemented recursively, the output signal of one compensation stage is used as the input of the next compensation stage. In each stage the first order theory is used to calculate the nonlinear distortions occurring in a distance much shorter than the entire fiber-optic link, which improves the accuracy and the summation of the signal field and the first order field of the previous stage is used as the unperturbed solution for the next stage, which further improves the accuracy. Moreover, the accumulated dispersion in one compensation stage is much smaller than that of the entire link which significantly reduces the size of the coefficient matrix X_{mn}, leading to reductions both in computational complexity and the required memory for storing X_{mn}. Numerical simulations of a single-channel fiber-optic system show that the multi-stage perturbation technique brings significant performance

improvements and computational complexity reduction as compared with the single-stage compensation scheme.

In Chapter 6, an ideal optical back propagation (OBP) scheme to compensate for dispersion and nonlinear effects of the transmission fibers is investigated [107]. The scheme consists of an optical phase conjugator (OPC), N spans of dispersion-decreasing fibers (DDFs) and amplifiers, placed at the end of the fiber optic link. In order to compensate for the nonlinear effects of the transmission fibers exactly, the nonlinear coefficient of the back propagation fiber has to increase exponentially with distance or equivalently the power in the back propagation fiber should increase exponentially with distance if the nonlinear coefficient is constant. We find that a combination of DDFs and amplifiers can compensate for the nonlinear effects exactly. An analytical expression for the dispersion profile of the DDF is derived. Numerical simulations of WDM fiber-optic systems show that the proposed OBP scheme can enhance the system reach significantly as compared to DBP.

In Chapter 7, an exact solution of NLSE is derived for impulse input in the presence of pre-dispersion [119]. The phase factor of the exact solution is obtained in a closed form using the exponential integral. The nonlinear interaction among periodically placed impulses launched at the input is investigated, and the condition under which these pulses do not exchange energy is examined. It is found that if the complex weights of the impulses at the input have a secant-hyperbolic envelope and a proper chirp factor, they will propagate over long distances without exchanging energy. To describe their interaction, a discrete version of NLSE is derived. The derived equation is a form of discrete self-trapping (DST) equation, which is found

to admit fundamental and higher order soliton solutions in the presence of high pre-dispersion. In the context of discrete NLSE, if the effective dispersion length is much longer than the effective nonlinear length, we have obtained the nonlinear eigenmodes of the highly pre-dispersed fiber-optic system which may be useful for the description of signal propagation, and signal and noise interaction.

8.2 Future work

This thesis provides theoretical analysis and simulation results of fiber nonlinear effects and the compensation techniques. Experimental research is one of the most important future works to validate the theoretical models and to measure the performance of digital and optical compensation schemes for mitigating fiber nonlinear effects. Moreover, most digital compensation schemes such as DBP and perturbation techniques are currently limited to off-line signal processing due to the high computational load. Therefore, simplification of digital signal processing (DSP) algorithms is an important and urgent research topic. Another problem of digital compensation schemes is the difficulty of application for fiber optic networks with complex mesh configurations, due to the potential lack of propagation path information of different signal channels. More research is required to seek a solution to this problem. For optical compensation methods, more research is required to optimize compensation scheme and to make them practically applicable to existing fiber optic communication systems.

DBP requires enormous computational resources since it necessitates a large number of steps and the computational cost mainly arises from the FFT operations. On the other hand, perturbation-based digital schemes require fewer number of stages

and are expected to reduce computational cost substantially. However, the cost of perturbation schemes is mainly in the double summations of the nonlinear operation, due to the larger size of the perturbation coefficient. One possible way to significantly reduce the computational cost is to simplify the double summation calculation of the perturbation scheme and find a more efficient way to calculate the nonlinear distortion. Another possible solution is to combine the SSFS-based DBP with the perturbation theory, such that the advantages of both high-efficiency FFT and high-accuracy perturbation calculation.

Another interesting research topic is the influence of accuracy of fiber parameters on the performance of digital and optical compensation methods. In practical systems, exact fiber parameters are sometimes unavailable or the parameters may fluctuate due to environment change. In this case, the performance of compensation schemes may be affected. It might be helpful to combine adaptive parameter estimation algorithms with DBP or perturbation-based digital compensation schemes.

Existing digital compensation schemes including DBP and perturbation-based techniques compensate for fiber nonlinear effects based on the information of signal propagation path and link parameters such as dispersion profiles and nonlinear coefficient. Such compensation schemes can be easily implemented in a point-to-point link. However, in the case of network communications, the implementations of DBP and perturbation-based techniques become difficult since the signal propagation path and link parameters become much complicated due to the complex network mesh and the presence of add/drop multiplexers. The optical back propagation (OBP) scheme with dispersion-decreasing fiber (DDF) investigated in Chapter 6 is a potential compensation scheme for the network communication systems. If the compensation block with

a DDF and amplifier is placed after the transmission fiber in each span (other than at the receiver only), the signal impairments of the transmission fiber will be fully compensated by the following compensation block. As a result, the compensation of a certain signal channel becomes independent of its propagation path and independent of the added/dropped channels within the propagation path.

The OBP scheme with DDF studied in Chapter 6 shows better performance than DBP even with a small step size and has a potential for fiber optic network systems. The OBP module is built using discrete optical components such as OPC, optical amplifier and DDF. It is very interesting to investigate if same function can be realized using integrated optical devices, such as silicon waveguides. If such an OBP scheme can be realized using photonic integrated circuits, the design of fiber optic communication systems will become much more simplified and much efficiently.

The nonlinear eigenmodes obtained in Chapter 7 based on the discrete NLSE for fiber-optic systems with large pre-dispersion may be useful for the description of signal evolution. If the effective dispersion length is much longer than the effective nonlinear length, which can be realized by properly choose the pre-dispersion, the discrete NLSE becomes much simpler since the dispersion term is negligible. Based on the eigenmodes of the discrete NLSE, it has a potential to develop a digital compensation scheme for fiber nonlinear effects that has much smaller computational complexity as compared with existing digital compensation schemes such as DBP and perturbation-based techniques.

Appendix A

Curve fitting using least squares method

The least squares method (LSM) and steepest descent algorithm are used for curve fitting. For a target function $h(t)$, we fit it by a summation of time-shifted Gaussian functions

$$h'(t) = \sum_{k=1}^{K} \xi_k \exp\left[-\frac{(t-\mu_k T_s)^2}{2(\theta_k T_s)^2}\right]. \tag{A.1}$$

The error function is

$$e(t) = h(t) - h'(t). \tag{A.2}$$

We discretize the time axis by

$$t = m\Delta t, \tag{A.3}$$

where Δt is the step size in the time axis; m is an integer. In order to find a good fitting, we need to minimize the cost function χ,

$$\chi = \sum_{m=1}^{M} e_m^2 = \sum_{m=1}^{M} [h_m - h'_m]^2, \tag{A.4}$$

where $e_m = e(m\Delta t), h_m = h(m\Delta t), h'_m = h'(m\Delta t)$. Substituting Eq. (A.1) into Eq. (A.4) and taking the derivatives of χ with respect to ξ_k, μ_k and θ_k respectively, we find

$$\frac{\partial \chi}{\partial \xi_k} = -2 \sum_m (h_m - h'_m) \exp\left[-\frac{(m\Delta t - \mu_k T_s)^2}{2(\theta_k T_s)^2} \right], \tag{A.5}$$

$$\frac{\partial \chi}{\partial \mu_k} = -2 \sum_m (h_m - h'_m) \frac{\xi_k (m\Delta t - \mu_k T_s)}{\theta_k^2 T_s} \exp\left[-\frac{(m\Delta t - \mu_k T_s)^2}{2(\theta_k T_s)^2} \right], \tag{A.6}$$

$$\frac{\partial \chi}{\partial \theta_k} = -2 \sum_m (h_m - h'_m) \frac{\xi_k (m\Delta t - \mu_k T_s)}{\theta_k^3 T_s^3} \exp\left[-\frac{(m\Delta t - \mu_k T_s)^2}{2(\theta_k T_s)^2} \right]. \tag{A.7}$$

The steepest descent algorithm is used to optimize ξ_k, μ_k and θ_k [127]. The parameters at the $(i+1)$th iteration are updated from the ith iteration by

$$\xi_k^{(i+1)} = \xi_k^{(i)} - \frac{\partial \chi}{\partial \xi_k} \Delta\xi, \quad \mu_k^{(i+1)} = \mu_k^{(i)} - \frac{\partial \chi}{\partial \mu_k} \Delta\mu, \quad \theta_k^{(i+1)} = \theta_k^{(i)} - \frac{\partial \chi}{\partial \theta_k} \Delta\theta, \tag{A.8}$$

where$\Delta\xi$, $\Delta\mu$ and $\Delta\theta$ are the step sizes. At the 0th iteration, $\xi_k^{(0)}$, $\mu_k^{(0)}$ and $\theta_k^{(0)}$ are randomly chosen from the interval (0 1).

Appendix B

Derivation of XPM distortions for non-Gaussian pulses

Consider two channels of a WDM system using a non-Gaussian pulse $h(t)$ which can be approximated by $h'(t)$ in Eq. (2.39). The input fields to the optical fiber are

$$u_1(0,t) = \sqrt{P}a_0 h'(t), \tag{B.1}$$

$$u_2(0,t) = \sqrt{P}\sum_{n=-N}^{N} b_n h'(t-nT_s)\exp(-i\Omega t), \tag{B.2}$$

The linear solution can be obtained by solving Eq. (2.11) in the frequency domain. Using the identity

$$\int_{-\infty}^{\infty} \exp(-ax^2 - bx)dx = \sqrt{\frac{\pi}{a}}\exp\left(\frac{b^2}{4a}\right), \tag{B.3}$$

we find the linear solution as

$$u_1^{(0)}(z,t) = \sqrt{P}a_0 \sum_{k=1}^{K} \xi_k \frac{\theta_k T_s}{T_{1,k}} \exp\left[-\frac{(t-\mu_k T_s)^2}{2T_{1,k}^2}\right], \tag{B.4}$$

$$u_2^{(0)}(z,t) = \sqrt{P} \sum_{n=-N}^{N} b_n \sum_{k=1}^{K} \xi_k \frac{\theta_k T_s}{T_{1,k}} \exp\left[-\frac{(t-\tau_{n,k})^2}{2T_{1,k}^2} - i\Omega t + i\theta(z)\right], \tag{B.5}$$

where

$$T_{1,k} = \sqrt{(\theta_k T_s)^2 - iS(z)}, \tag{B.6}$$

$$\tau_{n,k} = (n+\mu_k)T_s + S(z)\Omega. \tag{B.7}$$

For first-order correction of u_1, the forcing function of Eq. (2.19) is

$$F(z,t) = 2P^{3/2}a_0 \sum_m \sum_n b_m b_n^* \sum_{k_1=1}^{K} \sum_{k_2=1}^{K} \sum_{k_3=1}^{K} \eta(z) \exp\left[-\sum_{k'=1}^{3} [t - C_{k'}(z)]^2 R_{k'}(z)\right], \tag{B.8}$$

where

$$\eta(z) = -e^{-w(z)} \xi_{k_1}\xi_{k_2}\xi_{k_3} \frac{\theta_{k_1}\theta_{k_2}\theta_{k_3}T_s^2}{T_{1,k_1}T_{1,k_2}^* T_{1,k_3}}, \tag{B.9}$$

$$C_1(z) = \tau_{m,k_1}, \quad C_2(z) = \tau_{n,k_2}, \quad C_3(z) = \mu_{k_3}T_s, \tag{B.10}$$

$$R_1(z) = \frac{1}{2T_{1,k_1}^2}, \quad R_2(z) = \frac{1}{2(T_{1,k_2}^*)^2}, \quad R_3(z) = \frac{1}{2T_{1,k_3}^2}, \tag{B.11}$$

Using Eq. (2.21), the first order correction for u_1 due to XPM is found as

$$u_1^{(1),XPM,NG}(L_{tot},t) = i2P^{3/2}a_0 \sum_m \sum_n b_m b_n^* Y_{mn}(L_{tot},t), \tag{B.12}$$

where

$$Y_{mn}(L_{tot},t) = \int_{-\infty}^{\infty} V_{mn}(L_{tot},t') h_{RX}(t-t')dt', \tag{B.13}$$

$$V_{mn}(L_{tot},t)=\int_0^{L_{tot}}\sum_{k_1=1}^{K}\sum_{k_2=1}^{K}\sum_{k_3=1}^{K}\frac{-\eta'(s)}{\sqrt{\delta(L_{tot},s)R(s)}}\exp\left[\frac{(D+it)^2}{\delta(L_{tot},s)}\right]ds. \tag{B.14}$$

Bibliography

[1] G. P. Agrawal, *Fiber-Optic Communication Systems.* John Wiley & Sons, 1997.

[2] S. Kumar and M. J. Deen, *Fiber Optic Communications: Fundamentals and Applications.* Wiley, 2014.

[3] G. P. Agrawal, *Nonlinear Fiber Optics.* Academic Press, 2007.

[4] L. F. Mollenauer, S. G. Evangelides, and J. P. Gordon, "Wavelength division multiplexing with solitons in ultra-long distance transmission using lumped amplifiers," *J. Lightwave Technol.*, vol. 9, no. 3, pp. 362–367, 1991.

[5] A. Hasegawa, Y. Kodama, and S. Kumar, "Reduction of collision-induced time jitters in dispersion-managed soliton transmission systems," *Opt. Lett.*, vol. 21, no. 1, pp. 39–41, 1996.

[6] K. Inoue, "Four-wave mixing in an optical fiber in the zero-dispersion wavelength region," *J. Lightwave Technol.*, vol. 10, no. 11, pp. 1553–1561, 1992.

[7] R. Tkach, A. Chraplyvy, F. Forghieri, A. Gnauck, and R. Derosier, "Four-photon mixing and high-speed WDM systems," *J. Lightwave Technol.*, vol. 13, no. 5, pp. 841–849, 1995.

[8] P. Wai, W. Kath, C. Menyuk, and J. Zhang, "Nonlinear polarization-mode dispersion in optical fibers with randomly varying birefringence," *J. Opt. Soc. Am. B*, vol. 14, no. 11, pp. 2967–2979, 1997.

[9] C. Xie, "Interchannel nonlinearities in coherent polarization-division-multiplexed quadrature-phase-shift-keying systems," *IEEE Photon. Technol. Lett.*, vol. 21, no. 5, pp. 274–276, 2009.

[10] J. P. Gordon and L. F. Mollenauer, "Phase noise in photonic communications systems using linear amplifiers," *Opt. Lett.*, vol. 15, no. 23, pp. 1351–1353, 1990.

[11] D. Richardson, J. Fini, and L. Nelson, "Space-division multiplexing in optical fibres," *Nat. Photonics*, vol. 7, no. 5, pp. 354–362, 2013.

[12] A. J. Antos and D. K. Smith, "Design and characterization of dispersion compensating fiber based on the LP_{01} mode," *J. Lightwave Technol.*, vol. 12, no. 10, pp. 1739–1745, 1994.

[13] K. Hill, K. Takiguchi, F. Bilodeau, B. Malo, T. Kitagawa, S. Thériault, D. Johnson, and J. Albert, "Chirped in-fiber bragg gratings for compensation of optical-fiber dispersion," *Opt. Lett.*, vol. 19, no. 17, pp. 1314–1316, 1994.

[14] D. M. Pepper and A. Yariv, "Compensation for phase distortions in nonlinear media by phase conjugation," *Opt. Lett.*, vol. 5, no. 2, pp. 59–60, 1980.

[15] R. A. Fisher, B. Suydam, and D. Yevick, "Optical phase conjugation for time-domain undoing of dispersive self-phase-modulation effects," *Opt. Lett.*, vol. 8, no. 12, pp. 611–613, 1983.

[16] S. Watanabe and T. Chikama, "Cancellation of four-wave mixing in multichannel fibre transmission by midway optical phase conjugation," *Electron. Lett.*, vol. 30, no. 14, pp. 1156–1157, 1994.

[17] P. Martelli, P. Boffi, M. Ferrario, L. Marazzi, P. Parolari, R. Siano, V. Pusino, P. Minzioni, I. Cristiani, C. Langrock *et al.*, "All-optical wavelength conversion of a 100-Gb/s polarization-multiplexed signal," *Opt. Express*, vol. 17, no. 20, pp. 17 758–17 763, 2009.

[18] K. Solis-Trapala, T. Inoue, and S. Namiki, "Nearly-ideal optical phase conjugation based nonlinear compensation system," in *Optical Fiber Communication Conference*. Optical Society of America, 2014, p. W3F.8.

[19] S. Kumar and D. Yang, "Optical backpropagation for fiber-optic communications using highly nonlinear fibers," *Opt. Lett.*, vol. 36, no. 7, pp. 1038–1040, 2011.

[20] J. Shao and S. Kumar, "Optical backpropagation for fiber-optic communications using optical phase conjugation at the receiver," *Opt. Lett.*, vol. 37, no. 15, pp. 3012–3014, 2012.

[21] S. Kumar and J. Shao, "Optical back propagation with optimal step size for fiber optic transmission systems," *IEEE Photon. Technol. Lett.*, vol. 25, pp. 523–526, 2013.

[22] X. Liu, A. Chraplyvy, P. Winzer, R. Tkach, and S. Chandrasekhar, "Phase-conjugated twin waves for communication beyond the Kerr nonlinearity limit," *Nat. Photonics*, vol. 7, no. 7, pp. 560–568, 2013.

[23] T. Yoshida, T. Sugihara, K. Ishida, and T. Mizuochi, "Spectrally-efficient dual phase-conjugate twin waves with orthogonally multiplexed quadrature pulse-shaped signals," in *Optical Fiber Communication Conference*. Optical Society of America, 2014, p. M3C.6.

[24] X. Liu, S. Chandrasekhar, P. Winzer, R. Tkach, and A. Chraplyvy, "Fiber-nonlinearity-tolerant superchannel transmission via nonlinear noise squeezing and generalized phase-conjugated twin waves," *J. Lightwave Technol.*, vol. 32, no. 4, pp. 766–775, 2014.

[25] X. Yi, X. Chen, C. Li, M. Luo, Q. Yang, Z. Li, and K. Qiu, "Experimental demonstration of digital coherent superposition of optical OFDM subcarrier pairs for mitigation of linear and nonlinear phase noise," in *Optical Fiber Communication Conference*. Optical Society of America, 2014, p. Tu3G.6.

[26] G. Li, "Recent advances in coherent optical communication," *Adv. Opt. Photonics*, vol. 1, no. 2, pp. 279–307, 2009.

[27] M. G. Taylor, "Coherent detection method using DSP for demodulation of signal and subsequent equalization of propagation impairments," *IEEE Photon. Technol. Lett.*, vol. 16, no. 2, pp. 674–676, 2004.

[28] S. J. Savory, "Digital filters for coherent optical receivers," *Opt. Express*, vol. 16, no. 2, pp. 804–817, 2008.

[29] G. Goldfarb and G. Li, "Chromatic dispersion compensation using digital iir filtering with coherent detection," *IEEE Photon. Technol. Lett.*, vol. 19, no. 13, pp. 969–971, 2007.

[30] E. Ip and J. M. Kahn, "Digital equalization of chromatic dispersion and polarization mode dispersion," *J. Lightwave Technol.*, vol. 25, no. 8, pp. 2033–2043, 2007.

[31] S. Tsukamoto, K. Katoh, and K. Kikuchi, "Unrepeated transmission of 20-Gb/s optical quadrature phase-shift-keying signal over 200-km standard single-mode fiber based on digital processing of homodyne-detected signal for group-velocity dispersion compensation," *IEEE Photon. Technol. Lett.*, vol. 18, no. 9, pp. 1016–1018, 2006.

[32] K. Roberts, L. Chuandong, L. Strawczynski, M. O'SULLIVAN, and I. Hardcastle, "Electronic precompensation of optical nonlinearity," *IEEE Photon. Technol. Lett.*, vol. 18, no. 1-4, pp. 403–405, 2006.

[33] X. Li, X. Chen, G. Goldfarb, E. Mateo, I. Kim, F. Yaman, and G. Li, "Electronic post-compensation of WDM transmission impairments using coherent detection and digital signal processing," *Opt. Express*, vol. 16, no. 2, pp. 880–888, 2008.

[34] E. Ip and J. M. Kahn, "Compensation of dispersion and nonlinear impairments using digital backpropagation," *J. Lightwave Technol.*, vol. 26, no. 20, pp. 3416–3425, 2008.

[35] E. Mateo, L. Zhu, and G. Li, "Impact of XPM and FWM on the digital implementation of impairment compensation for WDM transmission using backward propagation," *Opt. Express*, vol. 16, no. 20, pp. 16 124–16 137, 2008.

[36] E. F. Mateo and G. Li, "Compensation of interchannel nonlinearities using enhanced coupled equations for digital backward propagation," *Appl. Opt.*, vol. 48, no. 25, pp. F6–F10, 2009.

[37] E. F. Mateo, F. Yaman, and G. Li, "Efficient compensation of inter-channel nonlinear effects via digital backward propagation in WDM optical transmission," *Opt. Express*, vol. 18, no. 14, pp. 15 144–15 154, 2010.

[38] L. B. Du and A. J. Lowery, "Improved single channel backpropagation for intra-channel fiber nonlinearity compensation in long-haul optical communication systems," *Opt. Express*, vol. 18, no. 16, pp. 17 075–17 088, 2010.

[39] L. Zhu and G. Li, "Folded digital backward propagation for dispersion-managed fiber-optic transmission," *Opt. Express*, vol. 19, no. 7, pp. 5953–5959, 2011.

[40] L. Zhu and G. LI, "Nonlinearity compensation using dispersion-folded digital backward propagation," *Opt. Express*, vol. 20, no. 13, pp. 14 362–14 370, 2012.

[41] X. Liu, S. Chandrasekhar, P. J. Winzer, B. Maheux-L, G. Brochu, and F. Trepanier, "Efficient fiber nonlinearity mitigation in 50-GHz-DWDM transmission of 256-Gb/s PDM-16QAM signals by folded digital-back-propagation and channelized FBG-DCMs," in *Optical Fiber Communication Conference*. Optical Society of America, 2014, p. Tu3A.8.

[42] F. Yaman and G. Li, "Nonlinear impairment compensation for polarization-division multiplexed WDM transmission using digital backward propagation," *Photonics J.*, vol. 2, no. 5, pp. 816–832, 2010.

[43] E. F. Mateo, X. Zhou, and G. Li, "Improved digital backward propagation for the compensation of inter-channel nonlinear effects in polarization-multiplexed WDM systems," *Opt. Express*, vol. 19, no. 2, pp. 570–583, 2011.

[44] A. Mecozzi, C. B. Clausen, and M. Shtaif, "Analysis of intrachannel nonlinear effects in highly dispersed optical pulse transmission," *IEEE Photon. Technol. Lett.*, vol. 12, no. 4, pp. 392–394, 2000.

[45] S. Kumar and D. Yang, "Second-order theory for self-phase modulation and cross-phase modulation in optical fibers," *J. Lightwave Technol.*, vol. 23, no. 6, pp. 2073–2080, 2005.

[46] P. Poggiolini, A. Carena, V. Curri, G. Bosco, and F. Forghieri, "Analytical modeling of nonlinear propagation in uncompensated optical transmission links," *IEEE Photon. Technol. Lett.*, vol. 23, no. 11, pp. 742–744, 2011.

[47] R. Dar, M. Feder, A. Mecozzi, and M. Shtaif, "Properties of nonlinear noise in long, dispersion-uncompensated fiber links," *Opt. Express*, vol. 21, no. 22, pp. 25 685–25 699, 2013.

[48] A. Mecozzi and R.-J. Essiambre, "Nonlinear shannon limit in pseudolinear coherent systems," *J. Lightwave Technol.*, vol. 30, no. 12, pp. 2011–2024, 2012.

[49] Z. Tao, L. Dou, W. Yan, L. Li, T. Hoshida, and J. C. Rasmussen, "Multiplier-free intrachannel nonlinearity compensating algorithm operating at symbol rate," *J. Lightwave Technol.*, vol. 29, no. 17, pp. 2570–2576, 2011.

[50] T. Oyama, H. Nakashima, S. Oda, T. Yamauchi, Z. Tao, T. Hoshida, and J. Rasmussen, "Robust and efficient receiver-side compensation method for

intra-channel nonlinear effects," in *Optical Fiber Communication Conference*. Optical Society of America, 2014, p. Tu3A.3.

[51] Y. Gao, J. Cartledge, A. Karar, and S. Yam, "Reducing the complexity of nonlinearity pre-compensation using symmetric edc and pulse shaping," in *European Conference on Optical Communications*, 2013, p. PD3. E.

[52] Y. Gao, J. C. Cartledge, A. S. Karar, S. S.-H. Yam, M. OSullivan, C. Laperle, A. Borowiec, and K. Roberts, "Reducing the complexity of perturbation based nonlinearity pre-compensation using symmetric edc and pulse shaping," *Opt. Express*, vol. 22, no. 2, pp. 1209–1219, 2014.

[53] Y. Gao, A. S. Karar, J. C. Cartledge, S. S.-H. Yam, C. Sullivan, Maurice Oand Laperle, A. Borowiec, and K. Roberts, "Joint pre-compensation and selective post-compensation for fiber nonlinearities," *IEEE Photon. Technol. Lett.*, vol. 26, no. 17, pp. 1746–1749, 2014.

[54] Q. Zhuge, M. Reimer, A. Borowiec, M. O'Sullivan, and D. V. Plant, "Aggressive quantization on perturbation coefficients for nonlinear pre-distortion," in *Optical Fiber Communication Conference*. Optical Society of America, 2014, p. Th4D.7.

[55] D. Marcuse, A. Chraplyvy, and R. Tkach, "Dependence of cross-phase modulation on channel number in fiber WDM systems," *J. Lightwave Technol.*, vol. 12, no. 5, pp. 885–890, 1994.

[56] T.-K. Chiang, N. Kagi, M. Marhic, and L. G. Kazovsky, "Cross-phase modulation in fiber links with multiple optical amplifiers and dispersion compensators," *J. Lightwave Technol.*, vol. 14, no. 3, pp. 249–260, 1996.

[57] R. Hui, Y. Wang, K. Demarest, and C. Allen, "Frequency response of cross-phase modulation in multispan WDM optical fiber systems," *IEEE Photon. Technol. Lett.*, vol. 10, no. 9, pp. 1271–1273, 1998.

[58] M. Shtaif and M. Eiselt, "Analysis of intensity interference caused by cross-phase modulation in dispersive optical fibers," *IEEE Photon. Technol. Lett.*, vol. 10, no. 7, pp. 979–981, 1998.

[59] R. Hui, K. Demarest, and C. T. Allen, "Cross-phase modulation in multispan WDM optical fiber systems," *J. Lightwave Technol.*, vol. 17, no. 6, pp. 1018–1026, 1999.

[60] A. V. Cartaxo, "Cross-phase modulation in intensity modulation-direct detection WDM systems with multiple optical amplifiers and dispersion compensators," *J. Lightwave Technol.*, vol. 17, no. 2, pp. 178–190, 1999.

[61] Z. Jiang and C. Fan, "A comprehensive study on XPM-and SRS-induced noise in cascaded IM-DD optical fiber transmission systems," *J. Lightwave Technol.*, vol. 21, no. 4, pp. 953–960, 2003.

[62] A. Carena, V. Curri, G. Bosco, P. Poggiolini, and F. Forghieri, "Modeling of the impact of nonlinear propagation effects in uncompensated optical coherent transmission links," *J. Lightwave Technol.*, vol. 30, no. 10, pp. 1524–1539, 2012.

[63] P. Poggiolini, "The GN model of non-linear propagation in uncompensated coherent optical systems," *J. Lightwave Technol.*, vol. 30, no. 24, pp. 3857–3879, 2012.

[64] G. Bosco, R. Cigliutti, A. Nespola, A. Carena, V. Curri, F. Forghieri, Y. Yamamoto, T. Sasaki, Y. Jiang, and P. Poggiolini, "Experimental investigation of nonlinear interference accumulation in uncompensated links," *IEEE Photon. Technol. Lett.*, vol. 24, no. 13, p. 1230, 2012.

[65] S. Turitsyn, M. Sorokina, and S. Derevyanko, "Dispersion-dominated nonlinear fiber-optic channel," *Opt. Lett.*, vol. 37, no. 14, pp. 2931–2933, 2012.

[66] P. Johannisson and M. Karlsson, "Perturbation analysis of nonlinear propagation in a strongly dispersive optical communication system," *J. Lightwave Technol.*, vol. 31, no. 8, pp. 1273–1282, 2013.

[67] R. Dar, M. Feder, A. Mecozzi, and M. Shtaif, "Time varying isi model for nonlinear interference noise," in *Optical Fiber Communication Conference*. Optical Society of America, 2014, p. W2A.62.

[68] R. Dar, M. Shtaif, and M. Feder, "New bounds on the capacity of the nonlinear fiber-optic channel," *Opt. Lett.*, vol. 39, no. 2, pp. 398–401, 2014.

[69] S. N. Shahi, S. Kumar, and X. Liang, "Analytical modeling of cross-phase modulation in coherent fiber-optic system," *Opt. Express*, vol. 22, no. 2, pp. 1426–1439, 2014.

[70] X. Liang and S. Kumar, "Analytical modeling of XPM in dispersion-managed

coherent fiber-optic systems," *Opt. Express*, vol. 22, no. 9, pp. 10 579–10 592, 2014.

[71] S. Kumar, S. N. Shahi, and D. Yang, "Analytical modeling of a single channel nonlinear fiber optic system based on QPSK," *Opt. Express*, vol. 20, no. 25, pp. 27 740–27 755, 2012.

[72] S. F. Boys, "Electronic wave functions. I. A general method of calculation for the stationary states of any molecular system," *Proceedings of the Royal Society of London. Series A. Mathematical and Physical Sciences*, vol. 200, no. 1063, pp. 542–554, 1950.

[73] A. Szabo and N. S. Ostlund, *Modern Quantum Chemistry: Introduction to Advanced Electronic Structure Theory*. Courier Dover Publications, 2012.

[74] E. Ip, "Nonlinear compensation using backpropagation for polarization-multiplexed transmission," *J. Lightwave Technol.*, vol. 28, no. 6, pp. 939–951, 2010.

[75] D. S. Millar, S. Makovejs, C. Behrens, S. Hellerbrand, R. I. Killey, P. Bayvel, and S. J. Savory, "Mitigation of fiber nonlinearity using a digital coherent receiver," *J. Select. Topics Quantum Electron.*, vol. 16, no. 5, pp. 1217–1226, 2010.

[76] D. Rafique and A. D. Ellis, "Impact of signal-ASE four-wave mixing on the effectiveness of digital back-propagation in 112 Gb/s PM-QPSK systems," *Opt. Express*, vol. 19, no. 4, pp. 3449–3454, 2011.

[77] G. Gao, X. Chen, and W. Shieh, "Influence of PMD on fiber nonlinearity compensation using digital back propagation," *Opt. Express*, vol. 20, no. 13, pp. 14 406–14 418, 2012.

[78] J. Shao, S. Kumar, and X. Liang, "Digital back propagation with optimal step size for polarization multiplexed transmission," *IEEE Photon. Technol. Lett.*, 2013.

[79] M. Matsumoto, Y. Akagi, and A. Hasegawa, "Propagation of solitons in fibers with randomly varying birefringence: Effects of soliton transmission control," *J. Lightwave Technol.*, vol. 15, no. 4, pp. 584–589, 1997.

[80] Z. Chen and S. Kumar, "A fiber-optic transmission system based on differential polarization-shift keying," *Opt. Commun.*, vol. 284, no. 16, pp. 4064–4069, 2011.

[81] W. Forysiak, F. Knox, and N. Doran, "Average soliton propagation in periodically amplified systems with stepwise dispersion-profiled fiber," *Opt. Lett.*, vol. 19, no. 3, pp. 174–176, 1994.

[82] J. Shao, X. Liang, and S. Kumar, "Comparison of split-step fourier schemes for simulating fiber optic communication systems," *IEEE Photonics J.*, vol. 6, no. 4, p. 7200515, 2014.

[83] S. Kumar, J. C. Mauro, S. Raghavan, and D. Q. Chowdhury, "Intrachannel nonlinear penalties in dispersion-managed transmission systems," *J. Select. Topics Quantum Electron.*, vol. 8, no. 3, pp. 626–631, 2002.

[84] R.-J. Essiambre, G. Raybon, and B. Mikkelsen, "Pseudo-linear transmission of

high-speed TDM signals: 40 and 160 Gb/s," *Optical fiber telecommunications IV B*, pp. 232–304, 2002.

[85] Y. Fan, L. Dou, Z. Tao, T. Hoshida, and J. Rasmussen, "A high performance nonlinear compensation algorithm with reduced complexity based on XPM model," in *Optical Fiber Communication Conference*. Optical Society of America, 2014, p. Th2A.8.

[86] Y. Gao, A. S. Karar, J. C. Cartledge, S. Yam, M. O'Sullivan, C. Laperle, A. Borowiec, and K. Roberts, "Simplified nonlinearity pre-compensation using a modified summation criteria and non-uniform power profile," in *Optical Fiber Communication Conference*. Optical Society of America, 2014, p. Tu3A.6.

[87] X. Liang, S. Kumar, J. Shao, M. Malekiha, and D. V. Plant, "Digital compensation of cross-phase modulation distortions using perturbation technique for dispersion-managed fiber-optic systems," *Opt. Express*, vol. 22, no. 17, pp. 20 634–20 645, 2014.

[88] X. Liu and S. Chandrasekhar, "Superchannel for next-generation optical networks," in *Optical Fiber Communication Conference*. Optical Society of America, 2014, p. W1H.5.

[89] X. Liu, S. Chandrasekhar, and P. J. Winzer, "Digital signal processing techniques enabling multi-Tbs superchannel transmission: An overview of recent advances in DSP-enabled superchannels," *Signal Proc. Mag.*, vol. 31, no. 2, pp. 16–24, 2014.

[90] T. Zeng, "Superchannel transmission system based on multi-channel equalization," *Opt. Express*, vol. 21, no. 12, pp. 14 799–14 807, 2013.

[91] T. Pfau, S. Hoffmann, and R. Noé, "Hardware-efficient coherent digital receiver concept with feedforward carrier recovery for m-QAM constellations," *J. Lightwave Technol.*, vol. 27, no. 8, pp. 989–999, 2009.

[92] Y. Gao, J. H. Ke, K. P. Zhong, J. C. Cartledge, and S. Yam, "Assessment of intrachannel nonlinear compensation for 112 Gb/s dual-polarization 16QAM systems," *J. Lightwave Technol.*, vol. 30, no. 24, pp. 3902–3910, 2012.

[93] A. Vannucci, P. Serena, and A. Bononi, "The RP method: A new tool for the iterative solution of the nonlinear schrödinger equation," *J. Lightwave Technol.*, vol. 20, no. 7, p. 1102, 2002.

[94] D. Yang and S. Kumar, "Intra-channel four-wave mixing impairments in dispersion-managed coherent fiber-optic systems based on binary phase-shift keying," *J. Lightwave Technol.*, vol. 27, no. 14, pp. 2916–2923, 2009.

[95] S. Kumar, "Analysis of nonlinear phase noise in coherent fiber-optic systems based on phase shift keying," *J. Lightwave Technol.*, vol. 27, no. 21, pp. 4722–4733, 2009.

[96] A. Mecozzi, "A unified theory of intrachannel nonlinearity in pseudolinear transmission," in *Impact of Nonlinearities on Fiber Optic Communications*. Springer, 2011, pp. 253–291.

[97] M. Secondini, D. Marsella, and E. Forestieri, "Enhanced split-step fourier

method for digital backpropagation," in *European Conference on Optical Communications*. Optical Society of America, 2014, p. We.3.

[98] X. Liang and S. Kumar, "Multi-stage perturbation theory for compensating intra-channel nonlinear impairments in fiber-optic links," *Opt. Express*, vol. 22, no. 24, pp. 29 733–29 745, 2014.

[99] Y. Fan, L. Dou, Z. Tao, L. Li, S. Oda, T. Hoshida, and J. C. Rasmussen, "Modulation format dependent phase noise caused by intra-channel nonlinearity," in *European Conference on Optical Communication*. Optical Society of America, 2012, p. We.2.

[100] R. Asif, C.-Y. Lin, M. Holtmannspoetter, and B. Schmauss, "Optimized digital backward propagation for phase modulated signals in mixed-optical fiber transmission link," *Opt. Express*, vol. 18, no. 22, pp. 22 796–22 807, 2010.

[101] A. Yariv, D. Fekete, and D. M. Pepper, "Compensation for channel dispersion by nonlinear optical phase conjugation," *Opt. Lett.*, vol. 4, no. 2, pp. 52–54, 1979.

[102] S. Watanabe and M. Shirasaki, "Exact compensation for both chromatic dispersion and Kerr effect in a transmission fiber using optical phase conjugation," *J. Lightwave Technol.*, vol. 14, no. 3, pp. 243–248, 1996.

[103] P. Minzioni, I. Cristiani, V. Degiorgio, L. Marazzi, M. Martinelli, C. Langrock, and M. Fejer, "Experimental demonstration of nonlinearity and dispersion compensation in an embedded link by optical phase conjugation," *IEEE Photon. Technol. Lett.*, vol. 18, no. 9, pp. 995–997, 2006.

[104] M. D. Pelusi, "WDM signal all-optical precompensation of Kerr nonlinearity in dispersion-managed fibers," *IEEE Photon. Technol. Lett.*, vol. 25, no. 1, pp. 71–74, 2013.

[105] M. Morshed, L. B. Du, B. Foo, M. D. Pelusi, and A. J. Lowery, "Optical phase conjugation for nonlinearity compensation of 1.21-Tb/s Pol-Mux coherent optical OFDM," in *OptoElectronics and Communications Conference and Photonics in Switching*. Optical Society of America, 2013, p. PD3_4.

[106] D. Rafique and A. D. Ellis, "Nonlinearity compensation via spectral inversion and digital back-propagation: A practical approach," in *Optical Fiber Communication Conference*. Optical Society of America, 2012, p. OM3A.1.

[107] X. Liang, S. Kumar, and J. Shao, "Ideal optical backpropagation of scalar NLSE using dispersion-decreasing fibers for WDM transmission," *Opt. Express*, vol. 21, no. 23, pp. 28 668–28 675, 2013.

[108] S. V. Chernikov, D. Richardson, D. Payne, and E. Dianov, "Soliton pulse compression in dispersion-decreasing fiber," *Opt. Lett.*, vol. 18, no. 7, pp. 476–478, 1993.

[109] A. J. Stentz, A. F. Evans, and R. W. Boyd, "Dramatically improved transmission of ultrashort solitons through 40 km of dispersion-decreasing fiber," *Opt. Lett.*, vol. 20, no. 17, pp. 1770–1772, 1995.

[110] I. Tomkos, D. Chowdhury, J. Conradi, D. Culverhouse, K. Ennser, C. Giroux, B. Hallock, T. Kennedy, A. Kruse, S. Kumar *et al.*, "Demonstration of negative

dispersion fibers for DWDM metropolitan area networks," *J. Select. Topics Quantum Electron.*, vol. 7, no. 3, pp. 439–460, 2001.

[111] J. Conradi, S. Kumar, and S. S. Rosenblum, "Negative dispersion single mode waveguide fiber," 2002, US Patent 6,430,346.

[112] S. Kumar, "Effect of dispersion on nonlinear phase noise in optical transmission systems," *Opt. Lett.*, vol. 30, no. 24, pp. 3278–3280, 2005.

[113] A. Hasegawa and F. Tappert, "Transmission of stationary nonlinear optical pulses in dispersive dielectric fibers. I. Anomalous dispersion," *Appl. Phys. Lett.*, vol. 23, no. 3, pp. 142–144, 1973.

[114] V. E. Zakharov and A. B. Shabat, "Exact theory of two-dimensional self-focusing and one-dimensional self-modulation of waves in nonlinear media," *Sov. Phys. JETP.*, vol. 34, pp. 62–69, 1972.

[115] G. L. Lamb Jr, *Elements of Soliton Theory*. Wiley-Interscience, 1980.

[116] P. G. Drazin and R. S. Johnson, *Solitons: An Introduction*. Cambridge University Press, 1989, vol. 2.

[117] Y. Xiao, D. N. Maywar, and G. P. Agrawal, "New approach to pulse propagation in nonlinear dispersive optical media," *J. Opt. Soc. Am. B*, vol. 29, no. 10, pp. 2958–2963, 2012.

[118] E. Ciaramella and E. Forestieri, "Analytical approximation of nonlinear distortions," *IEEE Photon. Technol. Lett.*, vol. 17, no. 1, pp. 91–93, 2005.

[119] S. Kumar, J. Shao, and X. Liang, "Impulse response of nonlinear schrödinger equation and its implications for pre-dispersed fiber-optic communication systems," *Opt. Express*, vol. 22, no. 26, pp. 32 282–32 292, 2014.

[120] R.-J. Essiambre, B. Mikkelsen, and G. Raybon, "Intra-channel cross-phase modulation and four-wave mixing in high-speed TDM systems," *Electron. Lett.*, vol. 35, no. 18, pp. 1576–1578, 1999.

[121] P. Mamyshev and N. Mamysheva, "Pulse-overlapped dispersion-managed data transmission and intrachannel four-wave mixing," *Opt. Lett.*, vol. 24, no. 21, pp. 1454–1456, 1999.

[122] I. S. Gradshtejn and I. M. Ryzhik, *Table of Integrals, Series and Products*. Academic Press, 1965.

[123] M. Ablowitz and B. Prinari, "Nonlinear Schrodinger systems: Continuous and discrete," *Scholarpedia*, vol. 3, no. 8, p. 5561, 2008.

[124] J. C. Eilbeck and M. Johansson, "The discrete nonlinear Schrödinger equation-20 years on," in *Conference on Localization and Energy Transfer in Nonlinear Systems*, 2003, p. 44.

[125] J. C. Eilbeck, P. Lomdahl, and A. Scott, "The discrete self-trapping equation," *Physica D: Nonlinear Phenomena*, vol. 16, no. 3, pp. 318–338, 1985.

[126] M. J. Ablowitz and T. Hirooka, "Managing nonlinearity in strongly dispersion-managed optical pulse transmission," *J. Opt. Soc. Am. B*, vol. 19, no. 3, pp. 425–439, 2002.

[127] M. Bakr, *Nonlinear Optimization in Electrical Engineering with Applications in Matlab*. The Institution of Engineering and Technology, 2013.